Supraglacial dust and debris characterization via in situ and optical remote sensing methods

Kimberly Ann Casey

Department of Geosciences

University of Oslo

A thesis submitted for the degree of

PhilosophiæDoctor (PhD)

2011

Series of dissertations submitted to the
Faculty of Mathematics and Natural Sciences, University of Oslo
No. 1113

ISSN 1501-7710

Cover: Inger Sandved Anfinsen.
Printed in Norway: AIT Oslo AS.

Produced in co-operation with Unipub.
The thesis is produced by Unipub merely in connection with the
thesis defence. Kindly direct all inquiries regarding the thesis to the copyright
holder or the unit which grants the doctorate.

Abstract

Supraglacial dust and debris affects many glaciologic variables, including radiative absorption, ablation, generation of supraglacial melt as well as mass flux. Earth observing satellite technology has advanced greatly in recent decades and allows for unprecedented spatial, temporal and spectral imaging of Earth's glaciers. While remote sensing of 'clean' glacier ice can be done quite successfully, strategies for satellite mapping of supraglacial debris remain in development. This work provides the first visible to thermal infrared full optical spectrum satellite data analysis of supraglacial dust and debris characterization and differentiation. Dust and debris covered glaciers in the following six contrasting study regions were targeted: Iceland, Nepal, New Zealand, southern Norway, Svalbard and Switzerland. A combination of field spectrometry and surface samples of snow, ice and debris were utilized to investigate supraglacial dust and debris diversity. This in situ data served as ground truth for evaluating spaceborne supraglacial debris mapping capabilities.

Glacier snow, ice and debris samples were analyzed for mineral composition and inorganic elemental abundances via the following analytical geochemical techniques: X-ray diffraction, X-ray fluorescence spectroscopy and inductively coupled plasma mass spectrometry. A synoptic data set from four contrasting alpine glacier regions – Svalbard, southern Norway, Nepal and New Zealand – and 70 surface snow, ice and debris samples was presented, comparing supraglacial composition variability. Distinct supraglacial geochemical abundances were found in major, trace and rare earth elemental concentrations between the four study regions. Elemental variations were attributed to both natural and anthropogenic processes.

Over 8800 glacier surface spectra were collected in Nepal, Svalbard and Switzerland, as well as from Nepal, New Zealand and Switzerland debris samples. Surface glacier debris mineralogy and moisture content were assessed from field spectra. Spaceborne supraglacial dust and debris mineral mapping techniques using visible to shortwave reflective and thermal emissive data were evaluated. Successful methods for mineral identification allowed mapping of volcanic vs. continental supraglacial debris, as well as different mineral classes within one glacier's supraglacial debris. Granite- vs. schist-dominant debris was mapped on Khumbu glacier in Nepal. Iron-rich vs. iron-poor serpentine debris was mapped on Zmutt glacier in the Swiss Alps. Satellite emissivity derived silica mapping suggested potential use of silica thresholds for delineation of debris covered glacier extent or sediment transport and weathering processes. Satellite derived surface temperatures were compared in Iceland, Nepal, Switzerland and New Zealand glacier study regions, with results demonstrating variations in supraglacial temperatures coincident with changing mineral abundances. Consistently higher surface temperatures with increasing dust and debris cover were mapped at all four glacier study regions. Repeat supraglacial debris imagery was used to estimate ablation area velocities and particulate transport times at debris covered glaciers. Velocity derivations used in conjunction with supraglacial composition variation analysis from shortwave and thermal infrared false color composites, allowed for estimation of glacial mass flux in the Khumbu Himalayas.

In short, the visible to thermal infrared satellite spectral analysis, combined with in situ spectral and geochemical ground truth data, proved that glacier dust and debris characterization is possible via satellite spectral data. Furthermore, this supraglacial dust and debris satellite characterization can be applied to a range of glaciologic studies, including thermal, mass balance and surface process interpretations on large spatial and temporal scales.

Acknowledgements

To place this dissertation in context, when I embarked upon this program my primary supervisor, Dr. Andreas Kääb shared with me that this was potentially the only time in my scientific career I would have the freedom to investigate any topic I desired without constraint (e.g. mandatory project deliverables). He encouraged me to delve into my burning scientific questions. Therefore, I had no hesitations at all. I wanted to test the capabilities of geochemical description of glaciers via satellite. My supervisor and the University of Oslo Department of Geosciences enthusiastically supported this scientific proposal, even when other scientists (i.e. reviewers) cautioned against 'trying to save the world'.

Funding of science for science's sake is an important principal of which I have been a grateful recipient over the years. As a child, my parents generously 'funded' all desired academic school supplies and in my later years even science club trips as they believe in the value of education. Similarly, in Oslo, Dr. Kääb and the University of Oslo, Department of Geosciences have bestowed an incredible gift of always providing me with the time and means to explore my scientific ideas. I am thus immensely grateful to Dr. Kääb and the University of Oslo, Department of Geosciences for supporting this scientific work. Both the opportunity to conduct research within an institution that values the pursuit of science, as well as the cultural experiences of working in Oslo and conducting field work in multiple countries have been exceptionally rewarding. In addition, I am thankful for scientific mentoring and encouragement from Dr. Oddvar Røyset and Dr. RuiKai Xie. I also thank Dr. Dorothy Hall for her unofficial mentoring of over a decade. I would like to acknowledge funding from the European Space Agency's GlobGlacier project and European Union's Brahmatwinn

project, and the receipt of field spectrometer instrument loans from Natural Environment Research Council Field Spectroscopy Facility and Analytical Spectral Devices Alexander Goetz Instrument Support Program (2010 recipient). Credit must also be given to the NASA Earth Observing System data that is freely available to the public; without this data and its availability, the goals of this project would have been much more difficult to achieve.

Of utmost importance, I sincerely thank my family, friends and colleagues for their support over the years. After science, (*joking*), many of life's most beautiful moments are within the company of loved ones and friends.

Oslo
31 May 2011
Kimberly A. Casey

. . .

To the continued value of the pursuit of science
and the scientists who dedicate even
"one percent inspiration and ninety-nine percent perspiration"
toward advancing our collective understanding
and applying it toward the greater good of all.

. . .

— *quote from Thomas Alva Edison*

List of Dissertation Publications

i. K.A. Casey. Proposed methodology for detection of geochemical species on glaciers, In: Proceedings of 10th Biennial Meeting of the Society for Geology Applied to Mineral Deposits (SGA), 16-22 August 2009. Townsville, Australia.

I. K.A. Casey, A. Kääb, D.I. Benn. Characterization of glacier debris cover via in situ and optical remote sensing methods: a case study in the Khumbu Himalaya, Nepal. The Cryosphere Discussions, 5, 499-564, 2011. *Revision submitted to The Cryosphere.*

II. K.A. Casey, R. Xie, O. Røyset, H. Keys. Supraglacial dust and debris geochemical variability: data from Svalbard, Norway, Nepal and New Zealand. *Revision submitted to Journal of Glaciology.*

III. K.A. Casey, A. Kääb. Supraglacial dust and debris reflectance and emissivity variability, relation to geochemical composition, surface temperature and glaciologic impacts. *Manuscript in preparation for submission.*

Contents

1

Introduction, Motivation and Objectives

Dust and debris is common to many of the world's glaciers and can impact radiative glaciologic processes (e.g. energy balance, melt rates, generation of supraglacial melt ponds or lakes) (Nakawo and Young, 1981; Pelto, 2000; Wessels and others, 2002), glacial kinematics (Iwata and others, 2000; Kääb and others, 2006), and may be spatially changing in coming years due to changing climate and atmospheric circulation patterns (Scherler and others, 2011; Oerlemans and others, 2009; Kok, 2011).

Spaceborne supraglacial dust and debris geochemical differentiation has received limited focus to date (e.g. Wientjes and Oerlemans, 2010, Greenland ablation zone 'dark region'). Several multi- and hyperspectral Earth observing sensors now offer over a decade of unprecedented spectral resolution glacier data and the opportunity to test supraglacial dust and debris mapping methods. Satellite remote sensing of glaciers is crucial to regional (e.g. Kääb and others, 2002; Schneider and others, 2007; Bolch and others, 2010a) and global glacier monitoring inventories (Raup and others, 2007; Paul and others, 2009). Although supraglacial dust and debris (or composition) are not currently central aims of glacier inventories, such information could be of key use in many glaciologic and climate applications. The geochemical composition of supraglacial dust and debris can reveal differing atmospheric and regional influences affecting glaciers.

With the motivation of characterizing surface glacier geochemical composition via multi- and hyperspectral remote sensing, the specific objectives of the dissertation work

are summarized as follows:

- Collect glacier surface samples in contrasting glaciologic and geographic regions. Measure geochemical composition of snow, ice and debris samples using inductively coupled plasma mass spectrometry, X-ray diffraction and X-ray fluorescence spectrometry.
- Collect in situ supraglacial spectral data in contrasting glaciologic and geographic regions. Assess in situ spectra for geochemical composition using spectral library geologic references. Compare field collected spectra with satellite spectral reflectance.
- Investigate full optical spectrum, visible to thermal infrared (reflective and emissive) differences of supraglacial dust and debris in distinct regions. Calculate reflectance, emissivity and surface temperatures of differing debris types and spatial distributions of debris.
- Evaluate optical satellite remote sensing methods to characterize composition and radiative properties of supraglacial dust and debris. Present preliminary results towards glaciologic implications of differing dust and debris types.

These objectives were addressed via the field collected glacier spectra, glacier surface samples, and satellite multi- and hyperspectral glacier reflectance and emissivity analysis in six diverse study locations. The following sections provide the scientific background, data and methods used, implications and outcomes of the work as well as the publications resulting from this dissertation.

2

Scientific Background

2.1 Glacial geochemistry

2.1.1 Influence of the atmosphere on glacier composition

Understanding the interactions between the Earth's atmosphere and cryosphere is of paramount importance to global radiative energy balance and climate. From glacier dust and soot radiative forcing studies (e.g. Hansen and Nazarenko, 2004; Paul and others, 2005) as well as ice core composition studies (e.g. Thompson, 2000; Gabrielli and others, 2010), particulate deposition on glaciers has been shown to be a significant variable requiring further definition. Emerging research suggests global atmospheric dust and soot flux may be underestimated, especially in consideration of changing climate and atmospheric circulation patterns (Kaspari and others, 2011; Kok, 2011). Consequently, these particulates may have larger impacts on glacier radiative energy balance than currently understood (e.g. Xu and others, 2009).

Natural environmental processes as well as human activities cause a vast amount of aerosols, or small particulates, to be injected into the atmosphere. In fact, 1000-5000 million tons of aerosols of all types – both natural (e.g. continental dust, volcanic ash, sea salt) and anthropogenic (e.g. fossil fuel emissions, metal production, waste incineration) are emitted into Earth's atmosphere each year (Tegen and Fung, 1995; Arimoto, 2001; Christopher and others, 2009). These particulates exist in seasonal cycles (Tegen and Schepanski, 2009), are derived from distinct origins (Mahowald and others, 2009), and their transport can be modeled (e.g. Figure 2.1) (Zender and others, 2003; Stohl and others, 2005; Yue and others, 2009). Atmospheric transport models

(e.g. FLEXPART, a Lagrangian particle dispersion model, see (Hirdman and others, 2010)) can potentially allow for estimations of supraglacial dust composition based on source regions. Atmospheric dust source regions modeled by Mahowald and others (2009) show African and Asian dust being the largest deposition contributor to northern hemisphere glaciers, while South American and Australian dust affects Antarctica, New Zealand and South American glaciers.

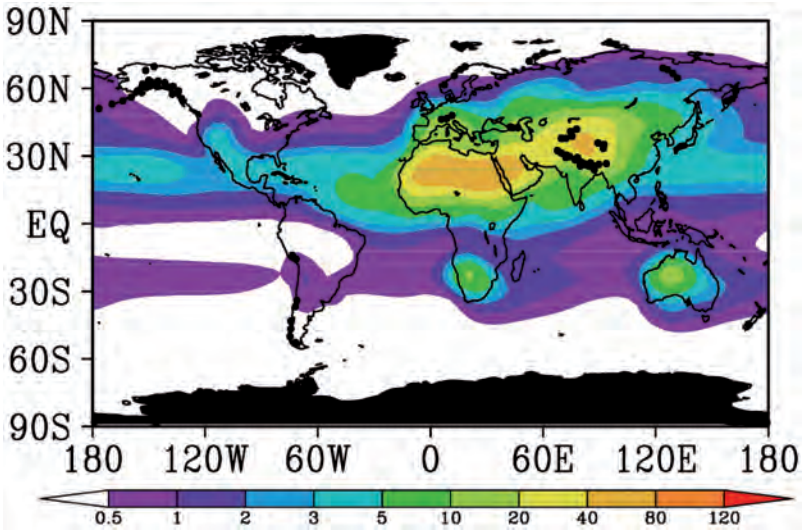

Figure 2.1: Atmospheric influence on glaciers - The figure shows the geographic distribution of land-based ice (in black after Global Land Ice Measurements from Space, GLIMS) on modeled mean annual wet and dry dust deposition after Yue and others (2009) (units g per meter squared per year).

In the atmosphere, as snow and ice crystals form, they nucleate about atmospheric particulates (except when temperatures are below -38°C and homogeneous freezing occurs without a nucleation particle) (Zimmermann and others, 2008; Cziczo and others, 2009; Knopf and others, 2011). Whether or not a particulate is at the center of a snow or ice crystal, as precipitation falls to Earth's surface, it can also assimilate other particulates. Both natural and anthropogenic particulates can be transported from source areas to remote locations and incorporated into precipitation which is deposited on glacier surfaces (Tatsumoto and Patterson, 1963; Barrie, 1985; Pacyna and Pacyna,

2001; Osterberg and others, 2008; Kaspari and others, 2009). As a result, a unique 'signature' of atmospheric aerosols is recorded in glacial geochemistry and can be analyzed in surface snow and ice or in ice cores (Thompson, 1980; Wake and others, 1993; Schwikowski and Eichler, 2010).

2.1.2 Evolution of ice composition

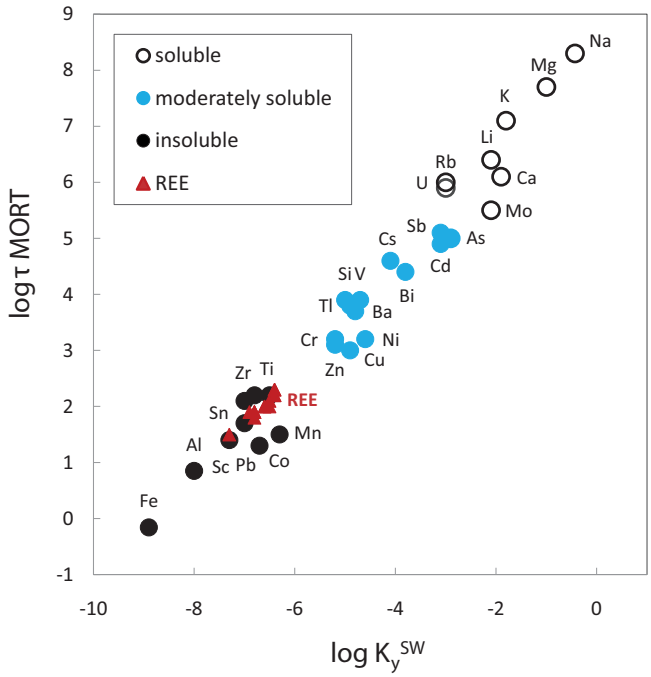

Figure 2.2: Solubility of the elements - The plot presents the meteoric solubility of the elements measured in the study regions, where the geochemical reference standard Mean Ocean Residence Time (MORT) is given relative to the chemical partition coefficient (of sea water to upper continental crust) (further detailed in Taylor and McLennan, 1985; Rudnick and Gao, 2003).

The geochemical composition of supraglacial ice evolves over days, seasons and years. Atmospheric deposition of particulates fluctuates with season, weather or emission event (e.g. a volcanic eruption, smelter emission). Proximity to the ocean, pollutant, dust or biomass emission sources can change specific element abundances (e.g.

Na, Ca, Fe) on the glacier surface (Barrie, 1985). Evidence of large seasonal dust variability affecting surface ice composition has been demonstrated by Himalayan ice core analysis (e.g. Kang and others, 2000; Kreutz and others, 2004), and much longer thousand year interglacial dust variability in glacial geochemical composition by Antarctic ice core measurements (Petit and others, 1999; Gabrielli and others, 2010).

Not only atmospheric wet and dry deposition, but also local dust or rock fall, biotic processes (Yoshimura and others, 2000; Takeuchi, 2002; Hodson and others, 2008), wind exposure, glacial slope and/or resurfacing of sediments and elements from englacial transport can influence supraglacial ice composition over time. Glacier motion can crush englacial sediments and bedrock to rock flour, allowing for remobilization of reactive trace elements within minerals to glacial ice (Tranter, 2003). There is also growing research on the role of biotic processes in supraglacial composition and processes (e.g. Kohshima and others, 1992; Hodson and others, 2005). For example, biota can change inorganic element oxidation states, and thus potentially affect solubility of inorganic species on glacier surfaces.

Chemical reactions at the glacier surface are regulated by factors including solar radiation, surface temperature, wind and the presence of melt water. These factors change glacier surface geochemical abundances as soluble species in particulates (e.g.: Na) are washed away in runoff, percolated downward in the snow pack with successive melt and refreeze cycles, or as particulates are concentrated by surface sublimation (Colbeck, 1981; Tranter and others, 1986; Fountain, 1996; Ginot and others, 2001). In polar regions, solar radiation can strongly influence seasonal atmospheric and supraglacial composition (e.g. Hg, detailed in Lu and others, 2001; Ferrari and others, 2008). The tendency for an element to be soluble is determined by intrinsic chemical properties (e.g. ionization potential, electronegativity and valency). Figure 2.2 displays meteoric solubility (i.e. solubility of elements in natural water with atmospheric interaction) of the elements measured in this dissertation work. Insoluble elements, metals and mineral grains tend to stay on the glacier surface (e.g. Kreutz and Sholkovitz, 2000), while salts dissolve readily. This insolubility can be utilized to identify source material (Taylor and McLennan, 1985; Rudnick and Gao, 2003). Insoluble elements are targeted by this work to investigate particulate origins and anthropogenic vs. natural influences to supraglacial dust and debris (further discussed in Section 2.1.3, **Publication II**).

2.1.3 Trace elements as indicators of provenance and anthropogenic or natural influences

Glacier dust and debris geochemical variability can be measured and used to further describe glacial environment variables, including provenance of dust and debris (Marx and others, 2005), anthropogenic or natural influences (Hong and others, 1996; Schwikowski and others, 1999) and even climate when assessed in ice cores (Thompson and others, 2006; Gabrielli and others, 2010). The rare earth elements (REE) provide a series of relatively insoluble elements with low chemical reactivity, and are thus amenable to provenance and geochemical cycling studies (Taylor and McLennan, 1985) including glaciologic (Kreutz and Sholkovitz, 2000; Zhang and others, 2009). Further, the simple presence of certain trace elements (or isotopes of trace elements) in supraglacial ice can signal anthropogenic influence (e.g. Olivier and others, 2003). For example, Pb, V are fossil fuel combustion and metal production byproducts with high atmospheric emission rates, yet very low crustal (i.e. natural) abundances. Conversely, the presence of Mn and Cr in supraglacial ice – elements which have high continental dust atmospheric emission rates, yet relatively low crustal abundances – can signal naturally derived atmospheric deposition sources (this sentence and previous sentence Pacyna and Pacyna, 2001; Hu and Gao, 2008). Trace element isotopes can also be used to investigate atmospheric, englacial and subglacial influences to glaciologic composition and residence times (Bhatia and others, 2011).

Glacier surface and ice core trace element abundance studies about the globe: for example, in the Arctic (Tao and others, 2001; Isaksson and others, 2003; Symon and Wilson, 2005), on the Greenland Ice Sheet (Hong and others, 1996; Bory and others, 2003; Osterberg and others, 2006; Banta and others, 2008), in the European Alps (Schwikowski and others, 1999; Barbante and others, 2004; Sodemann and others, 2005) and southern Alps (Marx and others, 2005; Purdie and others, 2010), in the tropics (Thompson and others, 2005), in the Himalayas (Wake and others, 1993; Thompson, 2000; Kreutz and Sholkovitz, 2000; Lee and others, 2008; Aizen and others, 2009; Kaspari and others, 2009; Zhang and others, 2009), in the Andes (Correia and others, 2003; Schwikowski and others, 2006; Vimeux and others, 2009) and on the Antarctic Ice Sheet (Ikegawa and others, 1999; Ruth and others, 2008; Marteel and others, 2008; Gabrielli and others, 2010) have to varying degrees measured and determined glacier particulate deposition sources as well as atmospheric, environmental and glaciologic

parameters. Not only trace elemental studies, but also studies measuring stable isotopes (δ^{18}O), major elements (e.g.: Na, Ca) as well as physical properties found in ice core layers (e.g. density), have been used to reconstruct climate and to determine accumulation rates over the past several hundred or thousand years (e.g. Thompson and others, 2006; Henderson and others, 2006). Research outcomes of these various glacier geochemical investigations have been indisputably ground-breaking in furthering understanding of climate, particulate provenance to glaciers, and glacier processes. Work completed in this dissertation provided a first-order data set of supraglacial dust and debris geochemical variability from diverse alpine glacier study regions and aimed to explore spaceborne geochemical measurement.

2.2 Debris covered glaciers

Glacial debris, for example shown on Susitna glacier in Alaska in Figure 2.3, has fascinated glaciologists for centuries (e.g. Russell, 1895; Ogilvie, 1904; Sharp, 1949; Sakai and others, 2002). Similar to analysis of dust composition revealing several glaciologic factors, the analysis of debris cover has been demonstrated to provide information on glacier kinematics (Barsch and Jakob, 1998; Kääb, 2005), mass wasting (Fort, 2000), weathering (Maisch and others, 1999; Anderson, 2005) and energy balance (Mihalcea and others, 2008; Scherler and others, 2011).

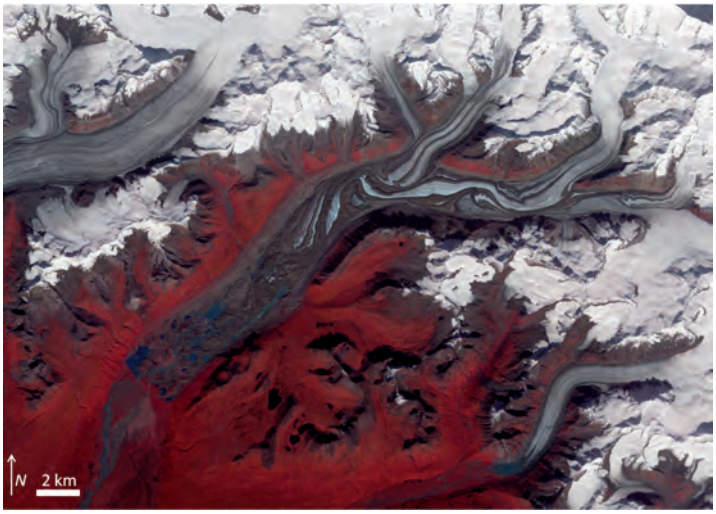

Figure 2.3: Susitna glacier, Alaska - ASTER image acquired 27 August 2009 of Susitna glacier, located in the Alaska Range in central Alaska. The supraglacial debris patterns on Susitna glacier indicate the differential flow of tributary accumulation area glaciers and historical surges. The image also displays supraglacial melt ponds and reveals chaotic disintegration toward the terminus. (Image processing by NASA Earth Observatory.)

2.2.1 Distribution and characteristics

While the majority of Earth's glaciers contain a degree of dust or debris cover in ablation zones, the heaviest debris covered glaciers are found in areas of extreme topographic relief (e.g. southern Himalayas, Alps) and around active volcanos (e.g. Iceland, north-

ern New Zealand, Andes). Debris cover on glaciers can range from fine particulates to several meter in diameter boulders, and can have even, gradual spatial distribution (e.g. dust, soot or heavy debris) or be arranged along longitudinal medial moraines (Paul and others, 2004a). Minimal to moderate glacier debris cover enhances melt rates (Warren and Wiscombe, 1980; Oerlemans and others, 2009) while extensive debris cover can insulate ice and reduce or dampen melt processes (Østrem, 1959; Fujii, 1977; Mattson and others, 1993; Takeuchi and others, 2000; Nicholson and Benn, 2006). Downwasting, or the stationary thinning of the glacier as a result of warming temperatures, has been studied, for example at debris covered glaciers in the Himalayas (Benn and others, 2000; Bolch and others, 2008), the European Alps (Paul and others, 2004b), the southern Alps (Hochstein and others, 1995; Quincey and Glasser, 2009), North America (Pelto, 2000; Schiefer and Menounos, 2010), and South America (Harrison and Winchester, 2000). Not only ablation rates, but also melt water discharge (Mattson, 1990, 2000) and backwasting (Nakawo and others, 1999), are additional glaciologic variables that are affected by debris cover.

Ice cored moraines and the generation of supraglacial melt are also key characteristics of debris covered glaciers (Richardson and Reynolds, 2000; Reynolds, 2000). The formation of supraglacial melt coupled with englacial drainage, pro-glacial lake calving and/or ice-cored moraine disintegration can result in chaotic loss of debris covered glacier ablation areas (Konrad, 1998; Gulley and Benn, 2007; Röhl, 2008). Consequent glacial lake outburst floods (GLOFs) can have extreme impacts on downstream ecosystems and settlements. This catastrophic geopotential of many debris covered glaciers, presents significant hazards and necessitates improved understanding and monitoring of heavily debris covered regions (Evans and Clague, 1994; Kargel and others, 2011).

2.2.2 Debris composition and weathering

Supraglacial debris composition consists primarily of surrounding and accumulation area glacier geology. Existing geologic maps can be used to predict supraglacial composition. For example, glaciologic field studies by Fushimi and others (1980) mapped spatial distribution of granitic vs. schistic supraglacial debris on Khumbu glacier correlating the supraglacial compositions to upper glacier geology.

The lithology of continental debris covered glaciers tends to be characterized by blocky angular boulders and sediments (Richardson and Reynolds, 2000; Benn and

Evans, 2010). Heavy volcanic supraglacial debris can be composed of fine grained volcanic ash, tephra or large ballistics ejected during eruptions (e.g. New Zealand's Mt. Ruapehu September 2007 eruption, described in Kilgour and others, 2010). The difference between volcanic tephra and continental sediment on glaciers provides potentially the largest mineral and lithologic supraglacial debris variety with regard to spectral investigations (**Publication III**). However, even within continental supraglacial debris, on one glacier, great compositional variety can exist and can be mapped via spectral data – e.g. Khumbu glacier leucogranite vs. schist supraglacial debris (mapped in **Publication I**) and Valais Swiss Alp Zmuttgletscher serpentine Fe-rich vs. Fe-poor supraglacial debris (mapped in **Publication III**). To note, as discussed in Section 2.1.1, the deposition of atmospherically transported particulates (e.g. dust) can also contribute significantly to heavily debris covered glaciers (e.g. Lirung glacier, studied by Adhikary and others, 2000).

Supraglacial dust and debris composition can evolve as weathering processes occur coincident with seasonal precipitation, melt/refreeze cycles or supraglacial activity (i.e. transport) rates. Diagenesis (discussed in **Publication I**) or precipitate coatings (discussed in **Publication III**) weathering processes are capable of changing the geochemical or lithologic characteristics of supraglacial dust and debris. The high activity of the Khumbu Himalayan glaciers, for example, enhance surface weathering processes (Benn and Owen, 2002). Further, glacial activity and comminution of englacial sediments and bedrock can also influence the composition of supraglacial debris, as en- or subglacial material is exchanged to the glacier surface over time (Tranter, 2003).

2.2.3 Debris kinematics, entrainment, mass flux

Past surges and flow processes can be evidenced by ogive patterns and looped and folded moraines (Post and LaChapelle, 1971) (Figure 2.3). Debris mantle assemblages indicate slope processes such as rock or ice falls or avalanches (Benn and Evans, 2010) or indicate glacier flow regimes described by glacial movement that is continuous, pulsed or of surge type (Kääb, 2005). Glacial mass flux can be further estimated by repeat spectral image matching to calculate velocity and theoretical particle transport time (Kääb, 2005; Haug and others, 2010; Scherler and others, 2011) (**Publication I**). Combined with spectral debris characterization methods, discussed in Section 3.2.2 such as the

shortwave-thermal infrared image composite (Kääb, 2005), a glacial kinematic history can be revealed.

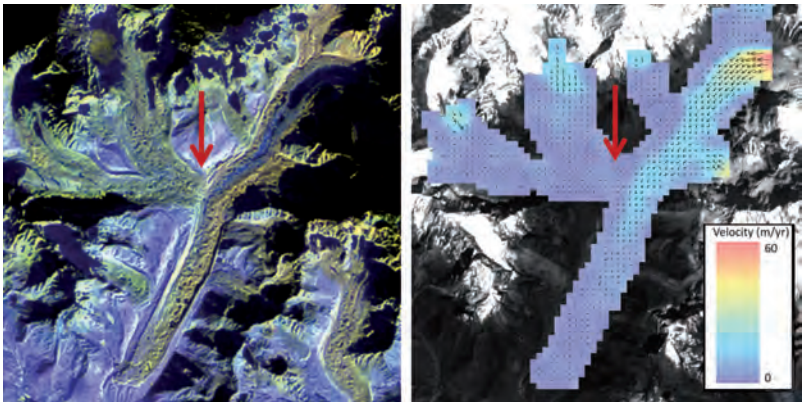

Figure 2.4: Debris covered glacier kinematics - The left image displays Khumbu glacier region using a Landsat ETM+ shortwave and thermal infrared false color composite (bands 5,7,6). The right image is a repeat image matching derived glacier velocity map of the same area. Limited mass flux from Khangri Nup and Khangri Shar glaciers into the Khumbu glacier (i.e. at red arrows) is indicated by the distinct break in surface lithology (blue corresponding with schistic debris, yellow with granitic debris) and reaffirmed by the near zero velocity in this region (further detailed in **Publication I**).

Distinct geologic sources derived from the accumulation zone, flowing down glacier or englacially, reemerging in the ablation zone can also be seen in supraglacial debris patterns (e.g. Kääb, 2005). Englacial transport as well as the magnitude of debris transported can be detected, demonstrated in **Publication I** at glacial confluences existing at both Ngozumpa and Khumbu glaciers. Figure 2.4 displays a false color composite of the Khumbu glacier and highlights mass flux at one such confluence (indicated by the red arrow). At this confluence of the Khangri Shar and Khumbu glaciers, just a few kilometers from the Khumbu icefall, evaluation of the lithologic and compositional differences reveal the limited or slight mass flux from Khangri Shar to Khumbu glacier. The repeat spectral image matching derived glacier velocity (right side, Figure 2.4) reaffirm negligible transfer of mass at the confluence from Khangri Shar toward Khumbu glacier, in agreement with the near zero velocities of Khangri Shar glacier toward Khumbu glacier (also detailed in **Publication I**).

3

Data and Methods

In order to characterize supraglacial dust and debris variability, field spectra and glacier snow, ice and debris samples were collected at several study glaciers and analyzed for reflectance as well as geochemical composition, respectively. Visible-to-thermal infrared satellite spectral data from the targeted study glaciers was used to investigate supraglacial reflectance, emissivity and geochemical composition.

Method \ Study	Abstract i	Publication I	Publication II	Publication III
VNIR-SWIR field spec	X	X		
VNIR-SWIR satellite	X	X		X
VNIR-SWIR hyperspectral satellite		X		X
TIR satellite		X		X
ICP-MS			X	
XRD / XRF		X	X	X
Global comparison	X		X	X

Figure 3.1: Study methods - An overview of the data used and methods applied in the dissertation are visualized in this table.

The following sections detail the in situ data collected as well as the spectral sensors and analytical geochemical techniques utilized. Methods for collecting data, using visible-to-thermal infrared spectral data and interpreting analytical geochemical data to investigate supraglacial dust and debris variability are presented. Figure 3.1 visually summarizes the combination of methods used by each dissertation publication. Lim-

itations of spectral remote sensing data usage and potential error sources inherent to analytical geochemistry measurements are also discussed in the following sections.

3.1 In situ glacier surface data

Glacier study regions were chosen based on distinct geographic and glaciologic characteristics, which are summarized in Table 3.1 and located on the map presented in Figure 3.2. The six regions provide contrasting mid to near-polar latitudes, continental to varying degrees of maritime climates, as well as volcanic influences. The diverse geographic locations allow for evaluation of a variety of regional geologic compositions as well as atmospheric circulation zones with differing particulate sources.

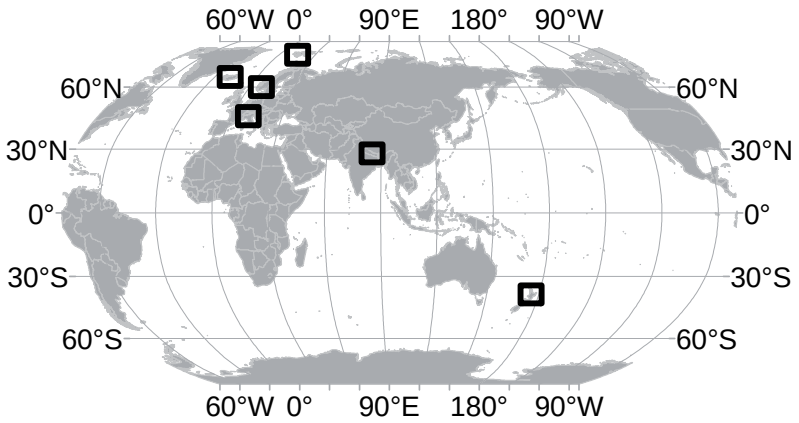

Figure 3.2: Location of glacier study regions - The black squares locate the diverse glacier study regions targeted in this dissertation.

In situ data, in the form of field spectroscopy and supraglacial snow, ice and debris samples were collected in five diverse study regions. At the sixth glacier study region, Iceland, in situ data was not collected but was extracted from existing published in situ geochemical data (e.g. from Gislason and others, 2011). The study regions are further detailed in the dissertation publications (i.e. **Abstract i** briefly details Svalbard, southern Norway, Nepal and New Zealand; **Publication I** details Nepal; **Publication II** details Svalbard, southern Norway, Nepal and New Zealand; and **Publication III** details Iceland, Switzerland, Nepal and New Zealand).

Table 3.1: Geographic, glaciologic and climate characteristics of glacier study regions.

Study region, Glacier (Latitude, Longitude)	Glacier type, Influences	Mean Annual Temp., Precip. Elevation (m.a.s.l.)
Svalbard Grønfjordbreen Aldegondabreen (77.98 N 14.12 E)	Arctic, small valley, polythermal, maritime influences	-6.0 °C, >400 mm 250-500 m[a]
Norway Jostedalsbreen Bødalsbreen (61.78 N 7.10 E)	Ice field and outlet valley glacier, temperate, slight maritime influence	6.4°C, 1200-3000 mm 740-1990 m[b]
Nepal Ngozumpa Khumbu (27.98 N 86.84 E)	Debris covered continental valley glaciers, Temperate, summer accumulation	-2.4°C, 470 mm 4900-8848 m[c]
New Zealand Mt. Ruapehu area (39.27 S 175.56 E)	Southern hemisphere, cirque glaciers, volcanic influences	6.1°C, 1100 mm 2200-2797 m[d]
Switzerland Zermatt area (46.00 N 7.65 E)	Mid-latitude, valley glaciers, dust and debris covered	3.5°C, 700 mm 2240-4450 m [e]
Iceland Central ice caps (64.30 N, 18.05 W)	Near-Arctic, maritime ice caps, volcanic influences	-0.4°C, 740 mm 0-2100 m [f]

[a]Climate data from Hagen and others (1993); elevation from Norwegian Polar Institute, 2004.

[b]Climate data from Norwegian Meteorological Institute; elevation from Andreassen and others (2008).

[c]Climate data from Tartari and others (1998); elevation from Hambrey and others (2008).

[d]Climate data from New Zealand National Institute of Water and Atmospheric Research; elevation from New Zealand Department of Conservation, 2004.

[e]Climate data from MeteoSwiss, Gruber and Hoelzle (2001); elevation from Swisstopo, 2004.

[f]Climate data from de Woul and others (2006); elevation from Gudmundsson and others (2010).

3.1.1 Supraglacial snow, ice and debris samples

Climate patterns and regional characteristics were studied prior to sample collection in order to plan collection, understand the context of samples (e.g. seasonal characteristics) and subsequently analyze results. For example, mining emissions occur near the Barentsburg, Svalbard study glaciers (visible in Figure 4.1), and Crater Lake volcanic outgassing emissions influence supraglacial geochemistry on the 8 glaciers about Mt. Ruapehu, New Zealand (Hurst and others, 1991; Werner and others, 2006). Ablation season samples were targeted (with the exception of both accumulation and ablation season samples acquired in Svalbard and New Zealand). Glacier surface snow and ice geochemical abundances of Jostedalsbreen ice field to Bødalsbreen outlet glacier were measured in southern Norway. Bare ice, dust, and heavy debris geochemical composition was compared using three neighboring glaciers in Valais, Switzerland. The largest in situ measurement campaign, conducted at Ngozumpa and Khumbu glaciers in Khumbu Himalaya, Nepal assessed snow, ice, various dust and debris types.

Overall, a total of 106 supraglacial snow, ice and debris samples were collected as follows: 8 snow samples from Grønfjordbreen in April 2009 and 2 ice samples from Aldegondabreen in western Svalbard in July 2009; 7 snow and ice samples from Jostedalsbreen and Bødalsbreen in southern Norway in June 2009; 18 snow and ice, and 22 debris samples from Ngozumpa and Khumbu glaciers in Nepal in November 2009 and December 2009; and 9 snow samples from New Zealand's Mt. Ruapehu Paretaetaitonga, Whakapapa and Whangaehu glaciers in August 2009 and 2 ice and 2 debris samples from Mangatoetoenui glacier in March 2010, and 6 ice and 30 debris samples from Findelengletscher and Zmuttgletscher in Valais, Switzerland in September and October 2010. (Note, the Svalbard 8 snow samples were collected by Dr. Rune Solberg in conjunction with snow field spectra, and 2 ice samples were collected by Øivind Due Trier. The Mt. Ruapehu Mangatoetoenui glacier 4 summer snow and debris samples were collected by Dr. Harry Keys.) Certainly more extensive sampling could have yielded data that could be used to more rigorously define regional influences. Yet, a first-order, synoptic analysis of surface glacier variability in these regions is presented by this work.

Preparation for trace element supraglacial snow and ice sample collection included the following: in a clean room, soaking low density polypropylene 500 mL Nalgene

bottles in an acid bath 48 hours, subsequently washing acid-soaked bottles with triple filtered deionized water, drying under laminar flow, and double bagging bottles prior to transport to the field. In the field, extreme care was taken during sample collection and treatment. Samples were collected with clean polyethylene gloves using standard trace element sampling procedures (e.g. Fitzgerald, 1999) and stored at room temperature in the dark until transported for analysis to the Norwegian Institute for Water Research in Oslo, Norway. All snow and ice samples were then nitric acid preserved and 45 mL sample subsets were extracted. A concentrated nitric acidification (Romil brand 67-69% HNO_3 assay for trace metal analysis) of 10% was conducted on snow and ice sample subsets, which were then allowed to react for 2 weeks to maximize dissolution. Trace element measurement is discussed further in Section 3.3, and **Publication II**.

Supraglacial debris samples were collected in the field in clean polyethylene bags, obtaining at least 100 grams of debris per sample, and double bagging for transport. All in situ samples were taken in duplicate. Supraglacial debris samples were analyzed for mineralogy and composition via powder XRD and XRF at the University of Oslo, Department of Geosciences. Debris samples were oven dried 2 days at 80°C, crushed to a fine powder (less than 125 μm particle size) via a vibratory ringmill. The fine powder was then prepared into XRD measurement discs and XRF sample tablets for measurement – further detailed in Section 3.3 and **Publication I**.

3.1.2 Field spectrometry

Field spectrometry derived reflective characteristics of surface materials are often used in conjunction with satellite spectral data as ground truth (e.g. Milton and others, 2009; Gleeson and others, 2010). Several field spectrometers exist, the FieldSpec Pro and FieldSpec 3 from Analytical Spectral Devices, Inc. (ASD) were used in this dissertation work. Both of these ASD FieldSpec spectrometers measure visible-to-shortwave infrared (0.35 - 2.5 μm) wavelengths, via three detectors in hyperspectral sampling steps of 1.4 nm from 0.35 - 1.05 μm and 2 nm from 1.05 - 2.5 μm (instrument characteristics further detailed in **Publication I**). In situ field spectrometry measurement techniques vary depending on research goals (e.g. Bourgeois and others, 2006; Takeuchi and Li, 2008). For this dissertation work, field spectrometry reflectance measurement methods after Hall and others (1992); Wiens and others (2002) and Takeuchi and Li (2008) among others, were used in the field and are further explained in **Publication**

I. Post-processing of spectra was conducted to remove instrument related hardware artifacts. To note, field spectrometry processing techniques remain in discussion (e.g. see Painter, 2011).

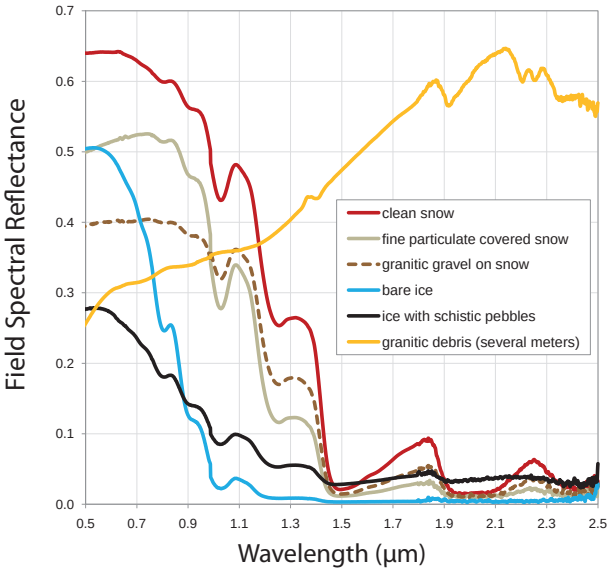

Figure 3.3: Field spectrometer collected glacier reflectance - The figure shows glacier surface reflectance as collected on the Khumbu and Ngozumpa glaciers in Nepal in November and December 2009. With increasing spatial coverage of debris, the change in glacial reflectance is demonstrated (e.g. red - snow and cyan - bare ice reflectance vs. heavy granitic debris cover - orange).

Supraglacial field spectrometry measurements were collected in Svalbard, Nepal, and Switzerland. Dr. Rune Solberg shared spectra collected at upper and lower Grønfjordbreen, Svalbard in April 2009. All other spectra were collected by the author as follows. Over 3360 spectra were collected at Ngozumpa and Khumbu glaciers in Khumbu Himalaya, Nepal in November and December 2009 (presented in **Publication I**). Over 3050 spectra were collected at Findelengletscher and Zmuttgletscher in Valais, Switzerland in September and October 2010. Contact probe spectra of supraglacial debris from Nepal, New Zealand and Switzerland were collected in laboratory conditions in November 2010, with over 2450 spectral acquisitions.

3.2 Satellite optical remote sensing of glaciers

Satellite optical remote sensing measures visible-to-thermal infrared radiance reflected and emitted from surface materials (Lillesand and others, 2004). The amount of radiance reflected and emitted from surface materials identifies targeted objects, as well as describes properties, for example, moisture content, temperature and lithologic or mineral composition (Gupta, 2003; Liang, 2004). This identification and property characterization task is done by measuring the reflective and emissive values at differing wavelengths targeted by the remote sensing spectral bands (visualized in Figure 3.4, methodology described in Section 3.2.2). Visible-to-near infrared (VNIR) reflectance has been demonstrated for differentiation snow, ice and debris (Hall and others, 1987; Paul and others, 2004a; Keshri and others, 2009). Shortwave infrared (SWIR) reflectance as well as thermal infrared (TIR) emissivity can also be used to describe supraglacial dust and debris composition. For this work, VNIR and SWIR reflective as well as TIR emissive radiance of supraglacial dust and debris was evaluated toward differentiating supraglacial dust and debris geochemical abundances.

3.2.1 Satellite multi- and hyperspectral sensors

The satellite sensors used in this study are part of the United States National Aeronautics and Space Administration (NASA) Earth Observing System (EOS) and include ALI, ASTER, Hyperion, Landsat and MODIS. Numerous other satellite sensors provide similar data, for example the European Space Agency's multispectral MERIS and hyperspectral Proba; the Indian Space Research Organization's multispectral IRS-1C/D; and the French space agency, Centre National d'Etudes Spatiales multispectral SPOT instruments. However, a great benefit of the NASA EOS data is that it is freely available by online download, with now over a decade of global data archived.

These NASA EOS hyper- and multispectral sensors acquire data in the full optical VNIR-TIR spectrum of wavelengths, with spatial resolutions ranging from 10 m - 1 km, and daily to 16-day temporal resolutions (Figure 3.4). The majority of the NASA EOS sensors listed are multispectral, that is to say they measure discrete VNIR-TIR spectral bands; Hyperion is the sole hyperspectral instrument, with 220 calibrated, discrete VNIR-SWIR spectral bands.

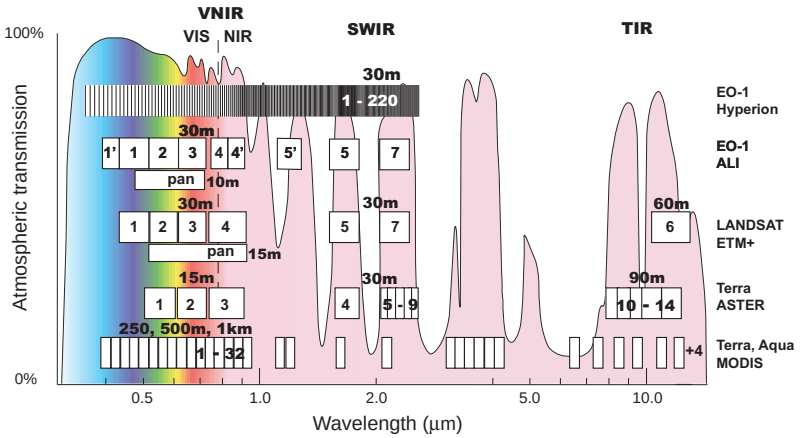

Figure 3.4: Satellite sensor spectral coverage - Hyper- and multispectral band coverage of NASA EOS satellite instruments used in this work are displayed with regard to atmospheric transmission. The spectral sensors take advantage of wavelengths free from water vapor, oxygen and carbon dioxide atmospheric absorption in order to measure reflective and emissive characteristics of surface materials.

An extensive description of the NASA EOS hyper- and multispectral sensors is given in **Publication I**. A short summary of sensor specifications follows. The Landsat Earth observing satellite program began in 1972 and has consisted of a several instruments over the past three decades: Landsat 1,2,3,4 - Multispectral Scanner System (MSS), Landsat 4, 5 - Thematic Mapper (TM), and Landsat 7 - Enhanced Thematic Mapper Plus (ETM+). Landsat 5 TM and Landsat 7 ETM+ continue to collect data at the date of this publication – with TM collecting 7 and ETM+ collecting 8 VNIR-TIR spectral bands at 15 - 60 m spatial resolution and 16-day temporal resolution. ASTER was launched onboard Terra in late 1999, and measures 14 VNIR-TIR bands at 15 to 90 m spatial resolutions and 16-day temporal resolution. Intended particularly for spectral studies (Abrams, 2000), ASTER's spectral coverage in SWIR and TIR is unprecedented via satellite instrumentation. Unfortunately, after nine years of operation, in April 2008, the SWIR bands began to fail and are no longer suitable for geologic analysis. To note, SWIR data from 2000 to 2008 are usable and VNIR and TIR bands continue to function well at the date of this publication. The ASTER SWIR and TIR spectral resolution was key to this dissertation and methods using this data are discussed in the following

section, as well as in **Publications I** and **III**. MODIS instruments are onboard both Terra and Aqua satellites, and each offer daily temporal resolution, meaning that most areas on Earth are imaged by MODIS more than once per day. The spatial resolution of MODIS is coarser than the other sensors discussed, with 250 m - 1 km spatial resolution, yet proves well suited to larger glaciers, ice caps (as demonstrated in **Publication III**), and the Greenland and Antarctic ice sheets. A total of 36 VNIR-TIR spectral bands are acquired by MODIS, offering the greatest SWIR and TIR spectral resolution behind ASTER. Finally, NASA's EO-1 satellite was launched in 2000 as a a technological demonstration and validation mission and operates on a 16-day repeat cycle (however does not acquire data continuously). EO-1 carries Hyperion and ALI (Advanced Land Imager): Hyperion acquires 242 VNIR-SWIR spectral bands at 30 m spatial resolution (220 bands of which are calibrated due to low response of detectors in non-calibrated bands), and ALI acquires one 10 m spatial resolution panchromatic band and 9 VNIR-SWIR bands at 30 m spatial resolution.

3.2.2 Methods for utilizing reflective and emissive data to describe glaciers

Often the first step in working with satellite VNIR-TIR spectral data is converting instrumental digital numbers to at-sensor radiance using sensor- and band-specific calibration settings (e.g.: gain, offset, solar irradiance). For calculation of satellite reflectance, at-sensor radiance is converted to at-sensor (top of atmosphere) planetary reflectance for each band after Markham and Barker (1986) (Equation 3.1).

$$\rho_p = \frac{(\pi \times L_\lambda \times d^2)}{(ESUN_\lambda \times \cos\theta_s)} \tag{3.1}$$

Where ρ_p is at-sensor planetary reflectance,
L_λ is at-sensor radiance,
d is the Earth-Sun distance,
$ESUN_\lambda$ is mean solar exoatmospheric irradiance,
θ_s is solar zenith angle.

For glacier surfaces, planetary reflectance (Hall and others, 1987; Keshri and others, 2009) or at-sensor radiance (Paul and others, 2004a) can be used to differentiate snow, ice and debris. However, planetary reflectance can vary from surface reflectance due to

absorption of gases and/or scattering effects of aerosols and gases in the atmosphere (Tanre and others, 1990). For example, at-satellite reflectance of Forbindels glacier in Greenland was found to be 5-17% higher after atmospheric corrections were applied to Landsat TM data (Hall and others, 1990). Over Bødalsbreen outlet glacier and Jostedalsbreen ice field in southern Norway, MODIS planetary reflectance vs. ASTER surface reflectance was similarly found to vary approximately 5-20% in VNIR (see **Abstract i**, Auxiliary material, Figure 4.2). Atmospheric correction for surface reflectance – especially over snow and ice – remains in development (Kaufman, 1989; Lu and others, 2002; Stamnes and others, 2004; Mars and Rowan, 2010). Another consideration in using planetary reflectance is variability due to the bidirectional reflectance factor (BRDF) topographic illumination influences (Nicodemus and others, 1977), especially in mountainous terrain (Sandmeier, 1995). For these reasons, atmospheric and BRDF corrections applied in validated satellite data products (e.g. ASTER AST_07XT 'VNIR & Crosstalk Corrected SWIR On Demand Surface Reflectance' (Thome and others, 1999); MODIS MOD09GA 'Daily L2G Global 500m Surface Reflectance' (Vermote and others, 2011) and Landsat derived surface temperature (atmospheric correction after Barsi and others, 2005) were used in this study. (Note, the following processing parameters for AST_07XT were chosen when ordering data: NCEP TOVS Daily Ozone for column ozone and GDAS0ZFH - NOAA/NCEP GDAS model at 6 hours, 1 degree resolution for moisture, temperature and pressure variables. Further, the MOD09GA product, gives a reflectance accuracy estimate of $+/-(0.005 + 0.05$ x reflectance) (Vermote and others, 2011).)

Reflectance data is used in spectral angle relational analysis (e.g. Kruse and others, 1993) (**Publications I**, **III**) and can be used to set classification thresholds (**Publication III**). SWIR radiance and TIR emissivity data were used to estimate mineral abundances of supraglacial debris after Ninomiya (2004). The calculations of SWIR estimated calcite, layered silicate, hydroxyl-bearing and alunite abundances and TIR estimated carbonate, quartz and mafic abundances are given in Equations 3.2– 3.8. These mineral abundance indices were calculated for Khumbu Himalayan supraglacial debris and are explained in detail in **Publication I**, and also visualized in **Abstract i**, Auxiliary material, Figure 4.3. Supraglacial mineral indicies can be used to inspect kinematics. For instance, a silicate SWIR mineral index was utilized on Ngozumpa

glacier to reveal previous glacial surges (**Publication I**, Figure 10).

$$CA = \frac{(AST6 \times AST9)}{(AST8^2)} \tag{3.2}$$

$$LS = \frac{(AST4 \times AST8)}{(AST5 \times AST6)} \tag{3.3}$$

$$OH = \frac{(AST4 \times AST7)}{(AST6^2)} \tag{3.4}$$

$$AL = \frac{(AST7^2)}{(AST5 \times AST8)} \tag{3.5}$$

$$CI = \frac{(AST13)}{(AST14)} \tag{3.6}$$

$$QI = \frac{(AST11^2)}{(AST10 \times AST12)} \tag{3.7}$$

$$MI = \frac{(AST12 \times AST14^3)}{(AST13^4)} \tag{3.8}$$

Where CA corresponds to calcite, LS corresponds to layered silicate, OH corresponds to hydroxyl-bearing, AL corresponds to alunite, CI corresponds to carbonate, QI corresponds to quartz and MI corresponds to mafic mineral abundances and ASTn corresponds to ASTER spectral band number n.

Another method used for calculation of supraglacial dust and debris geochemical composition is silica weight percent estimation (after Hook and others, 1992; Miyatake, 2000; Watanabe and Matsuo, 2003) (Equation 3.9 after Watanabe and Matsuo (2003)).

$$\mathrm{SiO_2} = 56.20 - 271.09 \times Log\left[\frac{(ASTe10 + ASTe11 + ASTe12)}{(3 \times ASTe13)}\right] \tag{3.9}$$

Where $\mathrm{SiO_2}$ is silica weight percent,
ASTen corresponds to ASTER AST_05 surface emissivity product band number n.

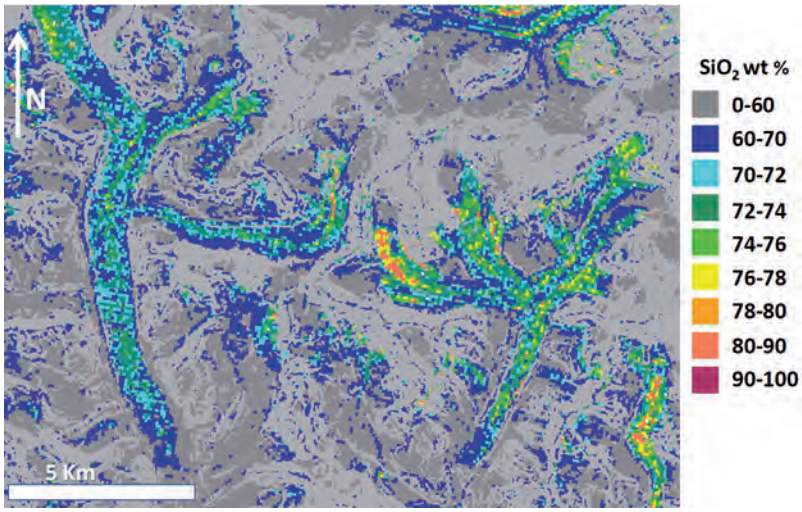

Figure 3.5: TIR estimated silica weight percent - The figure displays a thematic map of silica weight percent in the Khumbu Himalaya region. The Ngozumpa glacier (left) and Khumbu glacier (right) are delineated by the higher silica weight percent than most surrounding terrain. A digital elevation model derived slope mask of 35-90 degrees was applied to remove areas of high silica due to surrounding extreme terrain and active rock fall.

The silica weight percent calculation utilizes Si to O bonding variability of silicate minerals, specifically low (8-10 μm) absorption for mafic silicates (e.g. basalt) and higher (8-10 μm) absorption for felsic silicates (e.g. granite). TIR satellite estimated SiO_2 weight percent was calculated via ASTER emissive data (AST_05) in four study regions in **Publication III**, with silicate poor volcanic study regions displaying lower SiO_2 weight percent than continental silicate rich glacier debris study regions. As noted in Hook and others (2005), TIR SiO_2 estimates can be regionally fine tuned for greater accuracy – finding 2-7% improved accuracy with use of extensive field data.

The silica content mapping of supraglacial debris covered glacier areas may potentially provide a first order look at glacial activity, sediment transport, weathering processes, and/or glacial erosion. As shown in the silica percent thematic mapping of the Khumbu Himalaya region (Figure 3.5 and **Publications I** and **III**), the method may be useful in evaluating debris covered ice extent especially if used in conjunction with vegetation and digital elevation model calculated slope data. Region specific silica thresholds can be chosen, for example in **Publication I** 60% is chosen after total continental crust abundance (Rudnick and Gao, 2003). Supraglacial TIR SiO_2 estimates are due to innate silica properties of debris mineralogy, as well as due to diagenesis and lithology (e.g. grain size). For example, down Khumbu glacier areas of higher velocity and smaller grain sizes have the highest silica weight percents (Figure 3.5).

Further, surface temperature can be calculated from TIR data. Supraglacial temperatures were calculated over Khumbu Himalayan debris covered glaciers in **Publications I** and dust and debris covered ice in Iceland, Khumbu Himalayas, Swiss Alps and New Zealand in **Publication III**. Validated surface temperature data products provided by ASTER (AST_08 Surface Kinetic Temperature data product) and MODIS (MOD11_L2 Land Surface Temperature & Emissivity data product) were used along with Landsat TM and ETM+ thermal bands. Landsat TM and ETM+ thermal bands can be utilized to calculate surface temperature after Barsi and others (2005), procedure detailed in Hall and others (2008), used in **Publications I** and **III**. For this work, a 'dirty ice' emissivity value of 0.96 (from Qunzhu and others, 1985) was used for supraglacial dust and debris surface temperature calculation. Equation 3.10 denotes the at-sensor TIR radiance measured (for given wavelength) and its relation to surface temperature (for further description, see: Hall and others, 2008; Hook and others, 2007;

Barsi and others, 2005).

$$L_\lambda = [\varepsilon_\lambda \times L_{bb\lambda}(T) + (1 - \varepsilon_\lambda) \times L_{d\lambda}] \times \tau_\lambda + L_{u\lambda} \tag{3.10}$$

Where L_λ is at-sensor radiance at wavelength λ,
ε_λ is surface emissivity at wavelength λ,
$L_{bb\lambda}(T)$ is spectral radiance from a blackbody at surface temperature T,
$L_{d\lambda}$ is spectral downwelling radiance incident upon the surface from the atmosphere (also known as sky radiance),
τ_λ is spectral atmospheric transmission (transmittance), and
$L_{u\lambda}$ path radiance (the spectral upwelling radiance from atmospheric emission and scattering that reaches the sensor).

Other methods for qualitative reflectance analysis include true and false color composites. True and false color three spectral band based image composites can be used to quickly and simply visualize surface properties. Kääb (2005) utilized a SWIR and TIR false color composite of Hispar glacier in Karakorum, Pakistan to display surface lithology and geologic differences of supraglacial debris. As shown in **Publications I** and **III**, supraglacial debris compositional variations can be quickly visualized by SWIR/TIR false color composites. For example, the Khumbu glacier SWIR/TIR false color composite in Figure 2.4 differentiates schistic debris from granitic debris.

As an experimental technological demonstration sensor, Hyperion proves promising for spectral analysis of mineralogy and lithology (e.g. Griffin and others, 2005; Gleeson and others, 2010). Yet, the sensor is hindered by relatively low signal-to-noise ratios of approximately 50:1, compared with 500:1 for airborne hyperspectral imaging (Pearlman and others, 2003; Kruse and others, 2003) and the so-called 'smile' or spectral curvature effect (Dadon and others, 2010). Crude explorations of Hyperion at-sensor reflectance supraglacial dust and debris differentiation are shown in **Publications I** and **III**; work continues toward atmospherically corrected Hyperion supraglacial debris reflectance evaluation.

3.3 Analytical geochemistry of glacial samples

As detailed in Sections 1 and 2, many factors influence supraglacial geochemical composition (e.g. geology of accumulation zone or lateral surroundings, deposition of atmospherically transported particulates) and this geochemical composition can be measured to identify surrounding geologic contributions to glacial debris, to indicate weathering factors (e.g. high pH) or to signal provenance of atmospherically transported particulates. In order to accurately interpret such analytical geochemical results, use of known geologic information from the sample collection region is essential.

In this study, analytical geochemical techniques were use to measure glacial ice, snow, and surface debris sample elemental abundances and mineralogy. Supraglacial snow, ice and debris samples were collected as detailed in Section 3.1 and **Publications I** and **II**. Inductively coupled plasma mass spectrometry (ICP-MS) was used to measure trace element concentrations of snow and ice samples, while glacier debris samples were measured via X-ray diffraction (XRD) and X-ray fluorescence spectroscopy (XRF) to indicate mineralogic composition as well as quantify bulk oxide and elemental abundances. These techniques and the evaluation methods and potential error sources are covered in the following sections.

3.3.1 Inductively coupled plasma mass spectrometry

Inductively coupled plasma mass spectrometry is a key measurement technique for trace elemental presence and concentration. High resolution ICP-MS can determine very low part per billion or trillion concentrations for multiple elements simultaneously. For measurement, samples are acid dissolved (in solution) and subsequently vaporized by induction into a magnetic field. Characteristic emissions of light photons from atoms are measured by the mass spectrometry detector to determine elemental presence and concentration (Battey and Pring, 1997).

In this study, a Thermo Finnigan Element 2 high resolution ICP-MS was utilized for trace element measurement (sample collection and preparation discussed in Section 3.1 and **Publication II**). Using high resolution ICP-MS analysis we measured the following major elements: Na, Mg, Al, Si, S, K, and Ca; trace elements: Ti, V, Cr, Mn, Fe, Co, Ni, Cu, Zn, As, Rb, Zr, Mo, Cd, Sn, Sb, Cs, Ba, Tl, Pb, Bi, U; and rare earth elements (REE): La, Ce, Pr, Nd, Sm, Eu, Gd, Tb, Dy, Ho, Er, Tm, Yb, and Lu. The solubility of

these 43 elements (with regard to natural water) is shown in Figure 2.2. The elemental abundances of the supraglacial snow and ice samples are presented and evaluated in **Publication II**.

Inductively coupled plasma mass spectrometry laser ablation (ICP-MS-LA) is another technique which could be utilized in debris characterization. Instead of analyzing concentrations from solution, in ICP-MS-LA, a solid is vaporized by a laser ablator for elemental concentration measurement. Thus, this method is quite suitable to analysis of supraglacial debris when trace elemental abundances are required (e.g., see Risheng and others, 2003). This technique was not available, therefore, not utilized in this dissertation work.

3.3.2 X-ray diffraction and X-ray fluorescence spectroscopy

Both XRD and XRF are versatile, well-established analytical methods capable of simultaneously detecting a range of minerals (XRD) or elements and oxide compounds (XRF) in single measurements. For both techniques, X-rays are fired at samples. XRD utilizes the resultant deflection patterns to indicate of mineral structures present in the analyzed solid. In XRF, X-rays are fired at the sample in order to ionize atoms and measure characteristic emission fluorescence, and identify elemental composition. XRD can be used to determine the mineralogy of glacial dust and debris (Follmi and others, 2009; Gleeson and others, 2010; Bockheim, 2011), while XRF can be used to quantitatively measure bulk oxide weight percent and trace elemental abundances of glacial dust and debris. XRD and XRF together give an idea of both the mineral composition as well as the specific oxide compounds and trace element abundances found in the supraglacial sediment from the distinct glacier study locations.

In this work, glacial debris samples (collection and preparation discussed in Section 3.1 and **Publication I**) were assessed via powder XRD on a Philips XPERT diffractometer. Mineral components were identified via use of PANalytical's X'pert Highscore software, and dominant mineralogy was determined by semi-quantitative peak area (height x full width at half maximum) weight factor estimates (Moore D.M., 1997) and full pattern modeling (e.g. Chipera and Bish, 2002). Glacier debris samples were also measured on a Philips PW2400 XRF spectrometer run via SuperQ Version 3 software in TRACES 7B mode. The following oxide compounds and trace elements were measured: SiO_2, Al_2O_3, Fe_2O_3, MnO, MgO, CaO, Na_2O, K_2O, TiO_2, P_2O_5, and

V, Co, Zn, Rb, Pb, Sr, Y, Zr, Nb, Th, U, Ba, S. The accuracy of XRF results was 98% based on calibration data. XRD and XRF results are presented in **Publications I**, **II**, and **III**. XRD and XRF measurements along with field collected spectra (and spectral library references) provide greater confidence of supraglacial debris mineralogy and composition determinations.

3.3.3 Use of geochemical data for inspection of glacier characteristics

Several comparison methods can be used for inspecting analytical geochemistry composition results. The methods evaluated in this dissertation included reference to geochemical standards (e.g. upper continental crustal abundances), trace and REE signatures, enrichment factors and element abundance ratios. Geochemical standards provide reference elemental abundances to assess relative enrichment or depletion of inspected samples. For the purposes of this study, glacier snow and ice samples were referenced to upper continental crust (UCC) composition (after McLennan, 2001). The UCC composition can be used to compare elemental abundances found from diverse sample sets (e.g. distinct glacier study regions) to naturally found abundances (as opposed to anthropogenic influences).

Often trace and REE abundances are expressed normalized to a geochemical reference standard in a signature or spider diagram format (e.g. see **Publication II**, Figures 3 and 5). Spider diagrams visualize this element by element relative abundance and can also be used to identify, for example, classes of elements (e.g. transition metals or heavy rare earth elements HREE) and further speculate on environmental factors (e.g. pH, solubility) or enrichment sources.

An enrichment factor (EF) is used to evaluate elemental abundances relative to a standard. Calculation of relative environmental enrichment via the EF provides a simple, robust means to evaluate the abundance of an element in a sample compared to a known reference material such as upper continental crust and differentiate enrichment sources (Equation 3.11) (e.g. Kellerhals and others, 2010).

$$EF_x = \frac{(X/Ref)_{sample}}{(X/Ref)_{STD}} \tag{3.11}$$

Where EFx corresponds to the enrichment factor of element x,
X is the concentration of the element to be measured,
Ref is the concentration of the reference element,
sample indicates the concentration ratio of the sample,
and *STD* indicates the concentration ratio of the standard material chosen
(e.g. UCC).

An EF greater than 5 indicates significant enrichment of an element relative to the standard chosen. The EF significance threshold accounts for variability that can exist within the standard reference material chosen (e.g. crustal variability in UCC) or variability in mineralogy, solubility or atmospheric transport factors of the enrichment sources evaluated. The chemical composition of the enrichment sources must also be considered when using EF values. For example, in assessing enrichment sources such as mineral dust, volcanic or coal combustion emissions, if the geochemical abundances of the potential enrichment sources are similar, EF's must be used in conjunction with another technique to pinpoint the enrichment source (e.g. Correia and others, 2003; Xie and others, 2006).

Element abundance ratios are another means to inspect relative abundances (e.g. see **Publication II**, Figure 4). Comparison of ratio values can suggest different sources of inspected materials (e.g. Kreutz and Sholkovitz, 2000). Further, element abundance ratios can be expressed in bivariate plots where elemental ratios are inspected for correlation (e.g. Fortner, 2008). The above discussed geochemical comparison methods are further detailed and utilized in **Publication II**.

XRD measured mineralogy can be compared with other field, geochemical or remotely sensed mineral detection methods, (e.g. surface or satellite spectral VNIR-SWIR reflectance). XRF determined composition is amenable to comparison via spider diagrams, enrichment factors or element abundance ratios as discussed above. Additionally, XRF measured silica abundance was used in this dissertation to compare with silica weight percent calculated from satellite emissivity data (discussed Section 3.2.2). XRF measured transition metal abundances were also used with VNIR-SWIR spectral reflectance suggested transition metal presence. These XRD and XRF comparison principals and the XRD, XRF measured supraglacial debris composition results are used in **Publications I** and **III**.

3.3.4 Sources of analytical error

Sources of error in analytical methods can be introduced either in preparation of sampling material, while sampling or transporting samples, or in analytical techniques. Contamination of samples is possible when preparing sampling equipment or during field collection (e.g. sampling next to a contamination source). Samples can also be susceptible to contamination during transport, for example if dislodged from packaging, punctured or expanded in the presence of contaminants during transport. In analytical techniques, during preparation of samples for measurement, contamination can occur if there is mixing with residue from other materials in grinding or sorting prior to analytical measurement.

Calibration of instrumentation can also be a source of error or reduced accuracy or precision in geochemical sample results. In the analytical geochemistry methods presented, instruments were calibrated against known geochemical standard reference materials (e.g. XRF calibrated to several Govindaraju, 1994, standards). Calibration curves based on the measurement of geochemical reference standards are then used to determine sample results. Therefore, the accuracy and precision of sample measurements is dependant on the accuracy and precision of standard reference material measurements. Systematic errors or element contaminations are possible, and can be passed on to sample measurement results.

In situ collection as well as analytical geochemical preparation, sample measurement and data processing techniques used in this work aimed to reduce potential error sources to the greatest degree possible. Expected accuracy, instrumental limits of detection, and other limitations, were presented when detailing methods and publishing results in **Publications I**, **II** and **III**.

4

Summary of research

4.1 Extended Abstract i

K. A. Casey. Proposed methodology for detection of geochemical species on glaciers, In: Proceedings of 10th Biennial Meeting of the Society for Geology Applied to Mineral Deposits (SGA), 16-22 August 2009. Townsville, Australia.

Data: Multispectral satellite, in situ spectral data.
Study areas: Glaciers in Svalbard, southern Norway and Nepal.
Methods: VNIR-SWIR reflectance, TIR emissivity, band ratios.

Background scientific theories and proposed spectral and analytical geochemistry methods toward conducting spectral investigations on glacial dust and debris cover were presented to the geological community for peer review. Use of visible-to-shortwave infrared satellite and in situ reflectance and the wavelengths envisioned for element and mineral detection were discussed. The study evaluated glacier reflectance data in three regions – Svalbard, southern Norway and Khumbu Himalaya, Nepal. Field spectrometry collected at upper and lower Grønfjordbreen glacier in Svalbard in April 2009 was converted to reflectance and compared with atmospherically corrected multispectral satellite data from ASTER and MODIS (Auxiliary material, Figure 4.1). A comparison of satellite-derived planetary reflectance vs. surface reflectance was conducted over Bødalsbreen glacier and Jostedalsbreen ice field in southern Norway. Dust covered blue ice reflectance on Bødalsbreen was compared with dust covered firn on Jostedalsbreen ice field, showing an increase in overall VNIR-SWIR reflectance from ice to firn, yet similarity in SWIR ice and snow reflectance – hinting at the geologic signature of the region. This analysis also highlighted the significance of atmospheric correction (Auxiliary material, Figure 4.2). ASTER satellite shortwave infrared band ratio mineral indicies were calculated for Ngozumpa glacier in Khumbu Himalaya, Nepal and demonstrated marked supraglacial granite, calcite and hydroxide mineral abundance variability – suggesting that mineral abundances can be detected on debris covered glaciers (Auxiliary material, Figure 4.3). Envisioned spectral and temporal coverage limitations and bandwidth assumptions for spectral supraglacial mineralogy analysis were discussed. Analysis of in situ spectral reflectance and satellite multi-spectral reflectance in Svalbard, southern Norway and Khumbu Himalaya, Nepal aimed at testing

supraglacial dust and debris differentiation methods and yielded promising preliminary results. Supraglacial reflectance at the three study sites demonstrated clear differences, potentially attributable to geochemical supraglacial compositions. The study also revealed the importance of hyperspectral resolution data for spectral differentiation of mineralogy Figures 4.1, 4.2 as well as the importance of in situ sample collection for use as ground truth to satellite data.

4.1.1 Auxiliary material

The following section includes material not included in the published version, but discussed above and relevant to the dissertation analysis.

Field spectrometry and multispectral satellite comparison of soot affected glacier, Svalbard

Svalbard collected field spectrometry was compared with MODIS and ASTER satellite reflectance. Inorganic species present on these Arctic Svalbard glaciers result from long range atmospheric transport as well as local pollution sources. Grønfjordbreen is located approximately 10 km from a coal mine, therefore influenced almost directly by a distinct pollution source (see Figure 4.1). The field and satellite spectral analysis investigated the capability of fine scale pollution to glacier surfaces. In situ VNIR-SWIR glacier surface spectra were acquired with a FieldSpec Pro on the 17th and 18th of April 2009 at two sites (lower and upper glacier sites marked in Figure 4.1) on Grønfjordbreen in Svalbard. ASTER AST_07XT surface reflectance data from 30 April 2008 and MODIS MOD09GA reflectance data (17 April 2009) was used for satellite derived surface reflectance comparison. The study results highlighted the necessity of hyperspectral resolution for fine scale component analysis, as well as provided a preliminary data set to model future supraglacial dust and debris comparisons and in situ campaigns.

Planetary vs. surface reflectance multispectral comparison

Top of atmosphere planetary MODIS L1B derived reflectance (Equation 3.1) vs. atmospherically corrected surface reflectance from (ASTER AST_07XT) satellite data was analyzed for Bødalsbreen glacier and Jostedalsbreen ice field in southern Norway. MODIS planetary reflectance can be seen to be approximately 5-20% lower than surface

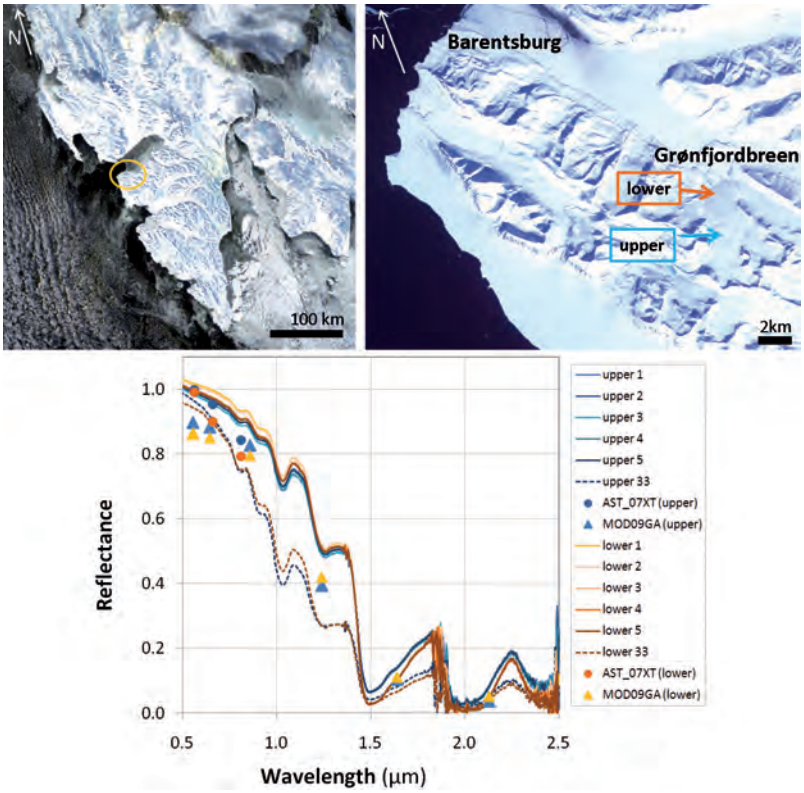

Figure 4.1: Field and satellite surface reflectance comparison, Svalbard - The MODIS (upper left image – acquired coincident with in situ spectra collection on 17 April 2009) and ASTER (upper right image – acquired 10 May 2003) detail the study areas. Note the coal mine soot deposition clearly visible around Barentsburg settlement, less than 10 km from the study glaciers. In situ spectral reflectance, MODIS MOD09GA (500 m) and ASTER AST_07XT (15 m VNIR) surface reflectance measurements are shown in the plot, yielding general agreement and highlighting the importance of hyperspectral data for compositional identification.

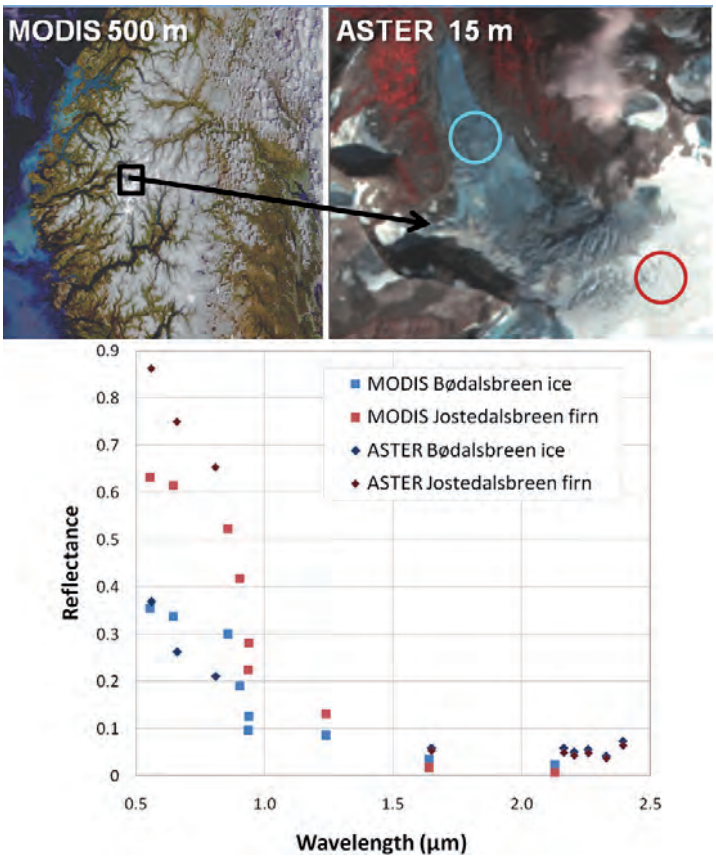

Figure 4.2: Southern Norway multispectral satellite reflectance - The upper left 500 m MODIS and upper right 15 m ASTER images locate the southern Norway Jostedalsbreen ice field and Bødalsbreen outlet glacier. MODIS L1B top of atmosphere planetary reflectance and ASTER AST_07XT surface reflectance was evaluated for Bødalsbreen ice (cyan circle) and Jostedalsbreen firn (red circle).

reflectance in VNIR bands, and nearly similar in SWIR bands.

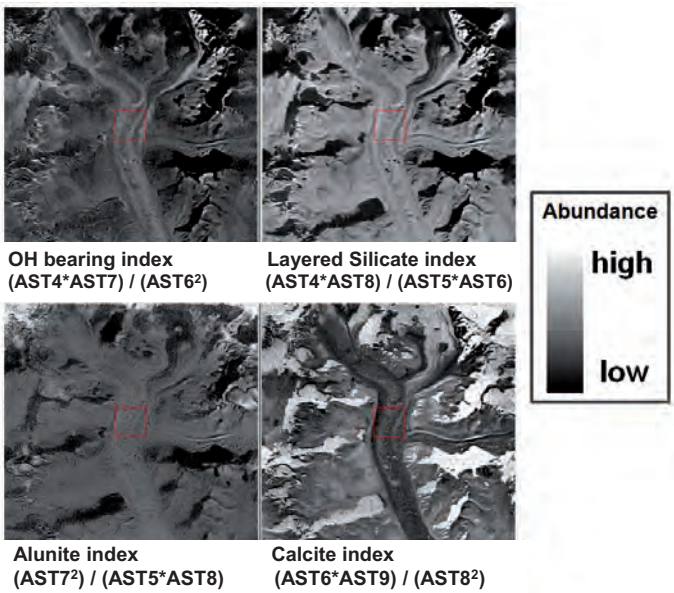

Figure 4.3: Mineral abundances on Ngozumpa glacier, Nepal - Satellite derived mineral abundances at Ngozumpa glacier, Khumbu Himalaya, Nepal. Clockwise from the top left, the mineral abundances estimated include: hydroxide-bearing, kaolinite, calcite and alunite (after Ninomiya, 2004). The mineral indices use ASTER SWIR radiance data with 30 m spatial resolution, scene date 29 November 2005 (North is toward the top of the scene).

Shortwave infrared mineral indices over heavy supraglacial debris, Nepal

Shortwave infrared mineral indices (after Ninomiya, 2004) were evaluated at heavily debris covered Ngozumpa glacier, in Khumbu Himalaya, Nepal. Differentiation of mineralogy on debris covered glaciers was strongly suggested by the diverse abundances revealed using the mineral maps for Ngozumpa glacier Figure 4.3. Indicies are further discussed in Section 3.2.2 and used in **Publication I**, however were not published in visual form, thus were included in this section.

4.2 Publication I

K.A. Casey, A. Kääb, D.I. Benn. Characterization of glacier debris cover via in situ and optical remote sensing methods: a case study in the Khumbu Himalaya, Nepal. The Cryosphere Discussions, 5, 499-564, 2011. Revision submitted for further publication as a final paper in The Cryosphere.

Data: Hyper-, multispectral satellite, in situ spectral, and geochemical data.
Study areas: Debris-covered glaciers in Khumbu Himalaya, Nepal.
Methods: VNIR-SWIR reflectance, TIR emissivity, band ratios.

Identification of surface materials and their characteristics (e.g. moisture content, spatial distribution) is a fundamental goal of satellite Earth observations. Despite the plethora of spectral glacier data, no publication prior to this focused on glacier dust and debris lithologic and compositional description via in situ VNIR-SWIR and full optical VNIR-TIR satellite spectral analysis. ALI, ASTER, Landsat and Hyperion data were used to test visible-to-thermal infrared reflectance and emissive methods for supraglacial debris characterization at several glaciers in the Khumbu Himalaya, Nepal. Supraglacial debris properties investigated via the spectral data included reflectance variability, mineral composition, moisture content, surface temperature variability, mass flux and velocity of these debris covered glaciers.

Over 3360 in situ spectra were collected from Ngozumpa and Khumbu glaciers in November and December 2009. Glacier debris samples were collected in conjunction with spectra in three ablation study areas on both the Khumbu and Ngozumpa glaciers (Publication I, Figure 3). Samples of supraglacial debris were analyzed geochemically via XRD and XRF for elemental abundances and mineral composition. In situ spectra were converted to absolute reflectance and processed to reveal mineralogic composition, debris moisture content, and reflectance variability with differing snow, ice and surface debris types. Both the in situ spectra and the supraglacial debris geochemical composition results were utilized as ground truth for comparison with satellite multispectral observations.

Hyper- and multispectral satellite data evaluation methods included comparison of reflectance variability with in situ results, satellite based mineralogic abundance

estimations via SWIR and TIR band indices, composition analysis via spectral angle mapping, silica weight percent thematic mapping, surface temperature comparisons of differing mineral debris compositions as well as velocity and theoretical particulate transport estimations.

Successful methods for mineral identification allowed for mapping of longitudinal bands of granite- vs. schist-dominant debris on Khumbu glacier from multispectral satellite data. Hyperspectral planetary reflectance data revealed potential to resolve different supraglacial mineral compositions on Lhotse Shar and Imja glaciers. Satellite emissivity derived silica-content thematic mapping suggested use of silica thresholds for delineation of debris covered glacier extent in the Khumbu Himalaya region. Silica thresholds were speculated to be attributable to active sediment transport and weathering processes. Further, velocity maps coupled with supraglacial debris compositions indicated by false color image composites, revealed mass flux and kinetic glacial patterns In short, this publication demonstrated a variety of supraglacial debris characteristics that can be extracted via use of VNIR-TIR spectral data. Glacier debris characterization is an important parameter relevant to energy balance and surface process glaciologic investigations. The methods presented in this study provide powerful remote sensing techniques for characterizing glacier debris.

4.3 Publication II

K.A. Casey, R. Xie, O. Røyset, H. Keys. Supraglacial dust and debris geochemical variability: data from Svalbard, Norway, Nepal and New Zealand. Revision submitted to Journal of Glaciology.

Data: ICP-MS, XRD, XRF of snow, ice, debris samples.
Study areas: Glaciers in Svalbard, southern Norway, Nepal and New Zealand.
Methods: Geochemical comparisons.

Trace and rare earth element glacier surface composition data is limited in glaciologic literature. In fact, the glacier study regions reported on in this paper have a small number or no previously published in trace and rare earth element glacier data available. In situ data collection and geochemical analysis is currently the most accurate method for deriving surface glacier composition. It is also a primary tool for use in developing and validating remote sensing based surface glacier composition methods.

This manuscript provides an important synoptic observation data set of four diverse alpine glacier regions. In sum, 70 snow, ice and debris samples were collected from glaciers in Svalbard, southern Norway, Nepal and New Zealand in 2009 and 2010. Glacier snow, ice and debris samples were analyzed for geochemical composition via inductively coupled plasma mass spectrometry, X-ray diffraction, and X-ray fluorescence. We present these uniform data collection, geochemical measurement, and subsequent global supraglacial composition comparisons in the manuscript. The focus is on investigation of supraglacial composition variability and the ability to assign compositional factors to the contrasting geographic, glaciologic, and climate conditions of the different regions. Thus, the study allowed for a first-order exploration of supraglacial particulate geochemical diversity. Analytical geochemical measurement methods are also evaluated in the study. Recommendations are suggested for further in situ geochemical studies, including use of XRF over ICP-MS for higher trace elemental precision and accuracy, especially of debris samples.

Expected region specific geochemical abundances were found, for example in the Khumbu Himalayas, a significantly higher magnitude of elemental abundances, including characteristic continental dust element abundances (e.g. Ca). Maritime influences

of high Na content and solute flush out with Arctic spring were found in Svalbard snow and ice spring to summer compositions. Volcanic influence was seen in the Mt. Ruapehu glacier sample results, with high S, Cr, Mn elemental abundances. Anthropogenic influence, for example, Bi, enrichment was found in all four study regions. Additionally, significant Pb enrichment was found in southern Norway and Svalbard, and U enrichment in Nepal. Rare earth element signatures were distinct in the four study areas; and suggested that more robust follow-on studies could utilize REE's to pinpoint provenance of atmospherically deposited supraglacial particulates.

This study is limited by the relatively small observation set in each region, which prevent larger statistical or temporal analysis approaches. The data set and methods evaluated nonetheless provide important initial steps to furthering global supraglacial composition variability. This study adds supraglacial trace and rare earth elemental compositions from northern and southern hemisphere; polar, mid-latitude and near-equatorial; as well as marine, continental and volcanically influenced glaciers. The evolving field of trace and rare earth element glaciology is important to study. Implications of supraglacial composition apply toward understanding ablation, and potentially atmospheric dust flux and transport as well as hydrologic water resource and global elemental cycling.

4.4 Publication III

K.A. Casey, A. Kääb. Supraglacial dust and debris reflectance and emissivity variability, relation to geochemical composition, surface temperature and glaciologic impacts. Manuscript in preparation for submission.

Data: Hyper- and multispectral satellite, and supraglacial debris geochemical data.
Study areas: Glaciers and ice caps in Iceland, Switzerland, Nepal, New Zealand.
Methods: VNIR-TIR reflectance, emissivity comparisons.

This study focused on four regions with distinct geologic, climatic and glaciologic differences affecting supraglacial dust and debris geochemical composition. The Khumbu Himalaya supraglacial debris characterization spectral remote sensing methods explored in **Publication I** are linked with the geochemical variability analysis of supraglacial dust and debris investigated in **Publication II**, to evaluate satellite reflectance variability of glacier dust and debris in several regions of contrasting geochemical dust and debris compositions. Satellite hyper- and multispectral NASA Earth Observing System sensors ALI, ASTER, Hyperion, Landsat and MODIS were used for the variability analysis. Geochemical composition data (measured via XRD and XRF) was used for ground truth to compare with satellite derived compositions. Continental supraglacial debris study regions included Khumbu Himalaya, Nepal and Valais, Swiss Alps; and volcanically influenced supraglacial debris study regions included Iceland and Mt. Ruapheu, New Zealand. VNIR-SWIR reflectance signatures as well as TIR emissivity for calculation of silica weight percent and surface temperature were presented at each of the glacier study regions. Significant VNIR-TIR spectral differences were quantified from satellite spectral data, not only between volcanic vs. continental supraglacial debris types, but also between different continental supraglacial debris types. Reflectance supraglacial debris differentiation thresholds were suggested from the study: VNIR reflectance values above 0.2 and SWIR signatures above 0.1 up to 0.4 are indicative of continental supraglacial debris; while VNIR-SWIR reflectance below 0.2 suggests basaltic volcanic tephra glacial debris. The supraglacial continental vs. volcanic threshold reflectance values identified in this study could be used in glacier

composition focused automated or semi-automated algorithms. Transition metal abundances of Fe and Mg were found to be spectrally detectable in continental supraglacial debris satellite data (and may be possible in volcanic supraglacial debris, but were outside the scope of our volcanic study region supraglacial compositions). Higher silica content characteristic of continental vs. volcanic basaltic tephra supraglacial debris was affirmed by ASTER TIR satellite estimated silica weight percent, ranging from an average of 68% for continental vs. 57% for volcanic supraglacial debris (agreeing generally well with in situ geochemical data silica abundance values). Surface temperatures were generally found to vary in excess of 10°C due to differing spatial distributions of dust and debris glacial cover. Overall, this study suggests spectral data can be used much more broadly in glacial debris analysis applications, ranging from estimation of radiative energy balance properties, surface temperatures, as well as satellite based composition determinations.

5

Conclusions and Perspectives

Particulate flux in the Earth's atmosphere is sizeable climatologically and remains a poorly-quantified component of Earth's energy balance (Tegen and Schepanski, 2009; Hansen and Nazarenko, 2004). Atmospheric particulate flux and the predicted changes to particulate flux patterns have significant implications toward the world's glaciers and ice sheets (Petit and others, 1999; Kaspari and others, 2009). Because supraglacial particulate coverage of just part per million concentrations can reduce albedo by 5-15% percent (Warren and Wiscombe, 1980), increased atmospheric deposition of dust, in conjunction with warming climate, could lead to greater than expected glacier melt rates, increased snow and ice mass loss, and ultimately contribution to sea level rise (Paul and others, 2005; Flanner and others, 2007; Xu and others, 2009).

Recent studies have highlighted changes in spatial distribution of heavily debris covered glaciers due to changing climate (Stokes and others, 2007; Scherler and others, 2011; Mayer and others, 2011). With warming climate, the insulation provided by heavy supraglacial debris can lessen, resulting in downwasting or thinning of many glaciers (e.g. southern Himalayas), changes to mass flux patterns, increased meltwater discharge, and/or increased supraglacial melt and glacier lake outburst flood potential. The types of supraglacial debris (e.g. granitic continental or basaltic tephra) can influence these supraglacial energy balance variables and are thus important to study.

Satellite remote sensing of supraglacial dust and debris is an efficient means to monitor glacier and climate variables. The full optical spectrum, VNIR-TIR satellite characterization of supraglacial dust and debris presented in this dissertation add

powerful spaceborne techniques toward dust and debris covered glacier mapping, and achieved the following specific results:

- Geochemical supraglacial dust and debris composition was detailed in diverse geographic and glaciologic study sites including: Khumbu Himalayas, northern New Zealand, southern Norway and Svalbard. Supraglacial geochemical compositions were compared between study regions, and elemental abundances were used to indicate regional, natural and anthropogenic influences to study glaciers.

- Geochemical components in supraglacial dust and debris were identified via in situ and satellite spectral data. Transition metals and mineral groups in supraglacial dust and debris were detected via VNIR-TIR spectral reflectance and emission analysis. Semi-automated threshold classifications of large geochemical composition differences between continental debris vs. volcanic tephra may be implemented using VNIR-SWIR reflectance thresholds.

- Spaceborne supraglacial dust and debris glaciologic analysis included: quantification of surface temperature by debris type and spatial distribution, supraglacial debris silica weight percent composition estimates related to weathering and glacial activity, use of mineral indicies to reveal glacial flow, and calculation of debris-covered glacier velocities and theoretical particulate transport times to inspect with regard to mass flux and glacial kinematics.

- Glaciologic implications of differing dust and debris types were discussed, including radiative absorption factors (e.g. albedo, ablation rate), kinematics (e.g. mass flux, pulse and surge supraglacial composition evidence) and monitoring of changes in spatial distribution and compositions (e.g. relevant to atmospheric transport of dust to glaciers, changes in debris covered extent).

As reaffirmed by this work, remote sensing is an efficient means to monitor glaciers globally, and a wealth of techniques have yet to be employed in surface characterization of dust and debris. Surface glacier properties such as spatial dust and debris coverage are included on a limited basis in many regional, national and global glacier inventories, yet, this information could be key to mass or energy balance studies. For example, calculation of relative surface glacier changes over decades, can quantify not only areal

extent changes, but also albedo variability (e.g. Paul and others, 2005; Schneider and others, 2007; Racoviteanu and others, 2008; Bolch and others, 2010b). Glacier inventory data from regional studies as well as global glacier databases (e.g. World Glacier Monitoring Service and Global Land Ice Measurements from Space) are of paramount importance to understanding changes in glaciers, climate and sea level.

In addition to the Earth observing optical sensors currently in operation, the upcoming European Space Agency Sentinel-2 pair of VNIR-SWIR sensors (expected launch 2013), are especially promising for global glacier monitoring as they are designed to collect data with 10-60 m spatial resolution on 2-5 day repeat temporal scale. Such improved spatial and temporal global coverage address one of the primary limitations of current optical glacier studies – the need for greater spatial and temporal coverage as optical sensors rely on clear-skies to collect reflective data. Further, high spectral resolution – including SWIR and TIR – is strongly recommended for forthcoming sensors with regard to glacier studies.

Application of the spectral remote sensing supraglacial dust and debris methods evaluated in **Publications I** and **III** offer rich potential toward global cryospheric surface mapping. An interesting implication of different supraglacial particulate types is consideration of post-deposition solubility, viscosity, and thermal impacts of the particulates to the glacier system (e.g. mentioned with regard to Eyjafjallajökull tephra deposition and runoff in Gislason and others, 2011). **Publication II** demonstrated that more robust geochemical abundance analysis could yield more precise provenance and dust transport information at studied glaciers – this work provided method analysis toward remotely sensed supraglacial geochemical composition description. Further spaceborne description of geochemical compositions (e.g. REE rich carbonatite differentiation using ASTER presented in Mars and Rowan, 2011) and particulates (e.g. 3-D MISR modeling of volcanic ash Scollo and others, 2010) and (e.g. lidar aerosol description Winker and others, 2009) prove promising. Recent research on mass loss of Alaskan glaciers and delivery of iron rich fine-grained glacial dust to ocean (Crusius and others, 2011) could be complemented with compositional description methods presented in this dissertation. Future work could also be recommended toward investigating topographic influences on supraglacial reflectance with respect to atmospheric transport mapping and tracking as well as incorporation of more robust radiative flux estimates due to differing supraglacial dust and debris types.

5. CONCLUSIONS AND PERSPECTIVES

Overall, this study provided a fundamental step in developing spaceborne supraglacial dust and debris characterization methods to spatially map surface composition, temperature and spectral variability. Supraglacial dust and debris mapping methods were applied toward glaciologic applications investigating radiative absorption and mass flux. Spaceborne supraglacial dust and debris characterization advances glacier remote sensing capabilities on a global scale, allowing for improved quantification of glacier dust and debris on large spatial and temporal scales. This improved quantification of glacier surface characteristics could prove promising in monitoring glaciers, modeling radiative energy balance and estimating ice mass flux.

6

References

Abrams, M.J., 2000. The Advanced Spaceborne Thermal Emission and Reflection Radiometer (ASTER): data products for the high spatial resolution imager on NASA's Terra platform, *International Journal of Remote Sensing*, **21(5)**, 847–859.

Adhikary, S., M. Nakawo and K. Seko, 2000. Dust influence on the melting process of glacier ice: experimental results from Lirung Glacier, Nepal Himalayas, Nakawo, M., C.F. Raymond and A. Fountain, eds., Debris-Covered Glaciers, IAHS, Oxfordshire, UK, no. 264, 43–52.

Aizen, V.B., P.A. Mayewski, E.M. Aizen, D.R. Joswiak, A.B. Surazakov, S. Kaspari, B. Grigholm, M. Krachler, M. Handley and A. Finaev, 2009. Stable-isotope and trace element time series from Fedchenko glacier (Pamirs) snow/firn cores, *Journal of Glaciology*, **55**, 275–291.

Anderson, S.P., 2005. Glaciers show direct linkage between erosion rate and chemical weathering fluxes, *Geomorphology*, **67**(1-2), 147–157.

Andreassen, L.M., F. Paul, A. Kääb and J.E. Hausberg, 2008. The new Landsat-derived glacier inventory for Jotunheimen, Norway, and deduced glacier changes since the 1930s, *The Cryosphere*, **2**, 131–145.

Arimoto, R., 2001. Eolian dust and climate: relationships to sources, tropospheric chemistry, transport and deposition, *Earth-Science Reviews*, **54**(1-3), 29–42.

Banta, J.R., J.R. McConnell, R. Edwards and J.P. Engelbrecht, 2008. Delineation of carbonate dust, aluminous dust, and sea salt deposition in a Greenland glaciochemical array using positive matrix factorization, *Geochemistry Geophysics Geosystems*, **9**(Q07013), 19 pp.

Barbante, C., M. Schwikowski, T. Doring, H.W. Gaggeler, U. Schotterer, L. Tobler, K. Van de Velde, C. Ferrari, G. Cozzi, A. Turetta, K. Rosman, M. Bolshov, G. Capodaglio, P. Cescon and C. Boutron, 2004. Historical Record of European Emissions of Heavy Metals to the Atmosphere Since the 1650s from Alpine Snow/Ice Cores Drilled near Monte Rosa, *Environmental Science & Technology*, **38**(15), 4085–4090.

Barrie, L.A., 1985. Atmospheric particles: their physical and chemical characteristics, and deposition processes relevant to the chemical composition of glaciers, *Annals of Glaciology*, **7**, 100–108.

Barsch, D. and M. Jakob, 1998. Mass transport by active rockglaciers in the Khumbu Himalaya, *Geomorphology*, **26**(1-3), 215–222.

Barsi, J.A., J.R. Schott, F.D. Palluconi and S.J. Hook, 2005. Validation of a web-based atmospheric correction tool for single thermal band instruments, SPIE, vol. 5882.

REFERENCES

Battey, M.H. and A. Pring, 1997. Mineralogy, Addison Wesley Longman, Essex, England, 3rd ed.

Benn, D.I. and D.J.A. Evans, 2010. Glaciers and Glaciation, Hodder Education.

Benn, D.I. and L.A. Owen, 2002. Himalayan glacial sedimentary environments: a framework for reconstructing and dating the former extent of glaciers in high mountains, *Quaternary International*, **97-98**, 3–25.

Benn, D.I., S. Wiseman and C.R. Warren, 2000. Rapid growth of a supraglacial lake, Ngozumpa Glacier, Khumbu Himal, Nepal, Nakawo, M., C.F. Raymond and A. Fountain, eds., Debris-Covered Glaciers, IAHS, Oxfordshire, UK, no. 264, 177–185.

Bhatia, M., S. Das, E. Kujawinski, P. Henderson, A. Burke and M. Charette, 2011. Seasonal evolution of water source contributions to discharge from a Greenland outlet glacier: Insight from a new isotope-mixing model, Accepted, *Journal of Glaciology*, 10J234.

Bockheim, J.G., 2011. Antarctic Earth Science, Cambridge University Press, chap. Use of soils in studying the behaviour of the McMurdo ice dome, 720 pp.

Bolch, T., M. Buchroithner, T. Pieczonka and A. Kunert, 2008. Planimetric and volumetric glacier changes in the Khumbu Himal, Nepal, since 1962 using Corona, Landsat TM and ASTER data, *Journal of Glaciology*, **54**, 592–600.

Bolch, T., B. Menounos and R. Wheate, 2010a. Landsat-based inventory of glaciers in western Canada, 1985-2005, *Remote Sensing of Environment*, **114**(1), 127–137.

Bolch, T., T. Yao, S. Kang, M.F. Buchroithner, D. Scherer, F. Maussion, E. Huintjes and C. Schneider, 2010b. A glacier inventory for the western Nyainqentanglha Range and the Nam Co Basin, Tibet, and glacier changes 1976-2009, *The Cryosphere*, **4**, 419–433.

Bory, A. J.-M., P. E. Biscaye, A. M. Piotrowski and J. P. Steffensen, 2003. Regional variability of ice core dust composition and provenance in Greenland, *Geochemistry Geophysics Geosystems*, **4**(12), 1107.

Bourgeois, C. S., P. Calanca and A. Ohmura, 2006. A field study of the hemispherical directional reflectance factor and spectral albedo of dry snow, *Journal of Geophysical Research*, **111**, D20108.

Chipera, S.J. and D.L. Bish, 2002. FULLPAT: a full-pattern quantitative analysis program for X-ray powder diffraction using measured and calculated patterns, *Journal of Applied Crystallography*, **35**(6), 744–749.

Christopher, S.A., B. Johnson, T.A. Jones and J. Haywood, 2009. Vertical and spatial distribution of dust from aircraft and satellite measurements during the GERBILS field campaign, *Geophysical Research Letters*, **36**(6), L06806.

Colbeck, S.C., 1981. A simulation of the enrichment of atmospheric pollutants in snow cover runoff, *Water Resources Research*, **17**(5), 1383–1388.

Correia, A., R. Freydier, R.J. Delmas, J.C. Simões, J.D. Taupin, B. Duprè and P. Artaxo, 2003. Trace elements in South America aerosol during 20th century inferred from a Nevado Illimani ice core, Eastern Bolivian Andes (6350 m asl), *Atmospheric Chemistry & Physics*, **3**, 1337–1352.

Crusius, J., A.W. Schroth, S. Gassò, C.M. Moy, R.C. Levy and M. Gatica, 2011. Glacial flour dust storms in the Gulf of Alaska: Hydrologic and meteorological controls and their importance as a source of bioavailable iron, *Geophysical Research Letters*, **38**(6), L06602.

Cziczo, D.J., K.D. Froyd, S.J. Gallavardin, O. Moehler, S. Benz, H. Saathoff and D.M. Murphy, 2009. Deactivation of ice nuclei due to atmospherically relevant surface coatings, *Environmental Research Letters*, **4**(4), 044013.

Dadon, A., E. Ben-Dor and A. Karnieli, 2010. Use of derivative calculations and minimum noise fraction transform for detecting and correcting the spectral curvature effect (smile) in Hyperion images, *IEEE Transactions on Geoscience and Remote Sensing*, **48**(6), 2603 –2612.

Evans, S.G. and J.J. Clague, 1994. Recent climatic change and catastrophic geomorphic processes in mountain environments, *Geomorphology*, **10**(1-4), 107–128.

Ferrari, C.P., C. Padova, X. Fain, P.-A. Gauchard, A. Dommergue, K. Aspmo, T. Berg, W. Cairns, C. Barbante, P. Cescon, L. Kaleschke, A. Richter, F. Wittrock and C. Boutron, 2008. Atmospheric mercury depletion event study in Ny-Alesund (Svalbard) in spring 2005. Deposition and transformation of Hg in surface snow during springtime, *Science of The Total Environment*, **397**(1-3), 167–177.

Fitzgerald, W.F., 1999. Clean hands: Clair Patterson's crusade against environmental lead contamination, Nova Science Publ., Commack, NY.

Flanner, M.G., C.S. Zender, J.T. Randerson and P.J. Rasch, 2007. Present-day climate forcing and response from black carbon in snow, *Journal Geophysical Research*, **112**, D11202.

Follmi, K.B., K. Arn, R. Hosein, T. Adatte and P. Steinmann, 2009. Biogeochemical weathering in sedimentary chronosequences of the Rhne and Oberaar Glaciers (Swiss Alps): Rates and mechanisms of biotite weathering, *Geoderma*, **151**(3-4), 270–281.

Fort, M., 2000. Glaciers and mass wasting processes: their influence on the shaping of the Kali Gandaki valley (higher Himalaya of Nepal), *Quaternary International*, **65-66**, 101–119.

Fortner, S.K., 2008. The geochemistry of glacier snow and melt: the Oregon Cascades and the Taylor Valley, Antarctica, (PhD thesis), The Ohio State University.

Fountain, A.G., 1996. Effect of snow and firn hydrology on the physical and chemical characteristics of glacial runoff, *Hydrological Processes*, **10**(4), 509–521.

Fujii, Y., 1977. Field experiment on glacier ablation under a layer of debris cover, *Journal of the Japanese Society of Snow and Ice, Seppyo*, **39**, 20–21.

Fushimi, H., M. Yoshida, O. Watanabe and B.P. Upadhyay, 1980. Distributions and grain sizes of supraglacial debris in the Khumbu glacier, Khumbu Region, East Nepal, *Journal of the Japanese Society of Snow and Ice, Seppyo*, **42**, 18–25.

Gabrielli, P., A. Wegner, J.R. Petit, B. Delmonte, P. De Deckker, V. Gaspari, H. Fischer, U. Ruth, M. Kriews, C. Boutron, P. Cescon and C. Barbante, 2010. A major glacial-interglacial change in aeolian dust composition inferred from Rare Earth Elements in Antarctic ice, *Quaternary Science Reviews*, **29**(1-2), 265–273.

Ginot, P., C. Kull, M. Schwikowski, U. Schotterer and H.W. Gäggeler, 2001. Effects of post-depositional processes on snow composition of a subtropical glacier (Cerro Tapado, Chilean Andes), *Journal Geophysical Research*, **106**, 32375–32386.

Gislason, S. R., T. Hassenkam, S. Nedel, N. Bovet, E. S. Eiriksdottir, H. A. Alfredsson, C. P. Hem, Z. I. Balogh, K. Dideriksen, N. Oskarsson, B. Sigfusson, G. Larsen and S. L. S. Stipp, 2011. Characterization of Eyjafjallajökull volcanic ash particles and a protocol for rapid risk assessment, *Proceedings of the National Academy of Sciences*, **108**(18), 7307–7312.

Gleeson, D.F., R.T. Pappalardo, S.E. Grasby, M.S. Anderson, B. Beauchamp, R. Castaño, S.A. Chien, T. Doggett, L. Mandrake and K.L. Wagstaff, 2010. Characterization of a sulfur-rich Arctic spring site and field analog to Europa using hyperspectral data, *Remote Sensing of Environment*, **114**(6), 1297–1311.

REFERENCES

Govindaraju, K., 1994. 1994 compilation of working values and sample description for 383 geostandards, *Geostandards Newsletter*, **18**(S1), 1–158.

Griffin, M.K., S.M. Hsu, H.K. Burke, S.M. Orloff and C.A. Upham, 2005. Examples of EO-1Hyperion data analysis, *Lincoln Laboratory Journal*, **15**(2), 271–298.

Gruber, S. and M. Hoelzle, 2001. Statistical modelling of mountain permafrost distribution: local calibration and incorporation of remotely sensed data, *Permafrost Periglacial Processes*, **12**, 69–77.

Gudmundsson, S., E. Magnússon, H. Björnsson, F. Pálsson, M.T. Gudmundsson, D. Högnadóttir, E. Berthier, T. Jóhannesson, O. Sigurdsson, D. Dorsteinsson and J. Dall, 2010. Volume and mass balance changes of ice caps in Iceland deduced from elevation data and in-situ mass balance observations, The SPOT image project Planet Action and the SPIRIT International Polar Year project.

Gulley, J. and D.I. Benn, 2007. Structural control of englacial drainage systems in Himalayan debris-covered glaciers, *Journal of Glaciology*, **53**(182), 399–412.

Gupta, R.P., 2003. Remote Sensing Geology, Springer, 2nd ed.

Hagen, J.O., O. Liestol, E. Roland and T. Jorgensen, 1993. Glacier Atlas of Svalbard and Jan Mayen, vol. 129, Norsk Polarinstitutt Meddelelser.

Hall, D.K., R.A. Bindschadler, J.L. Foster, A.T.C. Chang and H. Siddalingaiah, 1990. Comparison of in situ and satellite-derived reflectances of Forbindels Glacier, Greenland, *International Journal of Remote Sensing*, **11**(3), 493–504.

Hall, D.K., J.E. Box, K.A. Casey, S.J. Hook, C.A. Shuman and K. Steffen, 2008. Comparison of satellite-derived and in-situ observations of ice and snow surface temperatures over Greenland, *Remote Sensing of Environment*, **112**(10), 3739–3749.

Hall, D.K., J.L. Foster and A.T.C. Chang, 1992. Reflectance of snow measured in situ and from space in sub-Arctic areas in Canada and Alaska, *IEEE Transactions on Geoscience and Remote Sensing*, **30**(3), 634 –637.

Hall, D.K., J.P. Ormsby, R.A. Bindschadler and H. Siddalingaiah, 1987. Characterization of snow and ice reflectance zones on glaciers using Landsat thematic mapper data, *Annals of Glaciology*, **9**, 104–108.

Hambrey, M.J., D.J. Quincey, N.F. Glasser, J.M. Reynolds, S.J. Richardson and S. Clemmens, 2008. Sedimentological, geomorphological and dynamic context of debris-mantled glaciers, Mount Everest (Sagarmatha) region, Nepal, *Quaternary Science Reviews*, **27**(25-26), 2361–2389.

Hansen, J. and L. Nazarenko, 2004. Soot climate forcing via snow and ice albedos, *Proceedings of the National Academy of Sciences of the United States of America*, **101**(2), 423–428.

Harrison, S. and V. Winchester, 2000. Nineteenth- and Twentieth-Century Glacier Fluctuations and Climatic Implications in the Arco and Colonia Valleys, Hielo Patagònico Norte, Chile, *Arctic, Antarctic, and Alpine Research*, **32**(1), 55–63.

Haug, T., A. Kääb and P. Skvarca, 2010. Monitoring ice shelf velocities from repeat MODIS and Landsat data a method study on the Larsen C ice shelf, Antarctica Peninsula, and 10 other ice shelves around Antarctica, *The Cryosphere*, **4**, 161–178.

Henderson, K., A. Laube, H. Gäggeler, S. Olivier, T. Papina and M. Schwikowski, 2006. Temporal variations of accumulation and temperature during the past two centuries from Belukha ice core, Siberian Altai, *Journal of Geophysical Research*, **111**, D03104.

Hirdman, D., H. Sodemann, S. Eckhardt, J.F. Burkhart, A. Jefferson, T. Mefford, P.K. Quinn, S. Sharma, J. Ström and A. Stohl, 2010. Source identification of short-lived air pollutants in the Arctic using statistical analysis of measurement data and particle dispersion model output, *Atmospheric Chemistry & Physics*, **10**, 669–693.

Hochstein, M.P., D. Claridge, S.A. Henrys, A. Pyne, D.C. Nobes and S.F. Leary, 1995. Downwasting of the Tasman Glacier, South Island, New Zealand: Changes in the terminus region between 1971 and 1993, *New Zealand Journal of Geology and Geophysics*, **38**(1), 1–16.

Hodson, A., A.M. Anesio, M. Tranter, A. Fountain, M. Osborn, J. Priscu, J. Laybourn-Parry and B. Sattler, 2008. Glacial Ecosystems, *Ecological Monographs*, **78**(1), 41–67.

Hodson, A.J., P.N. Mumford, J. Kohler and P.M. Wynn, 2005. The High Arctic glacial ecosystem: new insights from nutrient budgets, *Biogeochemistry*, **72**(2), 233–256.

Hong, S., J.-P. Candelone, C. Turetta and C.F. Boutran, 1996. Changes in natural lead, copper, zinc and cadmium concentrations in central Greenland ice from 8250 to 149,100 years ago: Their association with climatic changes and resultant variations of dominant source contributions, *Earth and Planetary Science Letters*, **143**(1-4), 233–244.

Hook, S.J., J.E. Dmochowski, K.A. Howard, L.C. Rowan, K.E. Karlstrom and J.M. Stock, 2005. Mapping variations in weight percent silica measured from multispectral thermal infrared imagery – Examples from the Hiller Mountains, Nevada, USA and Tres Virgenes-La Reforma, Baja California Sur, Mexico, *Remote Sensing of Environment*, **95**(3), 273–289.

Hook, S.J., A.R. Gabell, A.A. Green and P.S. Kealy, 1992. A comparison of techniques for extracting emissivity information from thermal infrared data for geologic studies, *Remote Sensing of Environment*, **42**(2), 123–135.

Hook, S.J., R.G. Vaughan, H. Tonooka and S.G. Schladow, 2007. Absolute radiometric in-flight validation of mid infrared and thermal infrared data from ASTER and MODIS on Terra Spacecraft using the Lake Tahoe, CA/NV, USA, automated validation site, *IEEE Transactions on Geoscience and Remote Sensing*, **45**, 1798–1807.

Hu, Z. and S. Gao, 2008. Upper crustal abundances of trace elements: A revision and update, *Chemical Geology*, **253**(3-4), 205–221.

Hurst, A.W., H.M. Bibby, B.J. Scott and M.J. McGuinness, 1991. The heat source of Ruapehu crater lake; deductions from the energy and mass balances, *Journal of Volcanology and Geothermal Research*, **46**(1-2), 1–20.

Ikegawa, M., M. Kimura, K. Honda, I. Akabane, K. Makita, H. Motoyama, Y. Fujii and Y. Itokawa, 1999. Geographical variations of major and trace elements in East Antarctica, *Atmospheric Environment*, **33**(9), 1457–1467.

Isaksson, E., M. Hermanson, S. Hicks, M. Igarashi, K. Kamiyama, J. Moore, H. Motoyama, D. Muir, V. Pohjola, R. Vaikmae, R.S.W. van de Wal and O. Watanabe, 2003. Ice cores from Svalbard–useful archives of past climate and pollution history, *Physics and Chemistry of the Earth, Parts A/B/C*, **28**(28-32), 1217–1228.

Iwata, S., T. Aoki, T. Kadota, K. Seko and S. Yamaguchi, 2000. Morphological evolution of the debris cover on Khumbu Glacier, Nepal, between 1978 and 1995, Nakawo, M., C.F. Raymond and A. Fountain, eds., Debris-Covered Glaciers, IAHS, Oxfordshire, UK, no. 264, 3–11.

Kääb, A., 2005. Remote sensing of mountain glaciers and permafrost creep, vol. 48, Schriftenreihe Physische Geographie.

REFERENCES

Kääb, A., C. Huggel and L. Fischer, 2006. Remote sensing technologies for monitoring climate change impacts on glacier- and permafrost-related hazards, *ECI Conference on Geohazards*, 12pp.

Kääb, A., F. Paul, M. Maisch, M. Hoelzle and W. Haeberli, 2002. The new remote-sensing-derived Swiss glacier inventory: II. First results, *Annals of Glaciology*, **34**, 362–366.

Kang, S., C.P. Wake, Q. Dahe and P.A. Mayewski, 2000. Monsoon and dust signals recorded in Dasuopu glacier, Tibetan Plateau, *Journal of Glaciology*, **46**, 222–226.

Kargel, J., R. Furfaro, G. Kaser, G. Leonard, W. Fink, C. Huggel, A. Kääb, B. Raup, J. Reynolds, D. Wolfe and M. Zapata, 2011. ASTER imaging and analysis of glacier hazards, Springer, chap. 15, 325–373.

Kaspari, S., P.A. Mayewski, M. Handley, E. Osterberg, S. Kang, S. Sneed, S. Hou and D. Qin, 2009. Recent increases in atmospheric concentrations of Bi, U, Cs, S and Ca from a 350-year Mount Everest ice core record, *Journal Geophysical Research*, **114**(D04302), 14 pp.

Kaspari, S.D., M. Schwikowski, M. Gysel, M.G. Flanner, S. Kang, S. Hou and P.A. Mayewski, 2011. Recent increase in black carbon concentrations from a Mt. Everest ice core spanning 1860-2000 AD, *Geophysical Research Letters*, **38**, L04703.

Kaufman, Y.J., 1989. The atmospheric effect on remote sensing and its correction, Wiley, New York, chap. Theory and Application of Optical Remote Sensing, 341pp.

Kellerhals, T., L. Tobler, S. Brütsch, M. Sigl, L. Wacker, H.W. Gäggeler and M. Schwikowski, 2010. Thallium as a tracer for preindustrial volcanic eruptions in an ice core record from Illimani, Bolivia, *Environmental Science & Technology*, **44**, 888–893.

Keshri, A. K., A. Shukla and R. P. Gupta, 2009. ASTER ratio indices for supraglacial terrain mapping, *International Journal of Remote Sensing*, **30**(2), 519–524.

Kilgour, G., V. Manville, F. Della Pasqua, A. Graettinger, K.A. Hodgson and G.E. Jolly, 2010. The 25 September 2007 eruption of Mount Ruapehu, New Zealand: Directed ballistics, surtseyan jets, and ice-slurry lahars, *Journal of Volcanology and Geothermal Research*, **191**(1-2), 1–14.

Knopf, D.A., P.A. Alpert, B. Wang and J.Y. Aller, 2011. Stimulation of ice nucleation by marine diatoms, *Nature Geoscience*, **4**(2), 88–90.

Kohshima, S., K. Seko and Y. Yoshimura, 1992. Biotic Acceleration of Glacier Melting in Yala Glacier, Langtang Region, Nepal Himalaya, Snow and Glacier Hydrology, IAHS, vol. Proceedings of the Kathmandu Symposium, November 1992, 309–316.

Kok, J.F., 2011. A scaling theory for the size distribution of emitted dust aerosols suggests climate models underestimate the size of the global dust cycle, *Proceedings of the National Academy of Sciences*, **108**(3), 1016–1021.

Konrad, S.K., 1998. Possible Outburst Floods from Debris-Covered Glaciers in the Sierra Nevada, California, *Geografiska Annaler. Series A, Physical Geography*, **80**(3/4), 183–192.

Kreutz, K.J. and E.R. Sholkovitz, 2000. Major element, rare earth element, and sulfur isotopic composition of a high-elevation firn core: Sources and transport of mineral dust in central Asia, *Geochemistry Geophysics Geosystems*, **1**(11), 2000GC000082.

Kreutz, K., C. Wake, V. Aizen, L. Cecil, J. Green and H.-A. Synal, 2004. Event to Decadal-Scale Glaciochemical Variability on the Inilchek Glacier, Central Tien Shan, **9**, 61–79.

Kruse, F.A., J.W. Boardman and J.F. Huntington, 2003. Comparison of airborne hyperspectral data and EO-1 Hyperion for mineral mapping, *IEEE Transactions on Geoscience and Remote Sensing*, **41**(6), 1388–1400.

Kruse, F.A., A.B. Lefkoff, J.W. Boardman, K.B. Heidebrecht, A.T. Shapiro, P.J. Barloon and A.F.H. Goetz, 1993. The spectral image processing system (SIPS)–interactive visualization and analysis of imaging spectrometer data, *Remote Sensing of Environment*, **44**(2-3), 145–163.

Lee, K., S.D. Hur, S. Hou, S. Hong, X. Qin, J. Ren, Y. Liu, K.J.R. Rosman, C. Barbante and C.F. Boutron, 2008. Atmospheric pollution for trace elements in the remote high-altitude atmosphere in central Asia as recorded in snow from Mt. Qomolangma (Everest) of the Himalayas, *Science of The Total Environment*, **404**(1), 171–181.

Liang, S., 2004. Quantitative Remote Sensing of Land Surfaces, John Wiley & Sons, Inc., Hoboken, New Jersey, USA.

Lillesand, T.M., R.W. Kiefer and J.W. Chipman, 2004. Remote Sensing and Image Interpretation, Wiley, fifth edition ed.

Lu, D., P. Mausel, E. Brondizio and E. Moran, 2002. Assessment of atmospheric correction methods for Landsat TM data applicable to Amazon basin LBA research, *International Journal of Remote Sensing*, **23**(13), 2651–2671.

Lu, J.Y., W.H. Schroeder, L.A. Barrie, A. Steffen, H.E. Welch, K. Martin, L. Lockhart, R.V. Hunt, G. Boila and A. Richter, 2001. Magnification of atmospheric mercury deposition to polar regions in springtime: The link to tropospheric ozone depletion chemistry, *Geophysical Research Letters*, **28**(17), 3219–3222.

Mahowald, N.M., S. Engelstaedter, C. Luo, A. Sealy, P. Artaxo, C. Benitez-Nelson, S. Bonnet, Y. Chen, P.Y. Chuang, D.D. Cohen, F. Dulac, B. Herut, A.M. Johansen, N. Kubilay, R. Losno, W. Maenhaut, A. Paytan, J.M. Prospero, L.M. Shank and R.L. Siefert, 2009. Atmospheric Iron Deposition: Global Distribution, Variability, and Human Perturbations, *Annual Review Marine Science*, **1**(1), 245–278.

Maisch, M., W. Haeberli, M. Hoelzle and J. Wenzel, 1999. Occurrence of rocky and sedimentary glacier beds in the Swiss Alps as estimated from glacier-inventory data, *Annals of Glaciology*, **28**, 231–235.

Markham, B.L. and J.L. Barker, 1986. Landsat MSS and TM post-calibration dynamic ranges, exoatmospheric reflectances and at-satellite temperatures, *EOSAT Landsat Technical Notes*, **1**, 3–8.

Mars, J.C. and L.C. Rowan, 2010. Spectral assessment of new ASTER SWIR surface reflectance data products for spectroscopic mapping of rocks and minerals, *Remote Sensing of Environment*, **114**(9), 2011–2025.

Mars, J.C. and L.C. Rowan, 2011. ASTER spectral analysis and lithologic mapping of Khanneshin carbonatite volcano, Afghanistan, *Geosphere*, **7**(1), 276–289.

Marteel, A., C.F. Boutron, C. Barbante, P. Gabrielli, G. Cozzi, V. Gaspari, P. Cescon, C.P. Ferrari, A. Dommergue, K. Rosman, S. Hong and S.D. Hur, 2008. Changes in atmospheric heavy metals and metalloids in Dome C (East Antarctica) ice back to 672.0kyr BP (Marine Isotopic Stages 16.2), *Earth and Planetary Science Letters*, **272**(3-4), 579–590.

Marx, S.K., B.S. Kamber and H.A. McGowan, 2005. Provenance of long-travelled dust determined with ultra-trace-element composition: a pilot study with samples from New Zealand glaciers, *Earth Surface Processes and Landforms*, **30**(6), 699–716.

Mattson, L.E., 1990. The role of debris cover on glacial meltwater discharge, Canadian Rocky Mountains, Proceedings of the 47th Eastern Snow Conference, 237–242.

REFERENCES

Mattson, L.E., 2000. The influence of a debris cover on the mid-summer discharge of Dome glacier, Canadian Rocky Mountains, Nakawo, M., C.F. Raymond and A. Fountain, eds., Debris-Covered Glaciers, IAHS, Oxfordshire, UK, no. 264, 25–33.

Mattson, L.E., J.S. Gardner and G.J. Young, 1993. Ablation on debris covered glaciers: an example from the Rakhiot glacier, Punjab, Himalaya, Snow and Glacier Hydrology, no. 218, 289–296.

Mayer, C., A. Lambrecht, W. Hagg and Y. Narozhny, 2011. Glacial debris cover and melt water production for glaciers in the Atlay, Russia, *The Cryosphere Discussions*, **5**, 401–430.

McLennan, S.M., 2001. Relationships between the trace element composition of sedimentary rocks and upper continental crust, *Geochemistry Geophysics Geosystems*, **2**(4), 24 pp.

Mihalcea, C., C. Mayer, G. Diolaiuti, C. D'Agata and C. Smiraglia, 2008. Spatial distribution of debris thickness and melting from remote-sensing and meteorological data, at debris-covered Baltoro glacier, Karakoram, Pakistan, *Annals of Glaciology*, **48**, 49–57.

Milton, E.J., M.E. Schaepman, K. Anderson, M. Kneubühler and Nigel Fox, 2009. Progress in field spectroscopy, *Remote Sensing of Environment*, **113**(Supplement 1), S92–S109.

Miyatake, S., 2000. Technical development report: examination of indices for discriminating rocks and minerals and their universal validity, *Metal Mining Agency of Japan*, **3**, 1–31.

Moore D.M., R.C. Reynolds Jr., 1997. X-ray diffraction and the identification and analysis of clay minerals, Oxford University Press, New York, 2nd ed.

Nakawo, M., H. Yabuki and A. Sakai, 1999. Characteristics of Khumbu Glacier, Nepal Himalaya: recent changes in the debris-covered area, *Annals of Glaciology*, **28**(1), 118–122.

Nakawo, M. and G.J. Young, 1981. Field experiments to determine the effect of a debris layer on ablation of glacier ice., *Annals of Glaciology*, **2**, 85–91.

Nicholson, L. and D.I. Benn, 2006. Calculating ice melt beneath a debris layer using meteorological data, *Journal of Glaciology*, **52**(178), 463–470.

Nicodemus, F.E., J.C. Richmond, J.J. Hsia, I.W. Ginsberg and T. Limperis, 1977. Geometrical considerations and nomenclature for reflectance, *Monograph 160*, National Bureau of Standards, Washington, D.C.

Ninomiya, Y., 2004. Lithologic mapping with multispectral ASTER TIR and SWIR data, Society of Photo-Optical Instrumentation Engineers (SPIE) Conference Series, vol. 5234, 180–190.

Oerlemans, J., R.H. Giesen and M.R. van den Broeke, 2009. Retreating alpine glaciers: increased melt rates due to accumulation of dust (Vadret da Morteratsch, Switzerland), *Journal of Glaciology*, **55**(192), 729–736.

Ogilvie, I. H., 1904. The Effect of Superglacial Debris on the Advance and Retreat of Some Canadian Glaciers, *The Journal of Geology*, **12**(8), 722–743.

Olivier, S., M. Schwikowski, S. Brütsch, S. Eyrikh, H.W. Gäggeler, M. Lüthi, T. Papina, M. Saurer, U. Schotterer, L. Tobler and E. Vogel, 2003. Glaciochemical investigation of an ice core from Belukha glacier, Siberian Altai, *Geophysical Research Letters*, **30**(19), 2019.

Osterberg, E.C., M.J. Handley, S.B. Sneed, P.A. Mayewski and K.J. Kreutz, 2006. Continuous Ice Core Melter System with Discrete Sampling for Major Ion, Trace Element, and Stable Isotope Analyses, *Environmental Science & Technology*, **40**(10), 3355–3361.

Osterberg, E., P. Mayewski, K. Kreutz, D. Fisher, M. Handley, S. Sneed, C. Zdanowicz, J. Zheng, M. Demuth, M. Waskiewicz and J. Bourgeois, 2008. Ice core record of rising lead pollution in the North Pacific atmosphere, *Geophysical Research Letters*, **35**(5), L05810.

Østrem, G., 1959. Ice melting under a thin layer of moraine, and the existence of ice cores in moraine ridges, *Geografiska Annaler*, **41**(4), 228–230.

Pacyna, J.M. and E.G. Pacyna, 2001. An assessment of global and regional emissions of trace metals to the atmosphere from anthropogenic sources worldwide, *Environmental Reviews*, **9**(4), 269–298.

Painter, T., 2011. Comment on Singh and others, 'Hyperspectral analysis of snow reflectance to understand the effects of contamination and grain size', *Journal of Glaciology*, **57**, 183–185.

Paul, F., R.G. Barry, J.G. Cogley, H. Frey, W. Haeberli, A. Ohmura, C.S.L. Ommanney, B. Raup, A. Rivera and M. Zemp, 2009. Recommendations for the compilation of glacier inventory data from digital sources, *Annals of Glaciology*, **50**(53), 119–126.

Paul, F., C. Huggel and A. Kääb, 2004a. Combining satellite multispectral image data and a digital elevation model for mapping debris-covered glaciers, *Remote Sensing of Environment*, **89**(4), 510–518.

Paul, F., A. Kääb, M. Maisch, T. Kellenberger and W. Haeberli, 2004b. Rapid disintegration of Alpine glaciers observed with satellite data, *Geophysical Research Letters*, **31**(21), L21402.

Paul, F., H. Machguth and A. Kääb, 2005. On the impact of glacier albedo under conditions of extreme glacier melt: the summer of 2003 in the Alps, EARSeL eProceedings, vol. 4.

Pearlman, J.S., P.S. Barry, C.C. Segal, J. Shepanski, D. Beiso and S.L. Carman, 2003. Hyperion, a space-based imaging spectrometer, *IEEE Transactions on Geoscience and Remote Sensing*, **41**(6), 1160–1173.

Pelto, M.S., 2000. Mass balance of adjacent debris-covered and clean glacier ice in the North Cascades, Washington, Nakawo, M., C.F. Raymond and A. Fountain, eds., Debris-Covered Glaciers, IAHS, Oxfordshire, UK, no. 264, 35–42.

Petit, J.R., J. Jouzel, D. Raynaud, N.I. Barkov, J.-M. Barnola, I. Basile, M. Benders, J. Chappellaz, M. Davis, G. Delaygue, M. Delmotte, V.M. Kotlyakov, M. Legrand, V.Y. Lipenkov, C. Lorius, L. Pèpin, C. Ritz, E. Saltzman and M. Stievenard, 1999. Climate and atmospheric history of the past 420,000 years from the Vostok ice core, Antarctica, *Nature*, **399**, 429–436.

Post, A. and E.R. LaChapelle, 1971, 2000. Glacier Ice, Revised Edition, University of Washington Press, Seattle.

Purdie, H., N. Bertler, A. Mackintosh, J. Baker and R. Rhodes, 2010. Isotopic and Elemental Changes in Winter Snow Accumulation on Glaciers in the Southern Alps of New Zealand, *Journal of Climate*, **23**(18), 4737–4749.

Quincey, D.J. and N.F. Glasser, 2009. Morphological and ice-dynamical changes on the Tasman Glacier, New Zealand, 1990-2007, *Global and Planetary Change*, **68**(3), 185–197.

Qunzhu, Z., C. Meisheng, F. Xuezhi, L. Fengxian, C. Xianzhang and S. Wenkun, 1985. A study of spectral reflection characteristics for snow, ice and water in the north of China, Goodison, B.E., ed., Hydrological Applications of Remote Sensing and Remote Data Transmission: Proceedings of the Hamburg Symposium, IAHS, no. 145, 451–462.

Racoviteanu, A.E., Y. Arnaud, M.W. Williams and Ordo nez, 2008. Decadal changes in glacier parameters in the Cordillera Blanca, Peru, derived from remote sensing, *Journal of Glaciology*, **54**, 499–510.

REFERENCES

Raup, B., A. Racoviteanu, S.J.S. Khalsa, C. Helm, R. Armstrong and Y. Arnaud, 2007. The GLIMS geospatial glacier database: A new tool for studying glacier change, *Global and Planetary Change*, **56**(1-2), 101–110.

Reynolds, J.M., 2000. On the formation of supraglacial lakes on debris-covered glaciers, Nakawo, M., C.F. Raymond and A. Fountain, eds., Debris-Covered Glaciers, IAHS, Oxfordshire, UK, no. 264, 153–161.

Richardson, S.D. and J.M. Reynolds, 2000. Degradation of ice-cored moraine dams: implications for hazard development, Nakawo, M., C.F. Raymond and A. Fountain, eds., Debris-Covered Glaciers, IAHS, Oxfordshire, UK, no. 264, 187–197.

Risheng, L., C. Jun, L. Gengnian and C. Zhijiu, 2003. Characteristics of the subglacially-formed debris-rich chemical deposits and related subglacial processes of Qiangyong Glacier, Tibet, *Journal of Geographical Sciences*, **13**(4), 455–462.

Röhl, K., 2008. Characteristics and evolution of supraglacial ponds on debris-covered Tasman Glacier, New Zealand, *Journal of Glaciology*, **54**(188), 867–880.

Rudnick, R.L. and S. Gao, 2003. Composition of the Continental Crust, Holland, Heinrich D. and Karl K. Turekian, eds., Treatise on Geochemistry, Pergamon, Oxford, 1–64.

Russell, I.C., 1895. The Influence of Debris on the Flow of Glaciers, *The Journal of Geology*, **3**(7), 823–832.

Ruth, U., Barbante C., M. Bigler, B. Delmonte, H. Fischer, P. Gabrielli, V. Gaspari, P. Kaufmann, F. Lambert, V. Maggi, F. Marino, J.-R. Petit, R. Udisti, D. Wagenbach, A. Wegner and E.W. Wolff, 2008. Proxies and Measurement Techniques for Mineral Dust in Antarctic Ice Cores, *Environmental Science & Technology*, **42**(15), 5675–5681.

Sakai, A., M. Nakawo and K. Fujita, 2002. Distribution Characteristics and Energy Balance of Ice Cliffs on Debris-Covered Glaciers, Nepal Himalaya, *Arctic, Antarctic, and Alpine Research*, **34**(1), 12–19.

Sandmeier, S., 1995. A physically-based radiometric correction model. Correction of atmospheric and illumination effects in optical satellite data of rugged terrain., (PhD thesis), University of Zurich.

Scherler, D., B. Bookhagen and M.R. Strecker, 2011. Spatially variable response of Himalayan glaciers to climate change affected by debris cover, *Nature Geoscience*, **4**(3), 156–159.

Schiefer, E. and B. Menounos, 2010. Climatic and morphometric controls on the altitudinal range of glaciers, British Columbia, Canada, *The Holocene*, **20**(4), 517–523.

Schneider, C., M. Schnirch, C. Acuña, G. Casassa and R. Kilian, 2007. Glacier inventory of the Gran Campo Nevado Ice Cap in the Southern Andes and glacier changes observed during recent decades, *Global and Planetary Change*, **59**(1-4), 87–100.

Schwikowski, M., S. Brütsch, G. Casassa and A. Rivera, 2006. A potential high-elevation ice-core site at Hielo Patagònico Sur, *Annals of Glaciology*, **43**, 8–13.

Schwikowski, M., A. Döscher, H.W. Gäggler and U. Schotterer, 1999. Anthropogenic versus natural sources of atmospheric sulphate from an Alpine ice core, *Tellus B*, **51**(5), 938–951.

Schwikowski, M. and A. Eichler, 2010. Alpine Glaciers as Archives of Atmospheric Deposition, vol. 6, Springer Berlin / Heidelberg.

Scollo, S., A. Folch, M. Coltelli and V.J. Realmuto, 2010. Three-dimensional volcanic aerosol dispersal: a comparison between Multiangle Imaging Spectroradiometer (MISR) data and numerical simulations, *Journal of Geophysical Research*, **115**, D24210.

Sharp, R.P., 1949. Studies of superglacial debris on valley glaciers, *American Journal of Science*, **247**(5), 289–315.

Sodemann, H., A.S: Palmer, C. Schwierz, M. Schwikowski and H. Wernli, 2005. The transport history of two Saharan dust events archived in an Alpine ice core, *Atmospheric Chemistry & Physics Discussions*, **5**, 7497–7545.

Stamnes, K., W. Li, R. Spurr, H. Eide and J.J. Stamnes, 2004. Simultaneous retrieval of aerosol and surface properties over bright targets including snow and ice using multi- and hyperspectral data, Proceedings of SPIE, Bellingham, Washington, USA, vol. 5569, 56–67.

Stohl, A., C. Forster, A. Frank, P. Seibert and G. Wotawa, 2005. Technical note: The Lagrangian particle dispersion model FLEXPART version 6.2, *Atmospheric Chemistry & Physics Discussions*, **5**, 4739–4799.

Stokes, C.R., V. Popovnin, A. Aleynikov, S.D. Gurney and M. Shahgedanova, 2007. Recent glacier retreat in the Caucasus Mountains, Russia, and associated increase in supraglacial debris cover and supra-/proglacial lake development, *Annals of Glaciology*, **46**(1), 195–203.

Symon, C. and S.J. Wilson, eds., 2005. AMAP Assessment 2002: Heavy Metals in the Arctic, Arctic Monitoring and Assessment Programme, Oslo, Norway.

Takeuchi, N., 2002. Surface albedo and characteristics of cryoconite (biogenic surface dust) on an Alaska glacier, Gulkana Glacier in the Alaska Range, *Bulletin of Glaciological Research*, **19**, 63–70.

Takeuchi, N. and Z. Li, 2008. Characteristics of Surface Dust on Urumqi Glacier No. 1 in the Tien Shan Mountains, China, *Arctic, Antarctic, and Alpine Research*, **40**(4), 744–750.

Takeuchi, Y., R.B. Kayastha and M. Nakawo, 2000. Characteristics of ablation and heat balance in debris-free and debris-covered areas on Khumbu glacier, Nepal Himalayas, in the pre-monsoon season, Nakawo, M., C.F. Raymond and A. Fountain, eds., Debris-Covered Glaciers, IAHS, Oxfordshire, UK, no. 264, 53–61.

Tanre, D., C. Deroo, P. Duhaut, M. Herman, J.J. Morcrette, J. Perbos and P.Y. Deschamps, 1990. Description of a computer code to simulate the satellite signal in the solar spectrum: The 5S code, *International Journal of Remote Sensing*, **11**(4), 659–668.

Tao, G., R. Yamada, Y. Fujikawa, A. Kudo, J. Zheng, D.A. Fisher and R.M. Koerner, 2001. Determination of trace amounts of heavy metals in arctic ice core samples using inductively coupled plasma mass spectrometry, *Talanta*, **55**(4), 765–772.

Tartari, G., G. Verza and L. Bertolami, 1998. Meteorological data at the Pyramid Observatory Laboratory (Khumbu Valley, Sagarmatha National Park, Nepal), *Limnology of high altitude lakes in the Mt. Everest Region, Nepal*, **57**, 23–40.

Tatsumoto, M. and C.C. Patterson, 1963. Concentrations of common lead in some Atlantic and Mediterranean waters and in snow, *Nature*, **199**.

Taylor, S.R. and S.M. McLennan, 1985. The Continental Crust: its Composition and Evolution, Blackwell Scientific, Palo Alto, CA.

Tegen, I. and I. Fung, 1995. Contribution to the atmospheric mineral aerosol load from land surface modification, *Journal Geophysical Research*, **100**(D9), 18707–18726.

Tegen, I and K Schepanski, 2009. The global distribution of mineral dust, *IOP Conference Series: Earth and Environmental Science*, **7**(1), 012001.

REFERENCES

Thome, K., S. Biggar and T. Takashima, 1999. Algorithm Theoretical Basis Document for ASTER Surface Radiance and Reflectance, *NASA Technical Document*, **NAS5-31717**, 45 pp.

Thompson, L.G., 1980. Glaciological investigations of the tropical Quelccaya ice cap, Peru, *Journal of Glaciology*, **25**(91), 69–84.

Thompson, L.G., 2000. Ice core evidence for climate change in the Tropics: implications for our future, *Quaternary Science Reviews*, **19**(1-5), 19–35.

Thompson, L.G., M.E. Davis, E. Mosley-Thompson, P.N. Lin, K.A. Henderson and T.A. Mashiotta, 2005. Tropical ice core records: evidence for asynchronous glaciation on Milankovitch timescales, *Journal of Quaternary Science*, **80**(7-8), 723–733.

Thompson, L.G., E. Mosley-Thompson, H. Brecher, M. Davis, B. Leon, D. Les, P.-N. Lin, T. Mashiotta and K. Mountain, 2006. Abrupt tropical climate change: Past and present, *Proceedings of the National Academy of Sciences*, **103**(28), 10536–10543.

Tranter, M., 2003. Geochemical Weathering in Glacial and Proglacial Environments, Holland, Heinrich D. and Karl K. Turekian, eds., Treatise on Geochemistry, Pergamon, Oxford, 189–205.

Tranter, M., P. Brimblecombe, T.D. Davies, C.E. Vincent, P.W. Abrahams and I. Blackwood, 1986. The composition of snowfall, snowpack and meltwater in the Scottish Highlands - evidence for preferential elution, *Atmospheric Environment*, **20**(3), 517–525.

Vermote, E.F., S.Y. Kotchenova and J.P. Ray, 2011. MODIS Surface Reflectance User's Guide, *NASA Technical Document*, **1.3**, 40 pp.

Vimeux, F., P. Ginot, M. Schwikowski, M. Vuille, G. Hoffmann, L.G. Thompson and U. Schotterer, 2009. Climate variability during the last 1000 years inferred from Andean ice cores: A review of methodology and recent results, *Palaeogeography, Palaeoclimatology, Palaeoecology*, **281**, 229–241.

Wake, C.P., P.A. Mayewski, X. Zichu, W. Ping and L. Zhongqin, 1993. Regional distribution of monsoon and desert dust signals recorded in Asian glaciers, *Geophysical Research Letters*, **20**(14), 1411–1414.

Warren, S.G. and W.J. Wiscombe, 1980. A Model for the Spectral Albedo of Snow. II: Snow Containing Atmospheric Aerosols, *Journal of the Atmospheric Sciences*, **37**(12), 2734–2745.

Watanabe, H. and K. Matsuo, 2003. Rock type classification by multi-band TIR of ASTER, *Geosciences Journal*, **7**(4), 347–358.

Werner, C., B.W. Christenson, M. Hagerty and K. Britten, 2006. Variability of volcanic gas emissions during a crater lake heating cycle at Ruapehu Volcano, New Zealand, *Journal of Volcanology and Geothermal Research*, **154**(3-4), 291–302.

Wessels, R.L., J.S. Kargel and H.H. Kieffer, 2002. ASTER measurement of supraglacial lakes in the Mount Everest region of the Himalaya, *Annals of Glaciology*, **34**(1), 399–408.

Wiens, R.C., R.E. Arvidson, D.A. Cremers, M.J. Ferris, J.D. Blacic, IV Seelos, F.P. and K.S. Deal, 2002. Combined remote mineralogical and elemental identification from rovers: Field and laboratory tests using reflectance and laser-induced breakdown spectroscopy, *Journal of Geophysical Research*, **107**(E11), 8004.

Wientjes, I. G. M. and J. Oerlemans, 2010. An explanation for the dark region in the western melt zone of the Greenland ice sheet, *The Cryosphere*, **4**(3), 261–268.

Winker, D.A., M.A. Vaughan, A. Omar, Y. Hu and K.A. Powell, 2009. Overview of the CALIPSO Mission and CALIOP Data Processing Algorithms, *Journal of Atmospheric and Oceanic Technology*, **26**(11), 2310–2323.

de Woul, M., R. Hock, M. Braun, T. Thorsteinsson, T. Jóhannesson and S. Halldórsdóttir, 2006. Firn layer impact on glacial runoff: a case study at Hofsjökull, Iceland, *Hydrological Processes*, **20**, 2171–2185.

Xie, R., H.M. Seip, G. Wibetoe, S. Nori and C.W. McLeod, 2006. Heavy coal combustion as the dominant source of particualte pollution in Taiyuan, China, corroborated by high concentrations of arsenic and selenium in PM10, *Science of The Total Environment*, **370**, 409–415.

Xu, B., J. Cao, J. Hansen, T. Yao, D.R. Joswia, N. Wang, G. Wu, M. Wang, H. Zhao, W. Yang, X. Liu and J. He, 2009. Black soot and the survival of Tibetan glaciers, *Proceedings of the National Academy of Sciences*, **106**(52), 22114–22118.

Yoshimura, Y., S. Kohshima, N. Takeuchi, K. Seko and K. Fujita, 2000. Himalayan ice-core dating with snow algae, *Journal of Glaciology*, **46**(153), 335–340.

Yue, X., H. Wang, Z. Wang and K. Fan, 2009. Simulation of dust aerosol radiative feedback using the Global Transport Model of Dust: 1. Dust cycle and validation, *Journal of Geophysical Research*, **114**(D10), D10202.

Zender, C.S., H. Bian and D. Newman, 2003. Mineral Dust Entrainment and Deposition (DEAD) model: Description and 1990s dust climatology, *Journal of Geophysical Research*, **108**(D14), 4416.

Zhang, Q., S. Kang, S. Kaspari, C. Li, D. Qin, P.A. Mayewski and S. Hou, 2009. Rare earth elements in an ice core from Mt. Everest: Seasonal variations and potential sources, *Atmospheric Research*, **94**, 300–312.

Zimmermann, F., S. Weinbruch, L. Schutz, H. Hofmann, M. Ebert, K. Kandler and A. Worringen, 2008. Ice nucleation properties of the most abundant mineral dust phases, *Journal Geophysical Research*, **113**(D23), D23204.

7

Dissertation Publications

I

7.1 Extended Abstract i

K.A. Casey. Proposed methodology for detection of geochemical species on glaciers, In: Proceedings of 10th Biennial Meeting of the Society for Geology Applied to Mineral Deposits (SGA), 16-22 August 2009. Townsville, Australia.

Proposed methodology for detection of geochemical species on glaciers

Kimberly A. Casey
Department of Geosciences, University of Oslo, 0862 Oslo, Norway

Abstract. Remote sensing of inorganic geochemical species on glaciers is a key remaining challenge in cryospheric surface characterization and development of glacial and climate models. Cryospheric surface geochemistry via remote sensing is a powerful means to monitor atmospheric circulation and pollution dispersion. Extraction of geochemical information from remote sensing data would allow for an abundance of data to be used in a manner not previously possible – accessibility of near real time as well as historical data at large spatial scales. Traditional in-situ geochemical analyses often necessarily require considerable time and resources spent on field deployment and subsequent laboratory analysis. In this study, methodology for identifying geochemical species is proposed based on evaluation of glacial environments in Svalbard, the Himalayas and New Zealand. These sites were chosen due to availability of both remote sensing and in-situ data. Furthermore, in April 2009 field spectrometry data and in-situ snow samples were collected in Svalbard for use in methodological development and validation. Preliminary results indicate strong potential for development of a method to characterize inorganic geochemical species on snow and ice.

Keywords: remote sensing, glaciers, geochemistry

1 Background

Earth observing satellite technology has advanced greatly in the past decades and allows for unprecedented imaging of the Earth's surface, including difficult to access locations such as the polar regions. Satellites provide exceptionally detailed information at temporal resolutions of up to daily time scales and couple hundred meter spatial resolutions (i.e.: Moderate Resolution Imaging Spectroradiometer, MODIS) or finer spatial resolution of tens of meters and greater temporal resolutions (i.e.: Advanced Spaceborne Thermal Emission and Reflection Radiometer, ASTER and Landsat). Due to the finer spatial resolution, ASTER and Landsat data are commonly used in smaller glacier analysis (Andreassen et al. 2008; Kääb 2005; Hall et al. 2000; Hall et al. 1989), and are useful for geochemical studies of glaciers.

Previous geochemical remote sensing studies focus on arid terrain (Moore et al., 2008; Khan and Mahmood 2008; Gomez et al. 2005; Rowan et al. 2005; Mahoney et al. 2002; Sultan et al. 1987) and vegetation (Schellekens et al. 2005, Clevers et al. 2004; Horler et al. 1980). These studies have primarily used Landsat and ASTER remote sensing data, with some studies utilizing hyperspectral remote sensing data to more fully describe the spectral signature of investigated species (i.e.: Hyperion) (Mahoney et al. 2002).

Several in-situ cryospheric particulate matter studies have been conducted, ranging from glacial changes in mineral records in ice cores (Fischer et al. 2007; Kreutz and Sholkovitz 2000), Arctic pollution (Osterberg et al. 2008; Jacob 2007; Berg et al. 2008; Lu et al., 2001) and Antarctic trace element characterization (Marteel et al. 2008; Ruth et al. 2008; Gasparon and Matschullat 2006). In many cases, a significant expansion to such studies could be provided by remotely sensed geochemical data – greatly increasing spatial and possibly temporal coverage.

Laboratory spectroscopy is a well established scientific method for geochemical characterization. Further, the measurement of trace elements from geochemical samples has become possible within the past few decades. Mass and concentration detection instrumentation progression over the years from gravimetry and X-ray analysis to inductively coupled plasma mass spectrometry (ICP-MS) has allowed for a shift from larger scale mineralogical component measurements to small 'trace elemental' detection and measurement (Kreutz and Sholkovitz 2000; Berg et al. 1994; Steinnes et al. 1993). Ground breaking ICP-MS analysis allows for dozens of elements to be measured at very low concentrations (i.e.: concentrations in the parts per million or billion range). ICP-MS is the method envisioned to be used for comparison of remote sensing geochemical results and field collected geochemical analysis of data.

2 Methodology and Data

Methods used for detecting geochemical species on other land cover surfaces will be tested with respect to analysis of glacier surfaces in three regions: Kongsvegen and Grønfjordbreen in Svalbard, Norway; Kangxung and Khumbu glaciers in the Himalayas, and the Mt. Ruapehu glaciers in north New Zealand.

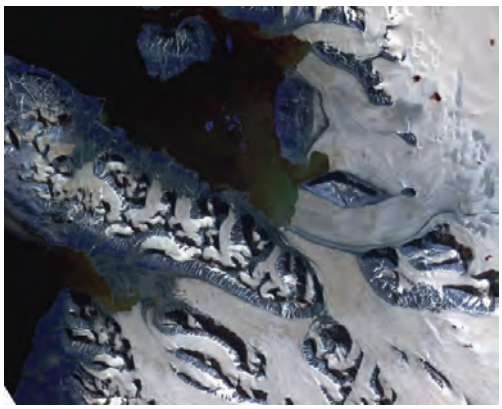

Figure 1. ASTER visible near infrared bands 1,2,3N image of Ny Ålesund area in Svalbard, highlighting Kongsvegen glacier which is targeted for geochemical analysis (image oriented

with North toward the top of the page, image resolution 15m, acquisition date 12 July 2002).

In-situ snow sample and field spectrometry data was acquired on the 17th and 18th of April 2009 on Grønfjordbreen and surrounding areas in Svalbard. A FieldSpec Pro instrument was used with data collection in the wavelength range of 350-2500 nm. Four areas in different regions on and surrounding Grønfjordbreen were chosen for sample collection in 1000 mL acid prepared (HCl) low density polyethylene bottles. Samples were collected in duplicate and will be analyzed via ICP-MS for snow trace element concentrations. Field spectrometry data will be compared with trace element concentrations.

Existing similar trace element concentration geochemical data is available in three areas: Ny Ålesund, Svalbard – via Berg et al. 2008; Mt. Everest snow and firn – Kang et al. 2007 and Zhang et al. 2007; and New Zealand - Marx et al 2005. ASTER level 1B scenes have been acquired for comparison with each geochemical data set (see Table 1) in time frames nearest in date and season to data collection are analyzed. For additional comparison purposes, for the April 2009 data set, MODIS data satellite data coinciding with field collection was also acquired.

Table 1. Listing the location, glacier; the date of remote sensing scene, and the in-situ data reference.

Svalbard, Kongsvegen glacier	12 Jul 2002	Berg (2008)
Himalaya, near Khumbu glacier	29 Nov 2005	Kang (2007)
New Zealand, Whangaehu glacier	18 Nov 2003	Kargel (1999)
Svalbard, Grønfjordbreen	4 Apr 2008	*this study*

* In addition to ASTER, MODIS satellite data has also been targeted for comparison with in situ data in this case.

Evaluations will include initial mineral specific spectral mapping after Moore (2008), and subsequent use of established (Ninomiya 2003, and others) or new ASTER visible-to-near, shortwave- and thermal-infrared reflectance band ratio analysis. The objective is to use distinctive metal or mineral spectral reflectance features to identify presence in the surface snow and ice of glaciers. Results will highlight optimal band ratio and suggested thresholds for geochemical species differentiation. Satellite data spectral band ratios and thresholds will be tested for each region with respect to expected inorganic geochemical species per in-situ data.

Geographically-varied regions provide an opportunity to test detection of various inorganic geochemical species under many glacier and geologic conditions. Trace inorganic element data is available for all three regions, yet, glacial type and geological conditions differ. The inorganic species present on Arctic Svalbard glaciers result from long range atmospheric transport as well as local pollution sources. Monsoon influenced Himalayan glaciers are heavily debris covered, with much of the inorganic glacial species expected to be representative of surrounding geology. Expected minerals on heavily debris covered Himalayan glaciers include leucogranite and low-grade schist (Benn, personal communication 2009). The temperate New Zealand Mt. Ruapehu glaciers provide volcanic tephra silica-rich surface geochemical signatures.

Kargel et al. (1999) presents investigation into trace elemental concentration required to affect the spectroscopic signature. Levels of trace elemental concentration will be evaluated with respect to cryospheric reflectance signatures.

3 Expected Results

Relative to the Khumbu and Whangaehu glaciers, Kongsvegen and Grønfjordbreen in Svalbard are expected to yield the highest glacial area mean reflectance. The distinct geologic surroundings of the Khumbu and Whangaehu glaciers should theoretically allow for differentiation of geochemical species over ice surfaces via established arid terrain mineral indicies.

It has been previously theorized that the visible region of the snow and ice spectral signature provides greatest potential for surface impurity and particulate signature distinction (Warren and Wiscombe 1980; Hall et al. 1989; Hansen and Nazarenko 2004; Moody et al. 2007). The visible region of the spectrum also contains absorption features for biological substances including glacial algae. It is well known that snow and ice grain size differences spectrally alter the near infrared region of the electromagnetic spectrum (Dozier et al., 2007 and others). Glacier facies i.e.: dry snow, percolation zone, wet snow, bare ice after Benson (1962) spectral characteristics are also well described (Williams et al. 1991). Mineral spectral absorption features distinct to the SWIR and TIR wavelengths suggest that a full spectral analysis will be part of the geochemical discrimination methodology.

Further, coordination of in-situ data with remote sensing data must include consideration of the temporal component. Gaps in data require consideration of many factors, including: seasonality, precipitation events, atmospheric events, as well as glacier velocities. An attempt was made to gather the most comparable remote sensing data relevant to the existing in-situ geochemical data. In consideration of the temporal gap with regards to glacial velocity, for example, Kongsvegen glacier in recent decades has been extremely low, only a few meters per year (Kääb et al. 2005), thus, this slow flowing glacier is amenable to comparisons which may have a small temporal gap of satellite and field acquisition of data. Faster glacier velocity (e.g. Khumbu glacier icefall -- 80 meters per year (Sherler et al. 2008)), may require larger spatial than point analysis in order to consider feature disposition if there is temporal inconsistency in data comparisons. When comparing in-situ and remote sensing data with large temporal gaps, analysis must also consider seasonal or other temporal surface deposit events (e.g. dust, volcanic).

A few studies begin to address the combination of cryospheric remote sensing and geochemistry - optical characteristics of surface dust over glaciers were studied by Takeuchi (2002). Although remote sensing data was not used in the study, factors including albedo and biological substances were explored. Wu (2006) conducted field spectroscopy measurements looking for

heavy metals in sediment.

These and other studies will be evaluated for development of remote sensing methodology for analysis of inorganic chemical species over glacier surfaces. Overall, detection of geochemical species via cryospheric remote sensing data is a powerful tool pertinent to a myriad of applications, from surface characterization, glacial and climate modeling, to pollution monitoring or understanding of atmospheric circulation patterns. Initial geochemical species remote sensing analysis proves promising for further development of geochemical remote sensing methodology.

Acknowledgements

I would like to thank Rune Solberg for collaboration on the Svalbard data collection as well as Andreas Kääb, Dorothy Hall and Oddvar Røyset for fruitful discussions. This work is supported by European Space Agency GlobGlacier project, Brahmatwinn, and the University of Oslo Department of Geosciences.

References

Andreassen L, et al. (2008) Landsat derived glacier inventory for Jotunheimen, Norway, and deduced glacier changes since the 1930s: Cryosphere 2:131-145

Benson C (1962) Stratigraphic studies in the snow and firn of the Greenland Ice Sheet: SIPRE Research Report 70 93 pp

Berg T, et al. (1994) PCA data for trace elements and main components in precipitation falling on Norway: Environmental Monitoring and Assessment 31:259-273

Berg T, et al. (2008) Atmospheric trace metal concentrations at Norwegian background sites during 25 years and its relation to European emissions: Atmospheric Environment 42:7494-7501

Clevers J, et al. (2004) Study of heavy metal contamination in river floodplains using the red-edge position in spectroscopic data: Intl J Remote Sensing 25(19):3883-3895

Dozier J, et al. (2007) Interpretation of Snow Properties from Imaging Spectrometry: Remote Sensing of Environment 51

Fischer H, et al. (2007) Glacial/interglacial changes in mineral dust and sea salt records in polar ice cores: sources, transport, Deposition: Dust and Sea Salt in Polar Ice Cores. *Rev. Geophys* 45

Gasparon M, Matschullat J (2006) Trace metals in Antarctic ecosystems: Results from the Larsemann Hills, East Antarctica: Applied Geochemistry 21:1593-1612

Gomez C, et al. (2005) Using ASTER remote sensing data set for geological mapping, in Namibia: Physics Chemistry of Earth 30:97-108

Hall D, et al. (2000) Evaluation of remote-sensing techniques to measure decadal-scale changes of Hofsjokull ice cap, Iceland: J Glaciology 46(154):375-388

Hall D, et al. (1989) Comparison of In Situ and Landsat Derived Reflectance of Alaskan Glaciers: Remote Sensing Environment 28:23-31

Hansen J, Nazarenko L (2004) Soot climate forcing via snow and ice albedos: Proceedings of the National Academy of Sciences of the United States of America 101(2):423-428

Horler D, et al. (1980) Effects of heavy metals on the absorbance and reflectance spectra of plants: Intl J Remote Sensing 1(2):121-136

Jacob D, et al. (2007) Arctic Research of the Composition of the Troposphere from Aircraft and Satellites (ARCTAS): Report, NASA Experiment for International Polar Year 31 pp

Kääb A, et al. (2005) Flow field of Kronebreen, Svalbard, using repeated Landsat 7 and ASTER Data: Annals of Glaciology 42:7-13

Kääb, A (2005) Remote sensing of mountain glaciers and permafrost creep. Schriftenreihe Physische Geographie 48.

Kang S, et al. (2007) Spatial and seasonal variations of elemental composition in Mt. Everest (Qomolangma) snow/firn: Atmospheric Environment 41:7208-7218

Kargel J, et al. (1999) Volcanogenic Sulfur on Earth and Io: Composition and Spectroscopy: Icarus 142:249-280

Khan SD, Mahmood K (2008) The application of remote sensing techniques to the study of ophiolites: Earth Science Reviews 89:135-143

Kreutz KJ, Sholkovitz ER (2000) Major element, rare earth element, and sulfur isotopic composition of a high-elevation firn core: Sources and transport of mineral dust in central Asia: Geochemistry Geophysics Geosystems 1:200GC000082

Lu J, et al. (2001) Magnification of atmospheric mercury deposition to polar regions in springtime: the link to tropospheric ozone depletion chemistry: Geophysical Research Letters 28(17):3219-3222

Mahoney S, et al. (2002) Geologic and regolith mapping for mineral exploration in the Gawler Craton of South Australia using Hyperion and other remote sensing techniques: IEEE 1779-1781

Marteel A, et al. (2008) Changes in atmospheric heavy metals and metalloids in Dome C (East Antarctica) ice back to 672.0 kyr BP (Marine Isotopic Stages 16.2): Earth and Planetary Science Letters 272:579-590

Moody E, et al. (2007) Northern Hemisphere five-year average (2000-2004) spectral albedos of surfaces in the presence of snow: Statistics computed from Terra MODIS land products: Remote Sensing Envmt 111:337-345

Moore F, et al. (2008) Mapping mineralogical alteration using principal-component analysis and matched filter processing in the Takab area, north-west Iran, from ASTER data: Int J Remote Sensing 29(10):2851-2867

Ninomiya Y (2003) A stabilized vegetation index and several mineralogic indicies defined for ASTER VNIR and SWIR data: IEEE 1552-1554

Osterberg E, et al. (2008) Ice core record of rising lead pollution in the North Pacific atmosphere: Geophysical Research Letters, 35:1-4 L05810

Rowan LC, et al. (2005) Lithologic mapping of the Mordor, NT, Australia ultramafic complex by using the Advanced Spaceborne Thermal Emission and Reflection Radiometer (ASTER): Remote Sensing Envmt, 99:105-126

Ruth U, et al. (2008) Proxies and Measurement Techniques for Mineral Dust in Antarctic Ice Cores: Environmental Science Technology 42:5675-5681

Scherler D, et al. (2008) Glacier-surface velocities in alpine terrain from optical satellite imagery-Accuracy improvement and quality assessment: Remote Sensing of Environment 112:3806-3819

Schellekens J, et al. (2005) Reflectance spectra of tropical vegetation as a response to metal enrichment in the substrate of west-central Puerto Rico: Caribbean Journal of Earth Science 39:9-12

Steinnes E, et al. (1993) Comparison of different multielement techniques for analysis of mosses used as biomonitors: Environmental Monitoring and Assessment 25:87-97

Sultan M, et al. (1987) Lithologic mapping in arid regions with Landsat thematic mapper data: Meatiq dome, Egypt: Geological Society of America Bulletin 99:748-762

Takeuchi, N (2002) Optical characteristics of cryoconite (surface dust) on glaciers: the relationship between light absorbency and the property of organic matter contained in the cryoconite: Annals of Glaciology 34:409-414

Warren SG, Wiscombe WJ (1980) A Model for the Spectral Albedo of Snow: Journal of the Atmospheric Sciences 37:2712-2745

Williams R, et al. (1991) Analysis of glacier facies using satellite techniques J Glaciology 37(125):120-128

Wu Y, et al. (2006) Visible and near infrared reflectance spectroscopy for measuring soil heavy metal content as a quick method: Chinese Journal of Geochemistry 25:225

Zhang YL, et al. (2007) The spatial distribution of trace elements in topsoil from the northern slope of Qomolangma (Everest) in China: Environ Geol 52:679-684

II

7.2 Publication I

K.A. Casey, A. Kääb, D.I. Benn. Characterization of glacier debris cover via in situ and optical remote sensing methods: a case study in the Khumbu Himalaya, Nepal. The Cryosphere Discussions, 5, 499-564, 2011. *Revision submitted to The Cryosphere.*

The Cryosphere Discuss., 5, 499–564, 2011
www.the-cryosphere-discuss.net/5/499/2011/
doi:10.5194/tcd-5-499-2011

The Cryosphere Discussions

Characterization of glacier debris cover via in situ and optical remote sensing methods: a case study in the Khumbu Himalaya, Nepal

K. A. Casey[1], **A. Kääb**[1], **and D. I. Benn**[2,3]

[1]Department of Geosciences, University of Oslo, P.O. Box 1047 Blindern, 0316 Oslo, Norway
[2]Department of Geography, University of St. Andrews, St. Andrews, UK
[3]The University Centre in Svalbard (UNIS), P.O. Box 156, 9171 Longyearbyen, Norway

Received: 28 November 2010 – Accepted: 22 January 2011 – Published: 7 February 2011

Correspondence to: K. Casey (k.a.casey@geo.uio.no)

Published by Copernicus Publications on behalf of the European Geosciences Union.

Abstract

Field spectrometry and physical samples of debris, snow and ice were collected from the ablation zones of Ngozumpa and Khumbu glaciers of the Khumbu Himalaya, Nepal in November and December 2009. Field acquired spectral reflectances and mineral and chemical composition of samples were used as ground truth for comparison with satellite optical remote sensing data. Supraglacial debris was characterized by several optical remote sensing methods, including hyperspectral reflectance analysis, multispectral band composites and indices, spectral angle relationships, thermal band temperature and emissivity analysis, as well as repeat image derived glacier velocity and theoretical supraglacial particle transport. Supraglacial mineral components were identified and mineral abundances were estimated on Khumbu Himalayan glaciers. Mass flux was estimated by false color composites and glacier velocity displacement fields. Supraglacial temperatures were compared with mineral abundances, implying potential parameters to estimate differential melt. Overall, glaciologic implications of debris cover characterizations are applicable to (1) glacier energy balance, (2) glacial kinematics and (3) mapping glacial extent. The methods presented can be used in synergy to improve supraglacial debris quantification and reduce errors associated with debris covered ice extent mapping, surface radiative properties, as well as debris covered ice mass flux and loss estimations.

1 Context

Many of the world's alpine glaciers have moderate to significant debris cover in their ablation zones, and this debris remains a challenge in optical satellite remote sensing glacier description. Previous optical remote sensing analysis of debris covered glaciers has largely focused on mapping glacial extent. While mapping "clean" bare glacier ice extent can be done quite successfully (Hall et al., 1988), even on a semi-automated basis (Paul et al., 2007); strategies for debris covered glacier extent mapping remain

in development and commonly utilize geomorphometric approaches (Taschner and Ranzi, 2002; Paul et al., 2004; Bolch et al., 2007; Buchroithner and Bolch, 2006; Shukla et al., 2010). A recent advance by Atwood et al. (2010) and Strozzi et al. (2010) involves the use of phase coherence between repeat synthetic aperture radar (SAR) data to delineate debris covered areas.

In addition to mapping glacier extent, glaciologic thermal properties as well as kinematic processes can be derived from optical remote sensing of glacier debris. Minimal to moderate glacier debris cover enhances ice and snow melt rates (Warren and Wiscombe, 1980; Oerlemans et al., 2009) while extensive debris cover – typical of several Himalayan glaciers – can insulate ice and dampen melt processes (Ostrem, 1959; Fujii, 1977; Mattson et al., 1993; Adhikary et al., 2000; Takeuchi et al., 2000; Nicholson and Benn, 2006). Ablation rates, melt water discharge (Mattson, 1990, 2000), and debris-cover regulated backwasting (Nakawo et al., 1999), are among the glaciologic variables that are affected by debris cover. Further, lithologic supraglacial patterns reveal the kinematic history of a debris covered glacier. Evidence of past surges and flow processes can be suggested by looped and folded moraines, as well as band and wave ogive patterns (Post and LaChapelle, 2000). Debris mantle patterns and assemblages indicate slope processes such as rock or ice falls or avalanches (Benn and Evans, 2010) as well as glacier flow regimes which can be described by glacial movement that is continuous, pulsed or of surge type (Kääb, 2005). Of course, flow dynamics from accumulation to ablation zones are complex and cannot be determined solely by surface optical remote sensing methods. However, inspecting supraglacial lithology can highlight distinct geologic sources in the accumulation zone which then reemerge supraglacially in the ablation zone, for example, giving an indication of englacial transport as well as the amount of debris transported.

Optical remote sensing multi-temporal image matching of debris cover can be utilized to estimate glacier velocities and theoretical surface particulate flow (Kääb et al., 1998; Frauenfelder and Kääb, 2000; Kääb, 2005). The synergy of glacier velocity and streamline information with supraglacial debris characterization can provide first-order

thermal- and kinematic-related glacier records of years, decades or centuries. Consideration of glacier transport and mass loss is relevant to glacier mass balance estimations at regional and global scales. Colloquially referred to as Earth's 3rd pole (Yao, 2010), the Himalayan glaciers are characterized by extensive debris cover. Sustained and widespread mass loss of ice in the Himalayas and in other regions can lead to crustal uplift (Tamisiea et al., 2001; Larsen et al., 2005), and of course, ultimately, sea level rise (Meier et al., 2007). Attention to and improved mapping of debris covered glaciers on a global scale is of paramount importance.

In this paper, we present several visible to thermal infrared multi- and hyperspectral remote sensing techniques for characterization of glacier debris which are applied to glacier energy balance, kinematic history and ice extent mapping. Glaciers in the Khumbu Himalayas will be used for testing the remote sensing techniques, with in situ field spectrometry and debris sample mineralogy and composition used as ground truth. To the authors' knowledge, no glaciologic study has explored full spectrum – visible to thermal infrared – data for qualitative and quantitative supraglacial debris characterization which is relevant to improving debris covered glacier mapping, understanding kinematic history as well as estimating thermal parameters of glaciers.

2 Optical remote sensing of glacier debris

In the following sections, we provide a review of optical satellite sensors used in this study and a brief background on spectral measurement of lithology.

2.1 Sensors

Earth observing satellite technology has advanced greatly in recent decades and allows for unprecedented spatial, temporal and spectral imaging of Earth's cryospheric surfaces, including difficult to access alpine and polar regions. Wavelength dependent spectral signatures can be used to identify surface material based on electromagnetic

reflection (0.4–3 µm) and emission (3–14 µm) (Goetz et al., 1983). Optical satellite instruments measure discrete spectral bands from the visible to the thermal infrared wavelengths (0.4–14 µm) and provide high resolution spectral information for determining surface materials (e.g.: snow, ice, rock, vegetation) at up to daily temporal resolutions and couple hundred meter spatial resolutions (e.g.: Medium Resolution Imaging Spectrometer Instrument, MERIS or Moderate Resolution Imaging Spectrometer, MODIS) or finer spatial resolutions of tens of meters and coarser temporal resolutions of more than ten days (e.g.: US/Japan Advanced Spaceborne Thermal Emission and Reflection Radiometer (ASTER) onboard the NASA Earth Observing System Terra satellite and US NASA/USGS Landsat mission satellites). Data from Landsat and ASTER are commonly used in glacier analysis, due to the finer spatial resolution (Hall et al., 1988; Paul et al., 2002; Andreassen et al., 2008) and will be among the sensors utilized in this study (Fig. 1).

The Landsat Earth observing satellite program began in 1972 (as Earth Resources Technology Satellite, ERTS) and has consisted of a several instruments over the past three decades: Landsat 1, 2, 3, 4 – Multispectral Scanner System (MSS), Landsat 4, 5 – Thematic Mapper (TM), and Landsat 7 – Enhanced Thematic Mapper Plus (ETM+). Landsat 7's ETM+ provides 16-day temporal resolution with 8 spectral bands: one panchromatic (pan) band at 15 m resolution, six visible to shortwave infrared bands at 30 m resolution, and one thermal band at approximately 60 m resolution. Unfortunately, the ETM+ scan line corrector (SLC) on the instrument failed in May 2003. ETM+ data post May 2003 exhibits wedge shaped gaps, resulting in a loss of approximately 22% of scene area (Storey et al., 2005). However, Landsat 7 ETM+ gap-filled data are available. Additionally, Landsat 5 TM, with similar spectral (7 bands) and spatial (30 m) resolution, continues to function at the date of this publication.

Launched onboard Terra in 1999, ASTER measures 14 optical bands at spatial resolutions from 15 to 90 m at 16-day temporal resolution. Specifically, ASTER offers three bands in the visible and near infrared (VNIR, 0.4–0.9 µm) at 15 m spatial resolution, six shortwave infrared bands (SWIR, 1.0–2.5 µm) at 30 m spatial resolution and

five thermal infrared bands (TIR, 3.0–12 µm) at 90 m spatial resolution. Intended particularly for spectral signature studies (Abrams, 2000), ASTER's spectral coverage in SWIR and TIR is unprecedented via satellite instrumentation. Unfortunately, after nine years of operation, in April 2008, the SWIR bands began to fail and are no longer suitable for geologic analysis. (To note, ASTER VNIR and TIR bands are still performing well at the date of this publication, SWIR data from 2000 to 2008 are usable.)

Part of a technological demonstration and validation mission, NASA's EO-1 satellite was launched in 2000 and operates in a sun-synchronous orbit on a 16-day repeat cycle (although images are not acquired continuously). EO-1 carries two pushbroom sensors: Hyperion and Advanced Land Imager (ALI). Hyperion uses a VNIR and a SWIR spectrometer to acquire 242 spectral bands from 0.4 to 2.5 µm (in 10 nm nominal increments) at 30 m spatial resolution. Of the 242 spectral bands, only 220 are calibrated due to low response of detectors in non-calibrated bands. Approximately 24 bands measure at the same wavelength between the VNIR and SWIR spectrometers. Thus, there are 196 distinct spectral bands – VNIR bands 8 through 57, and SWIR bands 77 through 224. Similar in spectral resolution to the Landsat series, ALI offers one pan band and 9 visible to shortwave infrared bands. Compared to Landsat TM and ETM+, ALI offers improved VNIR to SWIR spectral resolution at the same spatial resolution (30 m), and improved pan band spatial resolution (10 m vs. ETM+ pan 15 m). However, ALI offers no TIR spectral data. Although EO-1 was only planned to run for 2-years, operation has continued successfully and EO-1 is now managed by the United States Geological Survey (USGS) (all Hyperion and ALI instrument data after Beck et al., 2003).

2.2 Measuring lithology

The use of laboratory and field based spectroscopy in deriving mineral and chemical constituents began with pioneering investigations by McClure (1957, 1959); Lyon (1965); Hunt and Salisbury (1970a,b); Hunt et al. (1971a,b) as well as Clark and Lucey (1984) focusing strictly on ice/rock mixtures. Interpretation of reflectance and

emission spectra from optical satellite remote sensing for deriving mineral and chemical constituents has progressed over the past several decades (Vincent and Thomson, 1972; Goetz and Rowan, 1981; Clark et al., 1990; Hook et al., 1992; Rowan and Mars, 2003; Ninomiya, 2004). Laboratory and field based VNIR to SWIR and TIR spectral libraries serve as references for spectral analysis (Christensen et al., 2000; Baldridge et al., 2009) (Appendix A). Dominant anions, cations, trace constituents and crystal field structures strongly influence reflectance and emission spectra (Hunt, 1977; Gupta, 2003). Specifically, transition metal enrichment can be detected via use of VNIR (Rowan et al., 1986; Gupta, 2003; Rowan and Mars, 2003); hydroxide, sulfate and carbonate minerals can be analyzed using SWIR (Kruse, 1988; Rowan and Mars, 2003; Ninomiya et al., 2005); and silicate, carbonate, oxide, phosphate, and sulfate minerals via use of TIR (Gillespie et al., 1984; Hook et al., 1992; Gupta, 2003; Ninomiya et al., 2005). Traditionally, X-ray diffraction (XRD) can be used to semi-quantitatively identify mineralogy of in situ samples, while X-ray fluorescence spectrometry (XRF) can be used to provide a quantitative measurement of oxide compound weight percentage (e.g.: SiO_2, Al_2O_3, Fe_2O_3, CaO) as well as trace element concentration (part per million, ppm) (e.g.: V, Co, Zn, Pb). In this paper, we utilize XRD and XRF analysis of glacier debris samples to qualitatively and quantitatively and investigate lithology (which we define as the description of rock composition and texture) via remote sensing data in light of glacier dynamics.

Previous hyperspectral and satellite multispectral geologic or geochemical remote sensing differentiation studies focus largely on arid terrain (e.g. Goetz et al., 1983; Sultan et al., 1987; Rowan et al., 2005). Spectral investigations of debris cover on glacier surfaces to date include: glacier extent mapping via Landsat thermal imaging (Lougeay, 1974, 1982), SPOT pan imagery and an applied artificial neural network (Bishop et al., 1999), Landsat TM and ASTER VNIR, TIR data mapping (Taschner and Ranzi, 2002), and combined VNIR, 1 SWIR band, TIR and geomorphic data (Shukla et al., 2010). Further morphometric glacier mapping approaches are presented in Paul et al. (2004) and Bolch et al. (2007). In addition to glacier extent studies, Shroder et al.

(2000) inspected glacial debris cover via 4 SPOT VNIR bands to suggest mechanisms in which debris covered glaciers turn into rock glaciers; Wessels et al. (2002) used ASTER VNIR-TIR data to analyze spectral variability of supraglacial lakes in the Everest region; Suzuki et al. (2007) mapped thermal resistance of debris covered glaciers in the Lunana and Khumbu Himalayas, and Kääb (2005) utilized false color ASTER SWIR and TIR band composites to indicate debris patterns, source areas, and indication of flow regimes at Hispar glacier in the Karakorum, Pakistan and Unteraar glacier in the Grimsel region of the Swiss Alps. This study identifies VNIR-TIR multi- and hyperspectral satellite remote sensing methods for lithologic differentiation and characterization of supraglacial debris.

3 Study area

Fifteen percent of the Himalayan mountain range is covered by glaciers, constituting one of the largest areas of land-based ice outside of the Greenland and Antarctic ice sheets (Nesje and Dahl, 2000; Anthwal et al., 2006; Radic and Hock, 2010). We estimate glacier area in the Hindu Kush Himalayas to be around 65 000 km^2, and 8000 km^2 or roughly 15% of this glacier area is debris covered (unpublished initial Himalaya glacier inventory by the authors). Focusing on the Khumbu Himalaya study area (Fig. 2, 3), the Ngozumpa glacier is the longest glacier in Nepal at approximately 25 km (Benn et al., 2001) with Khumbu glacier measuring 17 km in length (Hambrey et al., 2008). The large size of these debris covered ablation areas provides ample spatial coverage to use remote sensing data (ranging from 15–90 m VNIR-TIR) in spectral debris cover analysis.

The climate in the region is strongly affected by the South Asian monsoon, mid-latitude westerlies, and El Niño Southern Oscillation (ENSO) (Benn and Owen, 2002). The Khumbu Himalayan glaciers experience summer precipitation that exceeds winter precipitation, allowing for simultaneously strong accumulation and ablation from late May through mid-September. Glaciologically referred to as summer accumulation type

(Ageta and Higuchi, 1984; Benn and Owen, 1998), significant melt can occur in late fall and early winter months as was observed at Khumbu glacier in December 2009. The Ngozumpa and Khumbu glaciers are heavily debris covered due to frequent rock and ice avalanches from surrounding extreme topographic relief. High rates of supraglacial activity in terms of sediment transport, deposition, and glacial erosion (Benn and Owen, 2002) as well as the extreme topographic relief are characteristics that differentiate Himalayan glaciers from polar and other alpine glaciers.

Ngozumpa and Khumbu glacier surface debris consists primarily of leucogranite, greenschist and sillimanite gneiss dust, silts, sands, gravels, rocks and boulders, with primary mineral components including quartz, potassium feldspars (in the form of orthoclase and microcline), feldspars (albite, calcium-rich albite), micas (muscovite, biotite, phlogopite), and carbonates (calcite) (Pognante and Benna, 1993; Carosi et al., 1999; Searle, 1999; Searle et al., 2003). Extensive debris cover on both glacier tongues increases in depth down glacier and insulates the underlying ice (Kadota, 1997; Kadota et al., 2000; Byers, 2007; Hambrey et al., 2008). Both Ngozumpa and Khumbu glaciers are characterized by numerous supraglacial melt ponds (Wessels et al., 2002) and considerable relief of supraglacial debris with the height difference between peaks and troughs estimated at 20–50 m as observed during field work in 2009 and reported in Benn and Owen (2002). Downwasting or thinning of Khumbu Himalayan glaciers has been observed over the past several decades (Bolch et al., 2008a). In addition to downwasting, backwasting, or the ablation which occurs on exposed ice faces in debris covered areas, is a primary melt mechanism active on these glaciers. Backwasting was found to account for up to 20% of the total ablation of debris covered area by Nakawo et al. (1999). Backwasting related topographic inversion processes that occur on these debris-mantled glaciers, yield complex debris assemblages (detailed in Benn and Evans, 2010). Fushimi et al. (1980) field based maps of supraglacial debris types on the Khumbu glacier show a longitudinal band of schistic debris and lateral granitic debris bands, traced from the icefall to the terminus. These Khumbu glacier longitudinal supraglacial debris bands are reflective of surrounding

lithology, and indicative of flow processes. Wave ogives occurring directly below the Khumbu icefall were noted by Hambrey et al. (2008), further suggesting glacial flow patterns also act as a control on the distribution of debris.

4 Data collection and methods

For this study, field work was conducted at the Ngozumpa and Khumbu glaciers in November and December 2009. Multiple glacier surface measurements were collected, including VNIR-SWIR field spectra, land surface temperature (LST), and physical samples of surface snow, ice, meltwater, and debris. Field measurements were conducted in the middle ablation area of the Ngozumpa glacier (approx 4735–4790 m a.s.l.) and in the upper ablation area of the Khumbu glacier (approx 5100–5285 m a.s.l). Figure 3 and Table 1 detail the glaciers studied and in situ measurement locations.

4.1 Field spectrometry

Field spectra were measured using an Analytical Spectral Devices (ASD) FieldSpec Pro. The backpack portable laptop-driven FieldSpec Pro is comprised of three detectors that measure spectral reflectance from visible to shortwave infrared (0.35–2.5 µm). One VNIR 512-channel silicon photodiode detector operates along with two separately cooled, scanning, grated index SWIR indium gallium arsenide (InGaAs) photodiode detectors. Instrumental spectral resolution (full-width at half maximum) is 3 nm at 0.7 µm, 10 nm at 1.4 µm, and 12 nm at 2.1 µm, with spectral sampling steps of 1.4 nm from 0.35–1.05 µm and 2 nm from 1.05–2.5 µm (Analytical Spectral Devices, 2002). Field spectrometry reflectance measurement methods after Hall et al. (1992); Wiens et al. (2002) and Takeuchi and Li (2008) among others, were used in the field in order to allow for optimal comparison with satellite remote sensing data. More sophisticated field spectra measurement techniques (e.g. Sandmeier and Itten, 1999; Painter et al., 2003; Bourgeois et al., 2006) would have been desirable, however such equipment was not available nor logistically possible for use in this study.

Over 3360 spectra were collected from glacier snow, ice, debris, and vegetation categories at the Ngozumpa and Khumbu glaciers. Specifically, in excess of 1800 spectra were collected at the Ngozumpa glacier from 26–29 November 2009, while more than 1560 spectra were collected at the Khumbu glacier from 4–6 December 2009. Spectra were measured in ASD's raw mode on clear sky days within two hours of local solar noon (10:00 a.m.–2:00 p.m. LT). An 18° foreoptic and distances ranging from 10 cm to 1 m above the surface (relating to approximately 3 cm^2 to 30 cm^2 surface resolution, respectively) were used for spectral data acquisitions. A Spectralon calibration panel provided the reference reflectance material. For each targeted surface material, at least 20–30 ground based spectrometry measurements were collected in the nadir viewing direction. In situ sample sites were selected to cover a range of surface types, of both pure (e.g.: bare ice, snow, debris) and mixed targets (e.g.: snow and rock, ice and snow) – maximizing spectral acquisitions while maneuvering on the active debris covered glacier in the short solar noon temporal window. Spectral measurements were collected with the aim of assessing in situ reflectance measurements of both pure and mixed pixel spectral targets. Geographic location (GPS), surface temperature and physical samples were collected in conjunction with each set of spectral class measurements.

Determination of field spectrometry results involved converting instrumental raw mode digital numbers to spectral reflectance after Nicodemus et al. (1977). Measured target reflectance was divided by Spectralon calibrated reference surface reflectance, and multiplied by both calibration panel offsets and the user defined reflectance scale for each wavelength (0.35–2.5 µm). Due to FieldSpec Pro instrument variability from the 57 VNIR/SWIR individual optical fiber responses (MacArthur et al., 2007) as well as signal-to-noise ratios (Analytical Spectral Devices, 2002) and in order to compare field spectra with satellite spectral data, repeat field spectra over each target were averaged to form field spectral reflectance class signatures (here after referred to as spectral signatures).

4.2 Sample acquisition and analysis by X-ray diffraction and X-ray fluorescence spectrometry

In conjunction with spectral measurements, 19 samples of snow, ice, and melt water were collected in acid prepared 500 mL low density polypropylene Nalgene bottles, and 22 samples of supraglacial debris were collected in clean polyethylene bags (obtaining approximately 100 g of material per sample). All in situ samples were taken in duplicate and double polyethylene bagged. For this study, Ngozumpa and Khumbu glacier debris samples were analyzed for mineralogy and composition via powder XRD and XRF at the University of Oslo, Department of Geosciences (snow, ice and melt water results are presented in Casey et al., 2010). Debris samples were oven dried (2 days at 80 °C), crushed to a fine powder (less than 125 µm particle size) via a vibratory ringmill. Powder XRD was conducted via use of a Philips XPERT diffractometer (manufactured by PANalytical B.V., Almelo) with samples analyzed in FORCE Bulk Mode measuring from 2° to 65° 2Θ. Mineralogy was derived via use of PANalytical's X'pert Highscore software, with semi-quantitative peak area and weight factor estimates of percent composition were calculated after Moore (1997). For XRF, ten grams of oven dried fine powder was prepared into sample tablets and measured on a Philips PW2400 XRF spectrometer run via SuperQ Version 3 software in TRACES 7B mode. The following oxide compounds and trace elements were measured: SiO_2, Al_2O_3, Fe_2O_3, MgO, CaO, Na_2O, K_2O, and V, Co, Zn, Pb, Zr, Th, U. Accuracy of XRF results is 98%. XRD and XRF measurements along with field collected spectra and spectral library references provide an indication of Ngozumpa and Khumbu supraglacial debris mineralogy and composition.

4.3 Optical satellite data

To assess the potential of the unprecedented spectral data provided by current Earth observing sensors, satellite data from ALI, ASTER, Hyperion, and Landsat TM, ETM+ was used to investigate glacier debris cover in the Khumbu Himalayas. Spectral

analysis methods for debris cover characterization included: hyperspectral reflectance, SWIR and TIR false color image composites, mineral abundance mapping via SWIR and TIR band indices and VNIR-TIR spectral angle relationships, TIR emissivity and land surface temperature (LST) mapping, and repeat image derived velocity and streamline estimations. The specific satellite data products used are as follows: Hyperion radiometrically corrected Level 1T data, Landsat TM Level 1T and ETM+ Level 1G radiometrically and geometrically corrected data, and the following ASTER products, Level 1B radiance-at-sensor data, Level 2 AST_07XT "Surface Reflectance VNIR & Crosstalk Corrected", AST_05 "Surface Emissivity", and AST_08 "Surface Kinetic Temperature". A full discussion of EO-1 products is given in Beck (2003), Landsat products in Tucker et al. (2004) and Storey et al. (2005) and ASTER products in Abrams (2000) and Abrams et al. (2002). Satellite data acquisition dates, product names and methods used to investigate Khumbu Himalayan glacier debris cover are summarized in Table 2. Satellite remote sensing data were acquired with the closest temporal and seasonal (post-monsoon dry season) correlation in light of the previously mentioned instrument anomalies (Landsat ETM+ data prior to 2003 and ASTER SWIR data prior to 2008 are used).

For satellite reflectance analysis, digital numbers were converted to at-sensor radiance using sensor- and band-specific calibration settings (e.g.: gain, offset, solar irradiance). At-sensor radiance was converted to at-sensor (top-of-atmosphere) planetary reflectance for each band after Markham and Barker (1986) (Eq. 1).

$$\rho_{\mathrm{p}} = \frac{(\pi \times L_{\lambda} \times d^2)}{(\mathrm{ESUN}_{\lambda} \times \cos\theta_{\mathrm{s}})} \quad (1)$$

Where ρ_{p} is at-sensor planetary reflectance (unitless value from 0 to 100%),
L_{λ} is at-sensor radiance ($\mathrm{m\,W\,cm^{-2}\,sr^{-1}\,\mu m^{-1}}$),
d is the Earth-Sun distance (in Astronomical Units),
ESUN_{λ} is mean solar exoatmospheric irradiance ($\mathrm{m\,W\,cm^{-2}\,\mu m^{-1}}$),
θ_{s} is solar zenith angle in degrees.

Planetary reflectance can vary from surface reflectance due to absorption of gases and/or scattering effects of aerosols and gases in the atmosphere (Tanre et al., 1990). For example, at-satellite reflectance was found to increase 5–17% after atmospheric corrections were applied to Landsat TM data at Forbindels glacier in Greenland (Hall et al., 1990). Atmospheric planetary to surface reflectance correction, especially over snow and ice, remains in development (Kaufman, 1989; Lu et al., 2002; Stamnes et al., 2004; Mars and Rowan, 2010). Thus, atmospheric corrections were restricted to those applied in validated products (i.e. AST_07XT) and in the Landsat derived LST (after Barsi et al., 2005). Planetary reflectance is presented with regard to Hyperion debris covered glacier analysis, however a brief overview of atmospheric correction options for use with hyperspectral satellite data are discussed in Sect. 5.3.1.

Horizontal surface displacements on the glaciers studied were derived using normalized cross-correlation between repeat Landsat TM near-infrared as well as repeat ETM+ pan data (Kääb and Vollmer, 2000; Debella-Gilo and Kääb, 2011). Relative surface ages were estimated from streamlines as interpolated from the horizontal surface displacement velocity fields (Haug et al., 2010). Such streamlines resemble real particle trajectories only under the assumption that a velocity field is constant over time.

5 Results

Khumbu Himalayan debris covered glacier field spectrometry, XRD and XRF debris sample analysis, and optical remote sensing methodology study results are presented in the following subsections.

5.1 Field spectrometry

This section provides an overview of the 3360 plus visible to shortwave infrared ice, snow, and debris spectral reflectance measurements collected at Ngozumpa and Khumbu glaciers. To begin, Fig. 4 displays spectral signatures acquired for Ngozumpa

glacier fresh snow and Khumbu glacier bare ice in comparison with previous snow and ice reflectance measurements by Qunzhu et al. (1985); ASTER derived visible reflectance of bare ice for the Khumbu glacier measurement site is over plotted. Average standard deviation for Ngozumpa glacier fresh snow and Khumbu glacier bare ice spectral signatures is 0.011 and 0.002, respectively. Ngozumpa glacier snow and Khumbu glacier bare ice spectral signatures and ASTER derived spectral reflectance plot within documented reflectance variability (Qunzhu et al., 1985; Hall et al., 1990; Winther, 1993; Takeuchi, 2009). Reduction in the Ngozumpa glacier snow spectral signature, relative to the Qunzhu et al. (1985) fresh snow reflectance can be attributed to melt of several days; snow reflectance diminishes as snow grain size increases and melt progresses (O'Brien and Munis, 1975; Choudhury and Chang, 1979; Wiscombe and Warren, 1980; Warren, 1982; Dozier, 1989; Nolin and Dozier, 2000). Reduction in the Khumbu glacier bare ice spectral signature is attributed to ice pinnacles of roughly 2 to 10 m in height at the measurement location on the upper Khumbu glacier, beneath the icefall: spectra are lower in reflectance partially due to the mitigation of light caused by the ice pinnacle topography. Several snow and ice spectral signatures (clean snow, small particulate covered snow, gravel covered snow, half snow half ice "mixed pixel", and bare ice) collected in the upper Khumbu glacier are presented in Fig. 5. The half snow half ice "mixed pixel" spectral signature is roughly a linear mixture of the end-member clean snow and bare ice pure spectral signatures. Both fine particulates and gravel reduce visible reflectance of snow, with fine particulates displaying an absorption feature minima at approximately 0.5 µm, while larger scale gravel shows a more marked broad reduction in snow reflectance in the visible to near infrared, with absorption features beginning much earlier, at approximately 0.38 µm. A detailed investigation of all gravel on snow spectra suggested that absorption features similar to sillimanite gneiss ca. 0.35–1.0 µm (reference spectrum seen in Appendix A) is resolved upon fine-scale spectral inspection.

Variability in snow optical reflectance can be attributed to a variety of components, including mineral composition of dust, soot, and organic material (Gajda, 1958; Warren and Wiscombe, 1980; Warren, 1982; Takeuchi et al., 2001). Snow carotinoid and chlorophyll absorption features at 0.55 and 0.68 µm, respectively, have been reported by Painter et al. (2001) and Takeuchi (2009). Absorption features near the chlorophyll absorption area were found in Khumbu snow spectra, however, fine debris was clearly visible in many of the snow samples and algal growth was not expected to dominate at the time of spectral measurements – though known to exist in the area (Yoshimura et al., 2000). Nevertheless, it is interesting to consider the factors affecting VNIR absorption, including metal cations within fine particulate debris or surface algal organisms and subsequent influence of these cations on spectral reflectance signatures (i.e. further investigation combining known metal cation absorption features (Appendix A) and XRD/XRF derived surface composition (Appendix B) with in situ and hyperspectral reflectance data).

Supraglacial debris field spectra were used to identify minerals present in Ngozumpa and Khumbu debris cover using spectral library references (Clark et al., 2007), with further validation provided by XRD analysis. Figure 6 presents an example of upper Ngozumpa glacier supraglacial debris mineral composition – a mixture of biotite, quartz and albite from field sample 3N (Table 3, Appendix B). This upper Ngozumpa glacier supraglacial debris spectra resulted in an approximately linear mixture of the three mineral components – biotite, quartz, and albite. Specifically, the slope of the biotite spectral library reference as well as the hydroxide related 1.4 µm OH bond absorption features from the quartz and albite reference spectra each are seen in the upper Ngozumpa debris mixture spectral signature. The standard deviation of the debris spectral signature was calculated at 0.013. Similar standard deviation magnitudes were found in the majority of spectral signatures – suggesting low variability within spectral measurements. To note, comparisons of debris spectral signatures with spectral library references should be regarded as qualitative – as spectral library reference spectra are from region specific, synthesized or altered materials, measured under

optimal or laboratory conditions with controlled factors that can impact spectral measurement (i.e.: illumination, temperature, pressure, humidity, wind) (Siegal and Abrams, 1976; Gupta, 2003).

Finally, the influence of melt water in fine particulate debris cover was observed in the supraglacial debris spectral signatures. The SWIR portion of the spectrum manifests characteristic water absorption features, which allow the amount of surface debris moisture to be estimated (Angstrom, 1925; Bowers and Hanks, 1965; Skidmore et al., 1975; Lobell and Asner, 2002). Ngozumpa supraglacial debris spectra presented in Fig. 7 of visually dry and wet mud display the subsequent variability in reflectance intensity. While general shapes of reflectance spectra are maintained, the amount of melt water determines the degree of reflectance intensity. Using reflectance moisture estimation (e.g. Bowers and Hanks, 1965; Liang, 2004; Zheng et al., 2005), water content was estimated at 5% and 15–20% from the two debris spectral signatures on the upper Ngozumpa glacier site. Spectral estimated supraglacial moisture content could be of key interest to glaciologic energy balance modelers, as debris moisture information is necessary for calculation of soil surface albedo (Liang, 2004). Improved supraglacial debris surface albedo could reduce errors in predictions of glacier ablation rates and mass loss.

5.2 X-ray diffraction and X-ray fluorescence measurements

Ngozumpa and Khumbu supraglacial debris rock, gravel, soil and silt mineralogy was determined by XRD to consist primarily of quartz, potassium feldspars (orthoclase and microcline), feldspars (albite, calcium albite), carbonates (calcite, ankerite, siderite), and micas (muscovite, phlogopite, biotite) (Table 3, Appendix B). These mineral classifications can be visualized in the reflectance and emission spectra of the dominant minerals (Appendix A) and will be further referred to in the optical remote sensing mineral mapping techniques discussed below (Sect. 5.3.3). Ngozumpa glacier samples were primarily quartz, feldspar – in the form of calcium albite, and mica – in the form of biotite, while Khumbu samples were primarily mica – in the form of muscovite, feldspar

– in the form of calcium albite and quartz. XRD mineralogy results indicated minor percentages of calcite in 7 of the 8 Ngozumpa glacier samples, and 2 of the 14 Khumbu glacier samples, and trace amounts of chlorites in 2 of the 8 Ngozumpa glacier samples, and 9 of the 14 Khumbu glacier samples. XRD results from this study were found to be comparable with published data by Searle et al. (2003) among others detailed in (Sect. 3).

XRF oxide and trace element quantitative results provide validation for supraglacial debris reflectance characteristic investigation – as briefly covered in the previous section. XRF silica measurements are also compared with ASTER based silicate mapping results (Sect. 5.3.3). Primary mineral and XRF determined silica weight percent results are displayed in Table 3 and full XRF analytical results are given in Appendix B. These XRD/XRF supraglacial debris results provide quantitative data on the Khumbu and Ngozumpa glaciers not previously reported.

5.3 Optical satellite data

The ASTER Level 2 atmospherically and cross-talk corrected surface reflectance data product (AST_07XT) was utilized for comparison with in situ surface reflectance (subsequent satellite methods investigate planetary reflectance of glacier surfaces). An average of nearest satellite reflectance pixels to the in situ sample location – 4 × 4 pixels in visible bands, and 2 × 2 pixels in SWIR bands, corresponding to a spatial resolution of 60 m^2 – was chosen for comparison due to the temporal disparity between in situ acquired data and satellite derived data (6 years) and the velocity of the glaciers (roughly from 10–50 m per year) (Sect. 5.3.5). Although these temporal and spatial disparities are not ideal for comparisons (due to potential surface movement of studied lithology over time or in situ point to 60 m^2 spatial differences), a first-order assessment of lithologic characteristics and mapping is worthwhile, especially in this region with the thick debris cover and relatively low velocities. The ASTER spectral signature shape and absorption features match relatively well with the in situ spectral signatures, for example, shown in ice and debris comparisons (Figs. 4 and 6, respectively).

In the following sections, the results of further VNIR-TIR methods for supraglacial debris characterization are presented, including: hyperspectral satellite reflectance, shortwave and thermal false color composites, mineralogic mapping, land surface temperature, and glacier velocity.

5.3.1 Hyperspectral remote sensing

Hyperion VNIR-SWIR hyperspectral satellite data is evaluated on Khumbu Himalayan debris covered glaciers. Although Hyperion coverage of in situ measurement sites does not exist at the time of publication, Hyperion imaging of nearby Lhotse Shar and Imja glaciers from 13 May 2002, and nearby Gyubanare and Khangri Nup glaciers (as well as approximately 100 m of the very terminus of Ngozumpa glacier) from 4 October 2010 were analyzed for general supraglacial debris characteristics. Hyperion Level 1 GST terrain-corrected data was converted from digital number to at-sensor radiance to planetary reflectance (Eq. 1). Hyperion planetary reflectance spectral signatures of Imja and Lhotse Shar supraglacial debris and ice are shown in (Fig. 8) along with an ALI true color 10 m pan enhanced image composite from 4 October 2010. The spectral planetary reflectance graph shows distinctions between the two supraglacial debris types; qualitative transition metal, hydroxyl and carbonate absorption area differences are demonstrated at 0.4–0.8, 2.1, and 2.1–2.3 µm, respectively. Ice, snow, and general mineral class qualitative differentiation was also achieved on Gyubanare and Khangri Nup glaciers in the 4 October 2010 Hyperion scene.

Quantitative VNIR-SWIR mineral differentiation via Hyperion requires atmospheric correction as seen in the Lhotse Shar ice planetary reflectance spectral signature with prominent atmospheric effects (Fig. 8). Another limitation to Hyperion data use is relatively low signal-to-noise ratios of approximately 50:1, compared with 500:1 for airborne hyperspectral imaging (Pearlman et al., 2003; Kruse et al., 2003). Several commercially available atmospheric and spectral correction software programs include, but are not limited to Atmospheric and Topographic Correction (ATCOR), ATmosphere REMoval algorithm (ATREM), and MODTRAN4 radiative transfer based Atmosphere

CORrection Now (ACORN) and Fast Line-of-sight Atmospheric Analysis of Spectral Hypercubes (FLAASH) and are described in Gao et al. (2009). Hyperion-specific atmospheric correction approaches remain in discussion (e.g. Dadon et al., 2010; Wang et al., 2010). Unfortunately, commercial atmospheric correction software was not available to the authors, and simplified atmospheric correction methods – such as dark object subtraction – rescale entire band arrays, potentially masking valuable spectral information (Kääb, 2005; Ninomiya et al., 2005). Thus, Hyperion planetary reflectance supraglacial debris evaluation is qualitative in this study.

Without atmospheric correction, a few other methods in addition to qualitative reflectance can be used to analyze Hyperion data. For example, true and false color composites as well as at-sensor radiance indices can be utilized and are discussed below in Sects. 5.3.2 and 5.3.3, respectively. As a technological demonstration, Hyperion VNIR-SWIR spectral analysis of mineralogy and lithology proves promising (e.g. Griffin et al., 2005; Gleeson et al., 2010). Theoretically, Hyperion data used in conjunction with commercial spectral and atmospheric correction software could be successful in discriminating small-scale wavelength and absorption depth-dependent characteristics of supraglacial debris (e.g. using continuum removal techniques (Clark and Lucey, 1984) to determine debris components and concentrations).

5.3.2 Shortwave and thermal false color composites

As suggested in the above hyperspectral remote sensing section, false color image composites highlight components not evident in true color images (e.g., Fig. 3). In addition to the VNIR-SWIR spectral resolution provided by ALI and Hyperion sensors, Landsat and ASTER offer thermal spectral bands (Fig. 1) that can be used to identify and classify glacier debris cover (Kääb, 2005). Landsat ETM+ thermal band 6 (11 µm) allows for spectral emission analysis of carbonate and silicate content in supraglacial debris, and Landsat ETM+ SWIR bands 5 and 7 (1.65 and 2.2 µm, respectively) indicate hydroxyl content, common to clays and hydrated silicates (see Appendix A for spectral features). Figure 9 displays a Landsat ETM+ SWIR band 5, 7 and TIR band

6 false color (red, green, blue – RGB) image composite from 24 January 2003 of Ngozumpa and Khumbu field study sites as well as regional glaciers. Supraglacial debris composition variability is displayed by the coloring – yellow indicates silica-rich granites, while blue highlights carbonate-rich gneiss. For example, the Khumbu glacier longitudinal schistic supraglacial debris band starting from the icefall down the center of the glacier reported by Fushimi et al. (1980) can be visualized in blue in the Fig. 9 false color composite, with lateral granite debris bands visualized in yellow. Similar carbonate-rich vs. silica-rich longitudinal supraglacial debris bands are visible on upper Ngozumpa glacier.

False color SWIR/TIR composites quickly visualize supraglacial mineral variability. Although similar total SiO_2 content was found at all six Ngozumpa and Khumbu in situ samples sites (Appendix B and Table 3), the more uniform spatial distribution of silicates on Ngozumpa glacier can be easily differentiated from the more distinct silicate-rich vs. carbonate-rich mineral classes found on the Khumbu glacier using the SWIR/TIR false color composite technique. Further, false color composites can provide an indication of mass flux. In Fig. 9, a suggestion of limited mass flux transferred to at glacier confluences can be seen at the Khangri Shar, Khangri Nup and Khumbu glacier confluence as well as the Gyubanare, Ngozumpa glacier confluence by the distinct shifts in supraglacial mineralogy.

5.3.3 Mineralogic mapping

The rich SWIR and TIR spectral resolution provided by ASTER allow for qualitative and quantitative approaches to mapping surface mineralogy. Three such approaches are presented in this section. First, SWIR and TIR based mineralogic indices are evaluated using ASTER at-sensor radiance data. Second, TIR emissivity silica weight percent mapping is presented. Third, the Spectral Angle Mapper (SAM) algorithm after Kruse et al. (1993), is discussed for semi-automated identification of supraglacial components. The three types of mineral mapping provide different advantages and limitations in characterizing supraglacial lithology. Of the methods, SAM is unique in the

potential to use discrete bands from the full VNIR-TIR spectrum, while TIR emissivity silica weight percent and mineral indices offer more quantitative estimates of specific mineral abundances.

SWIR Indices

SWIR mineral indices use wavelength dependant spectral absorption features to estimate mineral abundance. Several mineral indices are available and were evaluated (e.g. Vincent and Thomson, 1972; Ninomiya, 2003, 2004; Ninomiya et al., 2005). Based on the dominant minerals in the Khumbu Himalaya study area, the layered silicate index (LS) (Eq. 2) and calcite index (CA) (Eq. 3) after Ninomiya (2003) are presented in this study.

$$\mathrm{LS} = \frac{(\mathrm{AST4} \times \mathrm{AST8})}{(\mathrm{AST5} \times \mathrm{AST6})} \quad (2)$$

$$\mathrm{CA} = \frac{(\mathrm{AST6} \times \mathrm{AST9})}{(\mathrm{AST8}^2)} \quad (3)$$

Where AST*n* corresponds to ASTER spectral band number *n*.

The LS and CA SWIR indices target bands that measure hydroxyl (2.2 µm) and carbonate (2.35 µm) absorption features, respectively (See Appendix A). At-sensor radiance band ratios reduce atmospheric and topographic influences (including illumination variability) (Abrams et al., 1983; Mather, 1987; Kääb, 2005), highlight information not evident in single band or three-band true or false color composite images, and provide a quantitative estimate of mineral abundances. Layered silicate mineral abundance at Ngozumpa and Khumbu glaciers calculated from (Eq. 2), ASTER L1B at-sensor radiance data from 29 November 2005 is shown in Fig. 10. SWIR mineral index values can be further applied as thresholds in algorithms or in creation of thematic mineral abundance maps. For the scope of this study a grayscale image with darker shades indicating lower amounts of silicates and brighter shades indicate higher amounts of

silicates is presented. This grayscale silicate index map can also be used to quickly visualize kinematic flow, similar to that reported in Sect. 5.3.2. However, in addition to visualization, the SWIR LS and CA indices offer quantifiable mineral-specific abundances.

TIR Indices

Thermal at-sensor radiance indices after Ninomiya et al. (2005), offer the first strictly thermal spectrum based technique presented in this study. The thermal portion of the spectrum is described as the most important region of the spectrum for differentiating geology of terrestrial materials (Gupta, 2003). However, satellite spatial resolution in the thermal bands is considerably lower than VNIR or SWIR (e.g. in ASTER VNIR 15 m, SWIR 30 m, TIR 90 m spatial resolution). Nevertheless, TIR indices are utilized to study the abundance of the following minerals (and mineral groups) in the study region glacier debris cover: quartz, silicate, and carbonate. Rocks containing these mineral groups express characteristic emission features in the thermal infrared (see also Appendix A). TIR based band ratios to estimate carbonate, quartz and silica containing lithology are presented in Eqs. (4–6) (Ninomiya et al., 2005).

$$\mathrm{CI} = \frac{(\mathrm{AST13})}{(\mathrm{AST14})} \tag{4}$$

$$\mathrm{QI} = \frac{(\mathrm{AST11}^2)}{(\mathrm{AST10} \times \mathrm{AST12})} \tag{5}$$

$$\mathrm{MI} = \frac{(\mathrm{AST12} \times \mathrm{AST14}^3)}{(\mathrm{AST13}^4)} \tag{6}$$

Where AST*n* corresponds to ASTER spectral band number *n*.

The carbonate index (CI) is utilized to detect the primary carbonate minerals calcite and dolomite – with high values of CI indicating presence of these minerals (absorption features at 11.4 µm for calcite, 11.2 µm for dolomite). Further, pure carbonate will

provide a high CI value in conjunction with and low QI and MI values. The quartz index (QI) not only is indicative of quartz, but also low QI values signal potassium feldspar and gypsum. The mafic index (MI) correlates with silicate content, and is also sensitive to carbonate content in rocks. A simple silicate index ratio of band 12 to band 13 can be used – but for the differentiation from carbonates, Eq. (6) is used. A MI value greater than 0.90 corresponds to mafic rocks, while a MI value greater than 0.92 corresponds to ultramafic rocks (Ninomiya et al., 2005). To note, Ninomiya et al. (2005) concluded the stability of TIR mineral indices irrespective of surface temperature, elevation and atmospheric condition.

TIR emissivity to map silica abundance

Another technique to extract the dense geologic information available in the thermal bands is emissivity derived silica abundance mapping. Satellite emissivity weight percent of silica (SiO_2) after (Hook et al., 1992; Miyatake, 2000; Watanabe and Matsuo, 2003) is evaluated on Khumbu Himalaya supraglacial debris. Equation (7) (after Watanabe and Matsuo, 2003) displays the SiO_2 weight percent from emissivity values of ASTER TIR bands 10, 11, 12, and 13.

$$\mathrm{SiO_2} = 56.20 - 271.09 \times \log\left[\frac{(\mathrm{ASTe10} + \mathrm{ASTe11} + \mathrm{ASTe12})}{(3 \times \mathrm{ASTe13})}\right] \tag{7}$$

Where ASTe*n* corresponds to ASTER AST_05 surface emissivity product band number *n*.

Using the ASTER Surface Emissivity AST_05 product, silica weight percent abundance was derived for the Khumbu Himalaya region glaciers (Fig. 11). The ASTER derived silica weight percent estimates were compared with in situ XRF determined SiO_2 weight percent, with general agreement in consideration of the spatial resolution variation from in situ to 90 m^2 (ASTER TIR resolution) as well as the temporal resolution discrepancy of approximately 6 years (Table 3). Specifically, the difference between the XRF derived silica weight percent and TIR emissivity calculated silica weight percent

of the Ngozumpa and Khumbu glacier field measurement sites ranged from a 4.0 to 15.1 percent difference. This technique has been found to allow quantitative estimates of silica content from daytime TIR acquisitions (Hook et al., 2005). Further, mapping of silica content in supraglacial debris covered glacier areas may potentially provide a first order look at glacial activity, sediment transport, weathering processes, glacial erosion or areas prone to differential melt based on differing supraglacial debris composition. Further, in the Khumbu Himalaya test region, the silica percent thematic map outlined debris covered ice extent.

Spectral angle mapper

Finally, the spectral angle mapper (SAM) algorithm provides a powerful means to classify surface materials. The SAM classification algorithm evaluates general shape and angles user input spectral data to assign thematic mineral and non-mineral classes (Kruse et al., 1993). SAM is suggested by Dematte et al. (2004) and Chen et al. (2007) as the optimal method for classifying surface lithology due to the integration of VNIR, SWIR and TIR data for spectral signature identification. Chen et al. (2007), found SAM to particularly outperform other minimum-distance classification and spectral feature fitting when analyzing silicates, carbonates and other minerals expressing TIR absorption over arid terrain. SAM was evaluated in this study (using ASTER L1B data) and preliminary SAM analysis on Khumbu glacier provided successful first-order differentiation of bare ice, snow, silica, calcite, and vegetation land cover. In comparison to the previously mentioned lithologic mapping methods, an advantage of SAM is the ability to map not only mineralogy, but also other land cover types, including snow, ice, and vegetation within the same classification and without requiring a full hyperspectral data set. Further, sensitivity to illumination and albedo data acquisition effects are addressed by the SAM algorithm design.

5.3.4 Land surface temperature

Another thermal spectral band based glacier surface mapping technique is calculation of land surface temperature (LST) on glaciers. Thermal band derived LST was evaluated from the ASTER AST_08 Land Surface Temperature product, as well as from calculated Landsat the ETM+ and TM thermal band (after Barsi et al., 2005; explained in Hall et al., 2008) over Ngozumpa and Khumbu glaciers. Due to the nearly temporal coincidence of Landsat TM (31 October 2009) and in situ LST measurements (November, December 2009), Landsat TM data was utilized for satellite derived glacier debris cover LST analysis. Figure 12 shows Landsat TM calculated LST on Khumbu glacier, and Fig. 13 for Ngozumpa glacier. A longitudinal LST transect from the Khumbu icefall approximately 2 km down glacier displays a 15 °C increase in temperature. A similar Khumbu glacier LST trend is reported in Nakawo et al. (1999), and in Hall et al. (1987) using Landsat TM calculated LST.

In situ glacier surface temperatures measured in November and December 2009 field work sites were compared with the Landsat TM 31 October 2009 derived surface temperatures. In situ temperatures measured of snow, ice, and debris were averaged at each of the three Ngozumpa and three Khumbu glacier measurement locations. For example, in situ temperatures of 0.4 °C for upper Khumbu, 2.4 °C for mid-Khumbu, and 6.7 °C for lower Khumbu sample sites relate to Landsat TM 120 m pixel resolution LST's of −3.2, 4.8, 3.4 °C, respectively. In consideration of the spatial and temporal resolution disparities (satellite acquisition time 10 a.m. with some areas in shadows vs. in situ measurement disparity 2 h about solar noon, also point to 120 m^2 spatial disparity), general agreement was found between temperature measurements.

Used in conjunction with LST, other optical remote sensing supraglacial characterization methods may improve input toward glaciologic energy balance models. For example, LST and debris composition, could be analyzed to estimate differential solar absorption and subsequent impacts to ice melt rates (e.g.: Ngozumpa glacier measured gneiss surface temperature 24.1 °C vs. granitic debris 11.0 °C, and as shown in calcite index (Eq. 3), LST across Ngozumpa glacier transect Fig. 13).

5.3.5 Glacier velocity, streamlines

Repeat optical Landsat images were used to derive glacier velocities at Ngozumpa and Khumbu glaciers. Specifically, normalized cross-correlation between Landsat ETM+ orthorectified 15 m pan data from 30 October 2000 and 4 October 2002 was used to derive a velocity displacement field. Velocity measurement errors were detected and filtered using a threshold on the correlation coefficient. Some remaining spurious vectors were removed manually. To ensure that the glacier surface velocities did not change significantly between 2000–2002 and the time of our in situ sampling, displacements were also derived from 30 m spatial resolution near-infrared band Landsat TM data from 5 November 2005 and 31 October 2009. No significant temporal changes were found. Optical feature tracking based velocity of both the Ngozumpa and Khumbu glaciers is estimated at 60 m/yr in the upper ablation zones to less than 5 m/yr in the lower ablation zones with errors estimated to be approximately 8–15 m for the ETM+ pan derived displacements (0.5–1 pixel; i.e. 4–7 m/yr) (Fig. 14). Glacier velocity rates estimated in this study are comparable to Khumbu Himalayan glacier velocity rates derived from synthetic aperture radar (SAR) feature tracking (Luckman et al., 2007; Hambrey et al., 2008; Quincey et al., 2009) as well as optical imagery (SPOT – Seko et al., 1998; Ikonos and ASTER – Bolch et al., 2008b; and COSI-Corr (Co-registration of Optically Sensed Images and Correlation, from Leprince et al., 2007) derived ASTER – Scherler et al., 2008). (Note, Quincey et al. (2009) derived Ngozumpa glacier velocity, while all other listed references refer to Khumbu glacier velocity studies.)

Further, theoretical supraglacial particulate streamlines on Ngozumpa and Khumbu glaciers were calculated and indicate time scales of 380 and 450 years, respectively (Fig. 14). Streamline interpolation stops at locations on glacier when velocities decrease below the margin of error – around 4 m/yr. Thus, 380 year Ngozumpa and 450 year Khumbu glacier streamline estimations represent minimum glacier ablation area ages. The Khumbu glacier streamline estimate from this study corresponds well with the Fushimi (1978) in situ, structural-derived estimate of Khumbu glacier ice at 410 ± 110 years.

The glacier ablation area velocity rates, directional flow vectors, as well as streamline estimations provide a "time scale" of the glacier ablation zone. Use of optical satellite remote sensing velocity and streamline approximations provide a powerful tool to use in conjunction with the previously discussed lithologic mapping techniques. For example, streamline dating could be utilized to give a crude, first-order approximation of "debris age" by supraglacial debris type. First-order streamlines, used with robust glaciologic sediment dating studies, such as Benn and Owen (2002); Owen et al. (2009), could roughly estimate glacier sediments dates of regional glaciers lacking field studies.

Velocity vectors indicate debris transport paths which can be compared to debris source and glacial transport paths observed from multi- and hyperspectral derived lithologic differences. Difference between current velocity fields and cumulative transport paths derived from lithology suggests a change of glacial mass movement over time, for example, represented by surges and looped moraines. Further, velocities and streamlines together with supraglacial lithologic information can improve estimations of expected weathering and diagenesis of debris.

6 Synthesis

From the several methods explored in this study, some of the most significant synergistic applications include, spectral based supraglacial component identification, description of mass flux, indication toward weathering and activity, estimation of thermal parameters, as well as mapping of debris covered ice extent.

Use of in situ VNIR-SWIR spectral signatures allow for identification of supraglacial components, for example of Khumbu snow and ice types (Fig. 5) or Ngozumpa supraglacial debris variability and moisture content (Figs. 6 and 7). Supraglacial mineral compositions can be used to indicate sources of lithology and subsequent diagenesis. Satellite spectral reflectance – Hyperion and ALI with 196 and 9 VNIR to SWIR spectral bands, respectively, and ASTER and Landsat with 14 and 7 VNIR to TIR spectral bands, respectively – provide potential to identify supraglacial components by spectral signatures (e.g., Hyperion qualitative planetary reflectance Sect. 5.3.1,

Fig. 8, SAM algorithm Sect. 5.3.3). Differentiation of glacier debris can allow for analysis of glacier debris sources and multidimensional debris transport paths (Figs. 9 and 10). Further, mineral indices and emissivity can also be used for identification or relative abundances of minerals in supraglacial debris, such as calcite abundance on Ngozumpa glacier (Eq. 3, Fig. 13) or Khumbu Himalaya regional silicate supraglacial abundance (Figs. 10 and 11). Synergistic inspection of supraglacial debris variability can bridge the gap in detecting debris sources and using identified components to describe glaciologic parameters such as supra- or englacial glacial transport routes.

A second important combined application of the optical remote sensing methods is in describing glacier mass flux. False color composites visually allow for speculation of mass flux; in conjunction with repeat imagery velocity and supraglacial particulate flow estimations, a more quantitative estimate of mass transport can be made. For example, Fig. 9 visually indicates limited to negligible transport of mass from Khangri Shar and Khangri Nup glaciers at the convergence with Khumbu glacier by the distinct visual supraglacial debris types. Repeat optical image matching velocity and streamlines (Fig. 14) further give low velocities and flow from Khangri Shar and Khangri Nup glaciers into the Khumbu glacier. This limited mass flux can also be seen in such a false color composite, velocity comparison at Gyubanare glacier confluence with Ngozumpa glacier (Figs. 9 and 14). Streamlines provide a first-order assessment of supraglacial movement (Sect. 5.3.5). Further, input of material to glacier surfaces, such as from a rock avalanche of distinct lithology, can be detected and characterized with false color composites. This supraglacial mass flux analysis is describes not only present day, but also years and decades past due to the debris patterns archived in the supraglacial debris.

Description of supraglacial activity and weathering processes is a third important synergistic application of the optical remote sensing debris characterization methods. Emissivity percent silica mapping may provide information on glacier activity rates and diagenesis (Fig. 11). In the Khumbu Himalaya test region, a silica percent thematic map provided indication of debris covered ice extent, and compared with repeat image

velocity estimations, areas of higher velocities had correspondingly high silica composition. Supraglacial activity can also be indicated by the SWIR and TIR mineral indices – Fig. 10 suggests glacier kinematic pulses have occurred on the upper Ngozumpa glacier. Furthermore, the type of the material can be pinpointed by hyperspectral reflectance signature data – potentially confirming pre-weathered (or higher silica content) supraglacial debris material, for example in the upper ablation zone, and more heavily weathered (lower silica content) supraglacial debris in the lower ablation zone.

A fourth area of importance to glaciologic remote sensing is describing thermal supraglacial characteristics. Surface temperature can be calculated from sensors which acquire thermal data. In this study Landsat and ASTER surface temperature data was evaluated at Khumbu and Ngozumpa glaciers (Figs. 12 and 13). Glacier surface temperature was found to vary depending on the amount of debris cover as well as the composition of the debris and position on glacier. Temperature in conjunction with debris moisture content estimates (Fig. 7), hyperspectral mineral differentiation (Fig. 8), and/or mineral abundances (Fig. 10), more accurately describes surface parameters and could be crucial to reducing errors in satellite derived ablation rates and processes. Even further synergy of thermal and velocity data could be used to investigate climate interaction with debris covered ice, and to assess stagnation of flow toward the glacier terminus, the formation of supraglacial meltwater and subsequent glacial disintegration. Such glacier debris pattern analysis could reveal low magnitude, high repeat frequency mass events vs. episodic pattern high magnitude event, low frequency mass events. Spectral reflectance of debris covered ice can provide insight toward differential surface radiative absorption.

Finally, mapping of debris covered ice remains a challenge for optical remote sensing. Combination of methods presented in this study, for example the silica thematic mapping (Fig. 11), false color SWIR/TIR composites (Fig. 9), surface temperature (Figs. 12 and 13), and velocity (Fig. 14) methods all provide estimations of debris covered ice extent. Use of these techniques over debris covered ice area may be useful in improving debris covered glacier mapping.

7 Conclusions

Debris often covers a moderate to significant portion of glacier ablation areas. We estimate debris to cover approximately 15% of Hindu Kush Himalaya glaciers, relating to 8000 km^2 of debris covered ice. The presence and extent of supraglacial debris impacts radiative and surface processes of glaciers, and characterization of this debris can be used to indicate sources, paths and magnitudes of glacial transport as well as energy balance related glaciologic variables.

This study identified significant variability in the debris cover in the Khumbu Himalayan region glaciers. In situ hyperspectral imaging and XRD/XRF geochemical analysis was used to identify minerals, mineral mixtures, and moisture content of Ngozumpa and Khumbu glacier debris. Satellite planetary reflectance hyperspectral imaging was used to qualitatively differentiate surface components on Imja, Lhotse Shar, Gyubanare and Khangri Nup glaciers. We mapped supraglacial debris silica and calcite mineral abundances quantitatively with SWIR and TIR mineral indices, and silica weight percent quantitatively with TIR emissivity mapping across Khumbu Himalaya regional glaciers. Qualitatively, supraglacial mineral variability of Khumbu Himalayan glacier debris was mapped with false color SWIR/TIR image composites and differentiated silica-rich granite debris from carbonate-rich gneiss debris. Using false color image composites, mineral indices and repeat image derived velocity data, reduced glacial confluence mass flux of Gyubanare into Ngozumpa and Khangri Nup to Khumbu was determined. Similarly, the SWIR silica mineral index highlighted distinct kinematic pulses on the upper Ngozumpa glacier. Supraglacial temperatures were compared with calcite supraglacial debris abundance across Ngozumpa glacier and increased calcite supraglacial composition was found to correlate with increased supraglacial temperatures.

Synergistic application of the optical remote sensing supraglacial characterization methods presented are relevant to debris covered glaciers on a global scale in improving glaciologic interpretations of thermal, mass flux and debris covered ice extent.

Tuning the methods to the lithology of the region, debris covered glacier extent mapping may be delineated with combined use of false color composites, silica thematic mapping or region-specific mineral abundances, velocity fields and supraglacial temperature. Key methods applicable to thermal parameters include debris moisture estimations and use of mineral abundances to investigate supraglacial temperature variability. Kinematic processes are highlighted by combination of false color composites and mineral indices with velocity displacement fields and streamlines. Further, techniques can even be used to bridge the gap between field measurements and satellite based glacier estimations (e.g. with regard to improving glacier melt modeling).

Crucial to application of these methods in debris covered glacier monitoring is satellite sensor longevity and future sensors availability. As previously noted, some satellite instruments used in this study are no longer functioning optimally (Landsat ETM+ SLC gaps post 2003, ASTER SWIR failure post 2008). Landsat TM (and ETM+ gap-filled), ASTER VNIR and TIR as well as EO-1 ALI and Hyperion sensors offer current freely available spectral data sources. Forthcoming NASA optical satellite remote sensing missions include the National Polar-orbiting Operational Environmental Satellite System Preparatory Project (NPP) and National Polar-orbiting Operational Environmental Satellite System (NPOESS). ESA's Sentinel satellites with optical sensors aimed at collecting 10 m spatial resolution and 5 day temporal resolution prove extremely promising for glacier studies. Airborne hyperspectral sensors may be important tools to utilize during spaceborne instrumentation gaps.

High spectral and spatial resolution optical remote sensing is paramount for glacier monitoring. The wealth of current spectral satellite data has the potential to be used more broadly in supraglacial debris variability assessment. Improved satellite glacier debris cover characterization will lead to reduction of uncertainties in glacier extent mapping, glaciologic thermal parameters as well as glacial kinematic history and flow estimations, ultimately potentially advancing our understanding of debris covered ice ablation and mass loss.

Acknowledgements. This work was funded by the Department of Geosciences at the University of Oslo, Norway and European Space Agency's GlobGlacier project aimed at establishing protocols to map the world's glaciers via satellite remote sensing observations (Loan 585.1210 to DIB). We thank Alasdair MacArthur and Chris MacLellan of the Natural Environment Research Council Field Spectroscopy Facility for assistance with the field spectrometer loan. We also thank University of Oslo Department of Geosciences personnel Ruikai Xie and Berit Løken Berg as well as Misganu Debella-Gilo for assistance with XRD/XRF and velocity analysis, respectively. Thanks to Geir Moholdt for reviewing an earlier version of the manuscript. A special acknowledgement is due to Nima Sampang Rai for his help during field work in Nepal, as well as Rajesh Thapa and Samjwal Bajracharya at the International Centre for Integrated Mountain Development *ICIMOD* for logistic support in Kathmandu, Nepal.

References

Abrams, M. J.: The advanced spaceborne thermal emission and reflection radiometer (ASTER): data products for the high spatial resolution imager on NASA's Terra platform, Int. J. Remote Sens., 21(5), 847–859, 2000. 504, 511

Abrams, M. J., Brown, D., Lepley, L., and Sadowski, R.: Remote sensing for porphyry copper deposits in Southern Arizona, Econ. Geol., 78, 591–604, 1983. 520

Abrams, M. J., Hook, S. J., and Ramachandran, B.: ASTER user handbook, available at: http://asterweb.jpl.nasa.gov/content/03_data/04_documents/aster_user_guide_v2.pdf, last access: 4 August 2010, 2002. 511

Adhikary, S., Nakawo, M., and Seko, K.: Dust influence on the melting process of glacier ice: experimental results from Lirung Glacier, Nepal Himalayas, Chapt. Debris-Covered Glaciers, IAHS, Oxfordshire, UK, 43–52, 264, 2000. 501

Ageta, Y. and Higuchi, K.: Estimation of mass balance components of a summer-accumulation type glacier in the Nepal Himalaya, Geogr. Ann. A, 66, 249–255, 1984. 507

Analytical Spectral Devices, I.: FieldSpec Pro User's Guide, available at: http://support.asdi.com/Document/Viewer.aspx?id=19, last access: 5 October 2010, 2002. 508, 509

Andreassen, L. M., Paul, F., Kääb, A., and Hausberg, J. E.: Landsat-derived glacier inventory for Jotunheimen, Norway, and deduced glacier changes since the 1930s, The Cryosphere, 2, 131–145, doi:10.5194/tc-2-131-2008, 2008. 503

Angstrom, A.: The albedo of various surfaces of the ground, Geogr. Ann., 7, 323–342, 1925. 515

Anthwal, A., Joshi, V., Sharma, A., and Anthwal, S.: Retreat of Himalayan glaciers – indicators of climate change, Nat. Sci., 4(4), 53–59, 2006. 506

Atwood, D., Meyer, F., and Arendt, A.: Using L-band SAR coherence to delineate glacier extent, Can. J. Remote Sens., 36, S186–S195, 2010. 501

Baldridge, A., Hook, S., Grove, C., and Rivera, G.: The ASTER spectral library version 2.0, Remote Sens. Environ., 113, 711–715, 2009. 505

Barsi, J. A., Schott, J. R., Palluconi, F. D., and Hook, S. J.: Validation of a web-based atmospheric correction tool for single thermal band instruments, vol. 5882, Proceedings of SPIE, SPIE, Bellingham, Washington, USA, 2005. 512, 524

Beck, R.: EO-1 User Guide v.2.3, available at: http://edcsns17.cr.usgs.gov/eo1/documents/EO1userguidev2pt320030715UC.pdf, last access: 18 October 2010, 2003. 511

Benn, D. I. and Evans, D. J.: Glaciers and Glaciation, Hodder Education, London, 2010. 501, 507

Benn, D. I. and Owen, L. A.: The role of the indian summer monsoon and the mid-latitude westerlies in Himalayan glaciation: review and speculative discussion, J. Geol. Soc. London, 155, 353–363, 1998. 507

Benn, D. I. and Owen, L. A.: Himalayan glacial sedimentary environments: a framework for reconstructing and dating the former extent of glaciers in high mountains, Quatern. Int., 97–98, 3–25, 2002. 506, 507, 526

Benn, D., Wiseman, S., and Hands, K.: Growth and drainage of supraglacial lakes on the debris-mantled Ngozumpa Glacier, Khumbu Himal, Nepal, J. Glaciol., 47, 626–638, 2001. 506

Bishop, M. P. and Shroder Jr J.F., and Hickman, B.: SPOT panchromatic imagery and neural networks for information extraction in a complex mountain environment, Geocarto Int., 14(2), 19–28, 1999. 505

Bolch, T., Buchroithner, M. F., Kunert, A., and Kamp, U.: Automated delineation of debris-covered glaciers based on ASTER data, in: GeoInformation in Europe, in: Proceedings of 27th EARSeL Symposium, Bozen, Italy, 4–7 June 2007, 403–410, 2007. 501, 505

Bolch, T., Buchroithner, M., Pieczonka, T., and Kunert, A.: Planimetric and volumetric glacier changes in the Khumbu Himal, Nepal, since 1962 using Corona, Landsat TM and ASTER data, J. Glaciol., 54, 592–600, 2008a. 507

Bolch, T., Buchroithner, M. F., Peters, J., Baessler, M., and Bajracharya, S.: Identification of glacier motion and potentially dangerous glacial lakes in the Mt. Everest region/Nepal using spaceborne imagery, Nat. Hazards Earth Syst. Sci., 8, 1329–1340, doi:10.5194/nhess-8-1329-2008, 2008. 525

Bourgeois, C. S., Calanca, P., and Ohmura, A.: A field study of the hemispherical directional reflectance factor and spectral albedo of dry snow, J. Geophys. Res., 111, D20108, doi:10.1029/2006JD007296, 2006. 508

Bowers, S. A. and Hanks, R. J.: Reflection of radiant energy from soils, Soil Sci., 100, 130–138, 1965. 515

Buchroithner, M. F. and Bolch, T.: An automated method to delineate the ice extension of the debris-covered glaciers at Mt. Everest based on ASTER imagery, in: 9th International Symposium on High Mountain Remote Sensing Cartography, Graz, Austria, 14–22 September 2006, 71–78, 2006. 501

Byers, A. C.: An assessment of contemporary glacier fluctuations in Nepal's Khumbu Himal using repeat photography, Himal. J. Sci., 4(6), 21–26, 2007. 507

Carosi, R., Lombardo, B., Musumeci, G., and Pertusati, P. C.: Geology of the higher Himalayan crystallines in Khumbu Himal (Eastern Nepal), J. Asian Earth Sci., 17, 785–803, 1999. 507

Casey, K. A., Xie, R., Ryset, O., and Keys, H.: Alpine glaciers in the Himalayas, New Zealand and Norway: investigation of trace elemental abundances, in: International Symposium on Earth's Disappearing Ice, International Glaciological Society, Columbus, Ohio, USA, 15–20 August 2010, 59A029, 2010. 510

Chen, X., Warner, T. A., and Campagna, D. J.: Integrating visible, near-infrared and short-wave infrared hyperspectral and multispectral thermal imagery for geological mapping at Cuprite, Nevada, Remote Sens. Environ., 110, 344–356, 2007. 523

Choudhury, B. and Chang, A.: Two-stream theory of reflectance of snow, IEEE T. Geosci. Elect., 17, 63 –68, 1979. 513

Christensen, P. R., Bandfield, J. L., Hamilton, V. E., Howard, D. A., Lane, M. D., Piatek, J. L., Ruff, S. W., and Stefanov, W. L.: A thermal emission spectral library of rock-forming minerals, J. Geophys. Res., 105, 9735–9739, 2000. 505, 547

Clark, R. N.: Spectroscopy of Rocks and Minerals, and Principles of Spectroscopy, vol. 3, John Wiley and Sons, New York, 1999. 547

Clark, R. N. and Lucey, P. G.: Spectral properties of ice-particulate mixtures and implications for remote sensing 1. Intimate mixtures, J. Geophys. Res., 89, 6341–6348, 1984. 504, 518

Clark, R. N., King, T. V. V., Klejwa, M., Swayze, G. A., and Vergo, N.: High spectral resolution reflectance spectroscopy of minerals, J. Geophys. Res., 95, 12653–12680, 1990. 505

Clark, R. N., Swayze, G., Wise, R., Livo, E., Hoefen, T., Kokaly, R., and Sutley, S.: USGS spectral library splib06a, available at: http://speclab.cr.usgs.gov/spectral.lib06, 23 September 2010, 2007. 514

Dadon, A., Ben-Dor, E., and Karnieli, A.: Use of derivative calculations and minimum noise fraction transform for detecting and correcting the spectral curvature effect (smile) in Hyperion images, IEEE T. Geosci. Remote, 48, 2603–2612, 2010. 518

Debella-Gilo, M. and Kääb, A.: Sub-pixel precision image matching for measuring surface displacements on mass movements using normalized cross-correlation, Remote Sens. Environ., 115, 130–142, 2011. 512

Dematte, J. A. M., Campos, R. C., Alves, M. C., Fiorio, P. R., and Nanni, M. R.: Visible-NIR reflectance: a new approach on soil evaluation, Geoderma, 121, 95–112, 2004. 523

Dozier, J.: Spectral signature of alpine snow cover from the landsat thematic mapper, Remote Sens. Environ., 28, 9–22, 1989. 513

Frauenfelder, R. and Kääb, A.: Towards a palaeoclimatic model of rock-glacier formation in the Swiss Alps, Ann. Glaciol., 31, 281–286, 2000. 501

Fujii, Y.: Field experiment on glacier ablation under a layer of debris cover, J. Jap. Soc. Snow Ice, 39, 20–21, 1977. 501

Fushimi, H.: Glaciations in the Khumbu Himal, J. Jap. Soc. Snow Ice, 40, 71–77, 1978. 525

Fushimi, H., Yoshida, M., Watanabe, O., and Upadhyay, B.: Distributions and grain sizes of supraglacial debris in the Khumbu glacier, Khumbu Region, East Nepal, J. Jap. Soc. Snow Ice, 42, 18–25, 1980. 507, 519, 557

Gajda, R. T.: Cryoconite phenomena on the Greenland ice cap in the Thule area, Can. Geogr., 12, 35–44, 1958. 514

Gao, B.-C., Montes, M. J., Davis, C. O., and Goetz, A. F.: Atmospheric correction algorithms for hyperspectral remote sensing data of land and ocean, Remote Sens. Environ., imaging Spectroscopy Special Issue, 113, S17–S24, 2009. 518

Gillespie, A., Kahle, A., and Palluconi, F.: Mapping alluvial fans in Death Valley, California, using multichannel thermal infrared images, Geophys. Res. Lett., 11, 1153–1156, 1984. 505

Gleeson, D. F., Pappalardo, R. T., Grasby, S. E., Anderson, M. S., Beauchamp, B., Castao, R., Chien, S. A., Doggett, T., Mandrake, L., and Wagstaff, K. L.: Characterization of a sulfur-rich Arctic spring site and field analog to Europa using hyperspectral data, Remote Sens.

Environ., 114, 1297–1311, 2010. 518
Goetz, A. F. H. and Rowan, L. C.: Geologic remote sensing, Science, 211, 781–791, 1981. 505
Goetz, A. F. H., Rock, B. N., and Rowan, L. C.: Remote sensing for exploration, an overview, Econ. Geol., 78, 573–590, 1983. 503, 505
Govindaraju, K.: 1994 compilation of working values and sample description for 383 geostandards, Geostandard. Newslett., 18, 1–158, 1994. 548
Griffin, M., Hsu, S., Burke, H., Orloff, S., and Upham, C.: Examples of EO-1Hyperion data analysis, Lincoln Lab. J., 15, 271–298, 2005. 518
Gupta, R. P.: Remote Sensing Geology, 2nd edn., Springer, Berlin, 2003. 505, 515, 521, 547
Hall, D., Ormsby, J., Bindschadler, R., and Siddalingaiah, H.: Characterization of snow and ice reflectance zones on glaciers using Landsat thematic mapper data, Ann. Glaciol., 9, 104–108, 1987. 524
Hall, D., Bindschadler, R., Foster, J., Chang, A., and Siddalingaiah, H.: Comparison of in situ and satellite-derived reflectances of Forbindels Glacier, Greenland, Int. J. Remote Sens., 11, 493–504, 1990. 512, 513
Hall, D., Foster, J., and Chang, A.: Reflectance of snow measured in situ and from space in sub-Arctic areas in Canada and Alaska, IEEE T. Geosci. Remote, 30, 634 –637, 1992. 508
Hall, D. K., Chang, A. T., and Siddalingaiah, H.: Reflectances of glaciers as calculated using Landsat-5 Thematic Mapper data, Remote Sens. Environ., 25, 311–321, 1988. 500, 503
Hall, D. K., Box, J. E., Casey, K. A., Hook, S. J., Shuman, C. A., and Steffen, K.: Comparison of satellite-derived and in-situ observations of ice and snow surface temperatures over Greenland, Remote Sens. Environ., 112, 3739–3749, 2008. 524
Hambrey, M. J., Quincey, D. J., Glasser, N. F., Reynolds, J. M., Richardson, S. J., and Clemmens, S.: Sedimentological, geomorphological and dynamic context of debris-mantled glaciers, Mount Everest (Sagarmatha) region, Nepal, Quaternary Sci. Rev., 27, 2361–2389, 2008. 506, 507, 508, 525
Haug, T., Kääb, A., and Skvarca, P.: Monitoring ice shelf velocities from repeat MODIS and Landsat data – a method study on the Larsen C ice shelf, Antarctica Peninsula, and 10 other ice shelves around Antarctica, The Cryosphere, 4, 161–178, 2010, http://www.the-cryosphere-discuss.net/4/161/2010/. 512
Hook, S. J., Gabell, A., Green, A., and Kealy, P.: A comparison of techniques for extracting emissivity information from thermal infrared data for geologic studies, Remote Sens. Environ., 42, 123–135, 1992. 505, 522

Hook, S. J., Dmochowski, J. E., Howard, K. A., Rowan, L. C., Karlstrom, K. E., and Stock, J. M.: Mapping variations in weight percent silica measured from multispectral thermal infrared imagery – examples from the Hiller Mountains, Nevada, USA and Tres Virgenes-La Reforma, Baja California Sur, Mexico, Remote Sens. Environ., 95, 273–289, 2005. 523
Hunt, G. R.: Spectral signatures of particulate minerals in the visible and near infrared, Geophysics, 42, 501–513, 1977. 505, 547
Hunt, G. R. and Salisbury, J. W.: Visible and near-infrared spectra of minerals and rocks – I, silicates, Mod. Geol., 1, 283–300, 1970a. 504
Hunt, G. R. and Salisbury, J. W.: Visible and near-infrared spectra of minerals and rocks – II, carbonates, Mod. Geol., 2, 23–30, 1970b. 504
Hunt, G. R., Salisbury, J. W., and Lenhoff, C. J.: Visible and near-infrared spectra of minerals and rocks – III, oxides and hydroxides, Mod. Geol., 2, 195–205, 1971a. 504
Hunt, G. R., Salisbury, J. W., and Lenhoff, C. J.: Visible and near-infrared spectra of minerals and rocks – IV, sulphides and sulphates, Mod. Geol., 3, 1–14, 1971b. 504
Kääb, A.: Remote sensing of mountain glaciers and permafrost creep, Schrift. Phys. Geogr., 48, 266 pp., 2005. 501, 506, 518, 520, 549
Kääb, A. and Vollmer, M.: Surface geometry, thickness changes and flow fields on creeping mountain permafrost: automatic extraction by digital image analysis, Permafrost Periglac. Process., 11, 315–326, 2000. 512
Kääb, A., Gudmundsson, G. H., and Hoelzle, M.: Surface deformation of creeping moutnain permafrost. Photogrammetric investigations of rock glacier Murtel, Swiss Alps, in: Proceedings of the 7th International Permafrost Conference, Yellowknife, Northwest Territories, Canada, 23–27 June 1998, 531–537, 1998. 501
Kadota, T.: Study on the relation between climate and recent shrinkage of small glaciers in the Nepal Himalayas, Ph.D. thesis, Nagoya University, Nagoya, Japan, 1997. 507
Kadota, T., Seko, K., Oki, T., Iwata, S., and Yamaguchi, S.: Shrinkage of the Khumbu Glacier, East Nepal from 1978 to 1995, chapt. Debris-covered Glaciers, IAHS, Oxfordshire, UK, 235–243, 264, 2000. 507
Kaufman, Y.: The atmospheric effect on remote sensing and its correction, chapt. Theory and Application of Optical Remote Sensing, Wiley, New York, 341 pp., 1989. 512
Kruse, F., Lefkoff, A., Boardman, J., Heidebrecht, K., Shapiro, A., Barloon, P., and Goetz, A.: The spectral image processing system (SIPS) – interactive visualization and analysis of imaging spectrometer data, Remote Sens. Environ., 44, 145–163, 1993. 519, 523

Kruse, F., Boardman, J., and Huntington, J.: Comparison of airborne hyperspectral data and EO-1 Hyperion for mineral mapping, IEEE T. Geosci. Remote, 41, 1388–1400, 2003. 517
Kruse, F. A.: Use of airborne imaging spectrometer data to map minerals associated with hydrothermally altered rocks in the northern grapevine mountains, Nevada, and California, Remote Sens. Environ., 24, 31–51, 1988. 505
Larsen, C. F., Motyka, R. J., Freymueller, J. T., Echelmeyer, K. A., and Ivins, E. R.: Rapid viscoelastic uplift in Southeast Alaska caused by post-little ice age glacial retreat, Earth Planet. Sc. Lett., 237, 548–560, 2005. 502
Leprince, S., Barbot, S., Ayoub, F., and Avouac, J.-P.: Automatic and precise orthorectification, coregistration, and subpixel correlation of satellite images, application to ground deformation measurements, IEEE T. Geosci. Remote, 45, 1529–1558, 2007. 525
Liang, S.: Quantitative Remote Sensing of Land Surfaces, John Wiley & Sons, Inc., Hoboken, New Jersey, USA, 2004. 515
Lobell, D. B. and Asner, G. P.: Moisture effects on soil reflectance, Soil Sci. Soc. Am. J., 66, 722–727, 2002. 515
Lougeay, R.: Detection of buried glacial and ground ice with thermal infrared remote sensing, chap, Advanced Concepts and Techniques in the Study of Snow and Ice Resources, An Interdisciplinary Symposium, Monterey, California, USA, 2–6 December 1973, 487–493, 1974. 505
Lougeay, R.: Landsat thermal imaging of alpine regions, Photogramm. Eng. Rem. S., 48, 269–273, 1982. 505
Lu, D., Mausel, P., Brondizio, E., and Moran, E.: Assessment of atmospheric correction methods for Landsat TM data applicable to Amazon basin LBA research, Int. J. Remote Sens., 23, 2651–2671, 2002. 512
Luckman, A., Quincey, D., and Bevan, S.: The potential of satellite radar interferometry and feature tracking for monitoring flow rates of Himalayan glaciers, Remote Sens. Environ., remote Sensing of the Cryosphere Special Issue, 111, 172–181, 2007. 525
Lyon, R. J. P.: Analysis of rocks by spectral infrared emission (8 to 25 microns), Econ. Geol., 60, 715–736, 1965. 504
MacArthur, A., MacLellan, C., and Malthus, T.: The implications of non-uniformity in fields-of-view of commonly used field spectroradiometers, in: Geoscience and Remote Sensing Symposium, 2007, IGARSS 2007, Barcelona, Spain, 23–28 July 2007, IEEE International, 2890–2893, 2007. 509

Markham, B. and Barker, J.: Landsat MSS and TM post-calibration dynamic ranges, exoatmospheric reflectances and at-satellite temperatures, EOSAT Landsat Tech. Notes, 1, 3–8, 1986. 511
Mars, J. C. and Rowan, L. C.: Spectral assessment of new ASTER SWIR surface reflectance data products for spectroscopic mapping of rocks and minerals, Remote Sens. Environ., 114, 2011–2025, 2010. 512
Mather, P. M.: Computer Processing of Remotely Sensed Images, John Wiley & Sons, Ltd., Washington, D.C., USA, 1987. 520
Mattson, L.: The role of debris cover on glacial meltwater discharge, Canadian Rocky Mountains, in: Proceedings of the 47th Eastern Snow Conference, England, 3rd Edn., 237–242, 2004. 501
Mattson, L.: The influence of a debris cover on the mid-summer discharge of Dome glacier, Canadian Rocky Mountains, chapt. Debris-Covered Glaciers, IAHS, Bangor, Maine, USA, 7–8 June 1990, 25–33, 264, 2000. 501
Mattson, L., Gardner, J., and Young, G.: Ablation on debris covered glaciers: an example from the Rakhiot glacier, Punjab, Himalaya, IAHS-AISH P, 218, 289–296, 1993. 501
McClure, D.: The distribution of transition metal cations in spinels, J. Phys. Chem. Solids, 3, 3–4, 1957. 504, 547
McClure, D.: Electronic spectra of molecules and ions in crystals, Part II. spectra of ions in crystals, Solid State Phys., 9(C), 399–525, 1959. 504, 547
Meier, M., Dyurgerov, M., Rick, U., O'Neel, S., Pfeffer, W., Anderson, R., Anderson, S., and Glazovsky, A.: Glaciers dominate eustatic sea-level rise in the 21st century, Science, 317, 1064–1067, 2007. 502
Miyatake, S.: Technical development report: examination of indices for discriminating rocks and minerals and their universal validity, Met. Min. Agency Jap., 3, 1–31, 2000. 522, 559
Moore, D. M., Reynolds Jr., R. C.: X-ray diffraction and the identification and analysis of clay minerals, 2nd edn., Oxford University Press, New York, 1997. 510
Nakawo, M., Yabuki, H., and Sakai, A.: Characteristics of Khumbu Glacier, Nepal Himalaya: recent changes in the debris-covered area, Ann. Glaciol., 28, 118–122, 1999. 501, 507, 524
Nesje, A. and Dahl, S.: Glaciers and Environmental Change, Oxford University Press, Oxfordshire, UK, 2000. 506
Nicholson, L. and Benn, D.: Calculating ice melt beneath a debris layer using meteorological data, J. Glaciol., 52, 463–470, 2006. 501

Nicodemus, F., Richmond, J., Hsia, J., Ginsberg, I., and Limperis, T.: Geometrical considerations and nomenclature for reflectance, Tech. rep., London, 1977. 509
Ninomiya, Y.: Rock type mapping with indices defined for multispectral thermal infrared ASTER data: case studies, in: Society of Photo-Optical Instrumentation Engineers (SPIE) Conference Series, vol. 4886, National Bureau of Standards, Monograph 160, Washington, D.C., 123–132, 2003. 520
Ninomiya, Y.: Lithologic mapping with multispectral ASTER TIR and SWIR data, in: Society of Photo-Optical Instrumentation Engineers (SPIE) Conference Series, vol. 5234, SPIE, Bellingham, Washington, USA, 180–190, 2004. 505, 520
Ninomiya, Y., Fu, B., and Cudahy, T. J.: Detecting lithology with advanced spaceborne thermal emission and reflection radiometer (ASTER) multispectral thermal infrared radiance-at-sensor data, Remote Sens. Environ., 99, 127–139, 2005. 505, 518, 520, 521, 522, 558
Nolin, A. W. and Dozier, J.: A hyperspectral method for remotely sensing the grain size of snow, Remote Sens. Environ., 74, 207–216, 2000. 513
O'Brien, H. and Munis, R.: Red and near-infrared spectral reflectance of snow, in: Operational Applications of Satellite Snowcover Observations, NASA SP-391, proceedings of a workshop held in South Lake Tahoe, California, 345–360, 18–20 August, 1975. 513
Oerlemans, J., Giesen, R., and van den Broeke, M.: Retreating alpine glaciers: increased melt rates due to accumulation of dust (Vadret da Morteratsch, Switzerland), J. Glaciol., 55, 729–736, 2009. 501
Ostrem, G.: Ice melting under a thin layer of moraine, and the existence of ice cores in moraine ridges, Geogr. Ann., 41, 228–230, 1959. 501
Owen, L., Robinson, R., Benn, D., Finkel, R., Davis, N., Yi, C., Putkonen, J., Li, D., and Murray, A.: Quaternary glaciation of Mount Everest, Quaternary Sci. Rev., 28, 1412–1433, 2009. 526
Painter, T., Duval, B., Thomas, W., Mendez, M., Heintzelman, S. and Dozier, J.: Detection and quantification of snow algae with an airborne imaging spectrometer, Appl. Environ. Microbiol., 67, 5267–5272, 2001. 514, 547
Painter, T., Paden, B., and Dozier, J.: Automated spectro-goniometer: a spherical robot for the field measurement of the directional reflectance of snow, Rev. Sci. Instrum., 74, 5179–5188, 2003. 508
Paul, F., Kääb, A., Maisch, M., Kellenberger, T., and Haeberli, W.: The new remote-sensing-derived Swiss glacier inventory. I. methods, Ann. Glaciol., 34, 355–361, 2002. 503

Paul, F., Kääb, A., Maisch, M., Kellenberger, T., and Haeberli, W.: Rapid disintegration of Alpine glaciers observed with satellite data, Geophys. Res. Lett., 31, L21402, 4pp., 2004. 501, 505
Paul, F., Kääb, A., and Haeberli, W.: Recent glacier changes in the Alps observed by satellite: consequences for future monitoring strategies, Global Planet. Change, 56, 111–122, 2007. 500
Pearlman, J., Barry, P., Segal, C., Shepanski, J., Beiso, D., and Carman, S.: Hyperion, a space-based imaging spectrometer, IEEE T. Geosci. Remote, 41, 1160–1173, 2003. 517
Pognante, U. and Benna, P.: Metamorphic zonation, migmatization and leucogranites along the Everest transect of Eastern Nepal and Tibet: record of an exhumation history, Geol. Soc. Sp., 74, 323–340, 1993. 507
Post, A. and LaChapelle, E.: Glacier Ice, Revised Edition, University of Washington Press, Seattle, 2000. 501
Quincey, D., Luckman, A., and Benn, D.: Quantification of Everest region glacier velocities between 1992 and 2002, using satellite radar interferometry and feature tracking, J. Glaciol., 55, 596–606, 2009. 525
Qunzhu, Z., Meisheng, C., Xuezhi, F., Fengxian, L., Xianzhang, C., Wenkun, S.: A study of spectral reflection characteristics for snow, ice and water in the north of China, in: Hydrological Applications of Remote Sensing and Remote Data Transmission, edited by: Goodison, B. E., Proceedings of the Hamburg Symposium, August 1983, IAHS Publ No. 145, 451–462, 1985. 513, 552
Radic, V. and Hock, R.: Regional and global volumes of glaciers derived from statistical upscaling of glacier inventory data, J. Geophys. Res., 115, 2010. 506
Rowan, L. C. and Mars, J. C.: Lithologic mapping in the Mountain Pass, California area using advanced spaceborne thermal emission and reflection radiometer (ASTER) data, Remote Sens. Environ., 84, 350–366, 2003. 505
Rowan, L. C., Kingston, M. J., and Crowley, J. K.: Spectral reflectance of carbonatites and related alkalic igneous rocks; selected samples from four North American localities, Econ. Geol., 81, 857–871, 1986. 505
Rowan, L. C., Mars, J. C., and Simpson, C. J.: Lithologic mapping of the Mordor, NT, Australia ultramafic complex by using the advanced spaceborne thermal emission and reflection radiometer (ASTER), Remote Sens. Environ., 99, 105–126, 2005. 505
Sandmeier, S. and Itten, K.: A field goniometer system (FIGOS) for acquisition of hyperspectral BRDF data, IEEE T. Geosci. Remote, 37, 978–986, 1999. 508

Scherler, D., Leprince, S., and Strecker, M. R.: Glacier-surface velocities in alpine terrain from optical satellite imagery – accuracy improvement and quality assessment, Remote Sens. Environ., 112, 3806–3819, 2008. 525
Searle, M.: Extensional and compressional faults in the Everest Lhotse massif, Khumbu Himalaya, Nepal, J. Geol. Soc. London, 156, 227–240, 1999. 507
Searle, M., Simpson, R., Law, R., Parrish, R., and Waters, D.: The structural geometry, metamorphic and magmatic evolution of the Everest massif, High Himalaya of Nepal-South Tibet, J. Geol. Soc. London, 160, 345–366, 2003. 507, 516
Seko, K., Yabuki, H., Nakawo, M., Sakai, A., Kadota, T., and Yamada, Y.: Changing surface features of Khumbu Glacier, Nepal Himalayas revealed by SPOT images, Bull. Glac. Res., 16, 33–41, 1998. 525
Shroder, J. F., Bishop, M. P., Copland, L., and Sloan, V. F.: Debris-covered glaciers and rock glaciers in the Nanga Parbat Himalaya, Pakistan, Geogr. Ann. A, 82, 17–31, 2000. 505
Shukla, A., Arora, M., and Gupta, R.: Synergistic approach for mapping debris-covered glaciers using optical-thermal remote sensing data with inputs from geomorphometric parameters, Remote Sens. Environ., 114, 1378–1387, 2010. 501, 505
Siegal, B. and Abrams, M.: Geologic mapping using Landsat data, Photogramm. Eng. Rem. S., 42, 325–331, 1976. 515
Skidmore, E. L., Dickerson, J. D., and Schimmelpfennig, H.: Evaluating surface-soil water content by measuring reflectance, Soil Sci. Soc. Am. J., 39, 238–242, 1975. 515
Stamnes, K., Li, W., Spurr, R., Eide, H., and Stamnes, J.: Simultaneous retrieval of aerosol and surface properties over bright targets including snow and ice using multi- and hyperspectral data, Proc. SPIE, 5569, 56–67, 2004. 512
Storey, J., Scaramuzza, P., Schmidt, G., and Barsi, J.: Landsat 7 scan line corrector-off gap filled product development, in: Proceedings of Pecora 16 Global Priorities in Land Remote Sensing, Sioux Falls, South Dakota, USA, American Society for Photogrammetry and Remote Sensing, 23–27 October 2005, 2005. 503, 511
Strozzi, T., Paul, F., and Kääb, A.: Glacier mapping with ALOS PALSAR data within the ESA GlobGlacier project, in: Proceedings of the ESA Living Planet Symposium, Bergen, Norway 28 June–2 July 2010, 3223, 2010. 501
Sultan, M., Arvidson, R. E., Sturchio, N. C., and Guinness, E. A.: Lithologic mapping in arid regions with Landsat thematic mapper data: Meatiq dome, Egypt, Geol. Soc. Am. Bull., 99, 748–762, 1987. 505

Suzuki, R., Fujita, K., and Ageta, Y.: Spatial distribution of thermal properties on debris-covered glaciers in the Himalayas derived from ASTER data, Bull. Glaciol. Res., 24, 13–22, 2007. 506
Takeuchi, N.: Temporal and spatial variations in spectral reflectance and characteristics of surface dust on Gulkana Glacier, Alaska Range, J. Glaciol., 55, 701–709, 2009. 513, 514
Takeuchi, N. and Li, Z.: Characteristics of surface dust on Urumqi glacier no. 1 in the Tien Shan mountains, China, Arct. Antarct. Alp. Res., 40, 744–750, 2008. 508
Takeuchi, N., Kohshima, S., and Seko, K.: Structure, formation, and darkening process of albedo-reducing material (cryoconite) on a Himalayan glacier: a granular algal mat growing on the glacier, Arct. Antarct. Alp. Res., 33, 115–122, 2001. 514
Takeuchi, Y., Kayastha, R., and Nakawo, M.: Characteristics of ablation and heat balance in debris-free and debris-covered areas on Khumbu glacier, Nepal Himalayas, in the premonsoon season, in: Debris-Covered Glaciers, IAHS, Oxfordshire, UK, 53–61, 2000. 501
Tamisiea, M. E., Mitrovica, J. X., Milne, G. A., and Davis, J. L.: Global geoid and sea level changes due to present-day ice mass fluctuations, J. Geophys. Res., 106, 30849–30863, 2001. 502
Tanre, D., Deroo, C., Duhaut, P., Herman, M., Morcrette, J., Perbos, J., and Deschamps, P.: Description of a computer code to simulate the satellite signal in the solar spectrum: the 5S code, Int. J. Remote Sens., 11, 659–668, 1990. 512
Taschner, S. and Ranzi, R.: Comparing the opportunities of Landsat-TM and Aster data for monitoring a debris covered glacier in the Italian Alps within the GLIMS project, Int. Geosci. Remote Se., 2, 1044–1046, 2002. 501, 505
Tucker, C. J., Grant, D. M., and Dykstra, J. D.: NASA's global orthorectified Landsat data set, Photogramm. Eng. Rem. S., 70, 313–322, 2004. 511
Vincent, R. and Thomson, F.: Rock-type discrimination from ratioed infrared scanner images of Pisgah Crater, California, Science, 175, 986–988, 1972. 505, 520
Wang, T., Yan, G., Ren, H., and Mu, X.: Improved methods for spectral calibration of on-orbit imaging spectrometers, IEEE T. Geosci. Remote, 48, 3924–3931, 2010. 518
Warren, S.: Optical Properties of Snow, Rev. Geophys. Space Ge., 20, 67–89, 1982. 513, 514
Warren, S. and Wiscombe, W.: A model for the spectral albedo of snow. II: snow containing atmospheric aerosols, J. Atmos. Sci., 37, 2734–2745, 1980. 501, 514
Watanabe, H. and Matsuo, K.: Rock type classification by multi-band TIR of ASTER, Geosci. J., 7, 347–358, 2003. 522
Wessels, R., Kargel, J., and Kieffer, H.: ASTER measurement of supraglacial lakes in the Mount

Everest region of the Himalaya, Ann. Glaciol., 34, 399–408, 2002. 506, 507
Wiens, R. C., Arvidson, R. E., Cremers, D. A., Ferris, M. J., Blacic, J. D., Seelos, Frank, P. I., and Deal, K. S.: Combined remote mineralogical and elemental identification from rovers: field and laboratory tests using reflectance and laser-induced breakdown spectroscopy, J. Geophys. Res., 107, 8004, 2002. 508
Winther, J.-G.: Landsat TM derived and in situ summer reflectance of glaciers in Svalbard, Polar Res., 12, 37–55, 1993. 513
Wiscombe, W. J. and Warren, S. G.: A model for the spectral albedo of snow. I: pure snow, J. Atmos. Sci., 37, 2712–2733, 1980. 513
Yao, T.: Glacial retreat and its impact on hydrological processes on the third pole, in: International Symposium on Earth's Disappearing Ice, International Glaciological Society, Columbus, Ohio, USA, 15–20 August 2010, 59A100, 2010. 502
Yoshimura, Y., Kohshima, S., Takeuchi, N., Seko, K., and Fujita, K.: Himalayan ice-core dating with snow algae, J. Glaciol., 46, 335–340, 2000. 514
Zheng, L., Li, M., Sun, J., Zhang, X., and Zhao, P.: Estimating soil moisture based on image processing technologies, Proc. SPIE, San Diego, CA, USA, 5909, 548–555, 2005. 515

Table 1. Summary of in situ sample attributes. Corresponding sample numbers given in the final column refer to samples listed in Tables 3 and 1. The locations of the field measurement sites are mapped in the true color (Fig. 3) and in false color (Fig. 9) maps of the region.

Location	Date	Latitude / Longitude	Elevation (m a.s.l.)	Spectral signature class, (corresponding sample ID)
Upper Ngozumpa (UN)	27 Nov 2009	27.9568° N 86.6980° E	4760	snow, rock, gravel, sand, mud (1N–6N)
Mid-Ngozumpa (MN)	29 Nov 2009	27.9537° N 86.6992° E	4748	ice, snow, rock, gravel (7N, 8N)
Lower Ngozumpa (LN)	26 Nov 2009	27.9511° N 86.7020° E	4789	snow, boulders, gravel, soil
Upper Khumbu (UK)	6 Dec 2009	27.9998° N 86.8511° E	5284	ice, snow, gravel (19K–22K)
Mid-Khumbu (MK)	5 Dec 2009	27.9874° N 86.8405° E	5180	ice, snow, rock, sand (14K–18K)
Lower Khumbu (LK)	4 Dec 2009	27.9763° N 86.8304° E	5100	ice, snow, mud, rock (9K,10K)

Table 2. A listing of the satellite products and scene dates used for the optical remote sensing methods evaluated in this study.

Comparison method	Sensor, data product	Date(s) of scene(s), further details
Satellite derived reflectance		
multispectral	ASTER, AST_07XT	29 Nov 2005
hyperspectral	Hyperion, L1T	13 May 2002, 4 Oct 2010
True and false color composites	ALI, L1T	4 Oct 2010, 10 m pan enhanced true color
	ASTER, L1B	29 Nov 2005, SWIR/TIR false color
	Landsat TM, L1T	31 Oct 2009, true color
	Landsat ETM+, L1G	24 Jan 2003, SWIR/TIR false color
	Hyperion, L1T	13 May 2002, true color, SWIR false color
Mineralogic mapping:		
SWIR/TIR indices	ASTER, L1B	29 Nov 2005
SiO_2 weight percent	ASTER, AST_05	29 Nov 2005
Spectral Angle Mapper	ASTER, L1B, AST_07XT	29 Nov 2005
Land surface temperature	Landsat TM, L1T	31 Oct 2009
	ASTER, AST_08	29 Nov 2005
Glacier velocity, streamlines	Landsat TM, L1T	5 Nov 2005, 31 Oct 2009, 30 m near infrared
	Landsat ETM+, L1G	30 Oct 2000, 4 Oct 2002, 15 m pan

Table 3. In situ and satellite comparison of mineralogy and silica abundance at Ngozumpa and Khumbu glacier sample locations. XRD-derived minerals are listed in order of greatest abundance per sample. XRF SiO_2 weight percent and ASTER TIR estimated Eq. (7) SiO_2 composition are also listed. ASTER TIR SiO_2 weight percent is averaged from the nearest two 90 m pixels to the in situ sample site. In situ geochemical results compare generally well with the satellite derived estimates.

Sample ID	Debris type	XRD determined mineral classes in order of abundance	XRF derived SiO_2	ASTER TIR estimated SiO_2
1N	mud	quartz, feldspar, mica, K-feldspar, calcite	66.3	72.8
2N	mud	quartz, feldspar, mica, K-feldspar, calcite	66.4	
3N	sand	mica, quartz, feldspar, K-feldspar, calcite	62.7	
4N	sand	quartz, mica, feldspar, K-feldspar, calcite	65.1	
5N	gravel	feldspar, quartz, K-feldspar, mica, calcite	71.9	
6N	gravel	mica, feldspar, quartz, microcline, clinochlore	62.5	
7N	rock	feldspar, feldspar, calcite, quartz, K-feldspar	37.2	70.7
8N	rock	calcite, wollastonite	6.6	
9K	mud	mica, feldspar, quartz, microcline, clinochlore	61.4	77.9
10K	mud	mica, feldspar, quartz, K-feldspar, nimite	62.0	
11K	rock	phlogopite, feldspar, anorthite, quartz, nimite	63.8	
12K	rock	feldspar, mica, phlogopite, quartz, clinochlore	54.1	
13K	rock	calcite, feldspar, quartz	7.1	
14K	sand	quartz, feldspar, microcline, mica, mica	71.5	78.7
15K	sand	feldspar, quartz, K-feldspar, mica	71.7	
16K	soil	feldspar, feldspar, quartz, K-feldspar, mica, illite	71.1	
17K	soil	feldspar, quartz, mica, K-feldspar	68.1	
18K	soil	mica, quartz, feldspar, K-feldspar, nimite	69.2	
19K	gravel	mica, quartz, feldspar, clinochlore, K-feldspar	63.1	58.6
20K	gravel	mica, quartz, feldspar, ankerite, nimite	61.0	
21K	sand	phlogopite, quartz, feldspar, microcline, clinochlore	63.5	
22K	sand	mica, feldspar, quartz, microcline, calcite, nimite	62.8	

Table A1. Characteristic absorption feature values after Hunt (1977); Clark (1999); Gupta (2003) unless otherwise noted.

Wavelength	Component	Absorption feature (μm)
VNIR	Mg^{3+}	1.0
	Cr^{3+}	0.4, 0.55, 0.7
	Mn^{2+}	0.34, 0.37, 0.41, 0.45, 0.55 (McClure, 1959)
	Fe^{3+}, Fe^{2+}	0.44, 0.87, 0.95
	Ni^{2+}	0.4, 0.74, 1.25 (McClure, 1957)
	Cu^{2+}	0.8
	Rare Earth Ions, La^{2+}	0.5, 0.58
	Atmospheric O_2, Atmospheric H_2O	0.76, 0.94
	Water, Snow, Ice	0.98, 0.90, 1.03
	Algal snow	0.55, 0.68 (Painter et al., 2001)
SWIR	Carbonates	1.9, 2.35, 2.55
	Hydroxides, (Al-OH, Mg-OH)	2.7, overtone at 1.44, (2.2, 2.3)
	Water vapor	1.4, 1.7
	Snow	1.03, 1.25, 1.50
TIR	Chlorites	7.0
	Silicates	8.5–12.0 (e.g.: 8.7, 9.7 microcline; 9.2, 10.2 wollastonite; 10.0 hornblende) (Christensen et al., 2000)
	Carbonates	11.3 (11.4 calcite, 11.2 dolomite)
	Sulfates	9.0, 16.0
	Phosphates	9.25, 13.3
	Hydroxides	11.0

Table B1. In situ collected samples X-ray fluorescence (XRF) determined major oxide percent weights and part per million concentrations of trace elements. The locations and types of samples gathered are listed in Table 1, and mapped in Figs. 3 and 9. (XRF measurement accuracy is 98%. Basalt (BE-N, JB-1a, JB-2), diorite (DR-N) and disthene (DT-N) standards (after Govindaraju, 1994)) were utilized for XRF quality control. Over 100 total standards were used for XRF calibration.

Sample ID	SiO_2	Al_2O_3	Fe_2O_3	MgO	CaO	Na_2O	K_2O	V	Co	Zn	Pb	Zr	Th	U
1N	66.26	14.79	4.58	1.69	2.34	2.99	4.12	56	15	90	42	194	21	10
2N	66.38	14.69	4.85	1.70	2.34	2.96	4.10	56	17	92	42	188	19	11
3N	62.73	14.89	4.79	1.86	2.27	2.74	4.23	54	13	96	43	204	21	11
4N	65.09	13.10	3.42	1.28	2.29	2.94	3.77	37	10	69	40	174	18	7
5N	71.88	13.00	1.16	0.10	2.09	4.24	3.79	1	4	30	50	51	5	14
6N	62.45	14.34	6.42	2.55	2.19	2.29	4.60	79	19	84	27	309	26	6
7N	43.41	8.75	0.83	0.37	23.26	2.91	1.03	14	2	15	38	109	9	13
8N	10.21	1.90	1.80	0.83	48.61	0.01	0.23	19	4	34	13	90	5	10
9K	61.41	17.26	5.39	2.12	1.98	2.32	4.85	73	14	103	38	218	20	15
10K	61.96	17.80	5.79	2.25	1.89	2.33	4.98	82	18	107	37	233	22	17
11K	63.78	13.76	6.38	2.73	2.57	2.79	3.02	76	19	96	37	235	22	4
12K	54.08	18.94	7.42	3.00	5.40	3.33	2.83	130	18	108	30	450	38	9
13K	7.34	1.12	0.54	0.49	49.3	0.46	0.11	8	0	16	391	94	–	13
14K	71.52	12.28	2.63	0.57	2.86	3.73	2.85	23	5	179	40	151	10	12
15K	71.69	13.55	1.22	0.14	0.71	4.14	4.53	5	2	39	51	62	7	15
16K	71.08	13.32	1.41	0.22	0.86	3.69	4.62	8	1	27	55	83	10	8
17K	68.14	13.49	2.95	0.91	1.54	3.24	4.13	31	8	50	40	145	14	9
18K	69.21	11.78	5.35	2.18	2.75	1.90	3.30	72	14	71	24	501	28	7
19K	63.14	14.82	6.14	2.64	2.96	2.05	3.78	79	17	98	26	251	21	6
20K	61.01	14.24	6.24	2.73	3.47	1.96	3.48	78	17	95	30	289	22	7
21K	63.50	14.62	5.14	2.24	2.59	2.24	4.24	64	16	84	32	202	17	7
22K	62.82	14.59	5.39	2.36	2.57	2.19	4.18	71	17	82	33	209	18	8

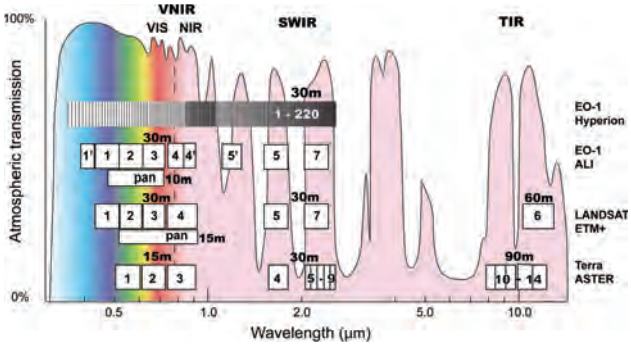

Fig. 1. Spectral coverage of Hyperion, ASTER and Landsat ETM+ sensors with regard to atmospheric transmission in the visible to thermal infrared wavelength range (Adapted after Kääb, 2005).

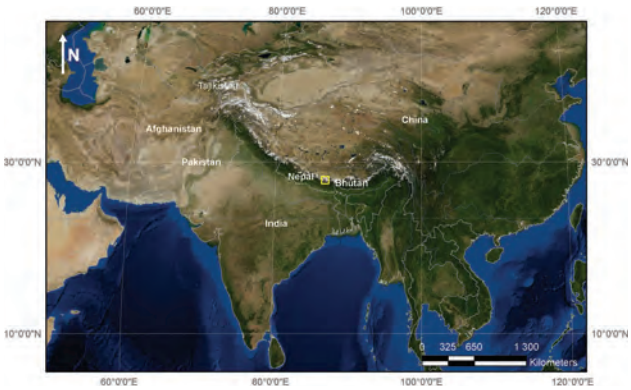

Fig. 2. Overview map of study region, with the Khumbu Himalaya, Nepal area highlighted by the yellow box. (Background image courtesy of MODIS based NASA Earth Observatory Blue Marble.)

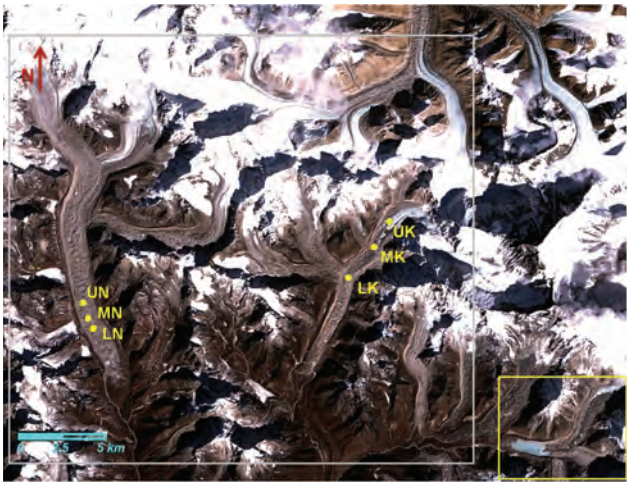

Fig. 3. Landsat TM true color composite (31 October 2009, Bands 3, 2, 1) of the Khumbu Himalaya study area. Ngozumpa glacier (left) and Khumbu glacier (right) in situ measurement locations are labeled as follows: Upper Ngozumpa – UN, Mid-Ngozumpa – MN, Lower Ngozumpa – LN, Upper Khumbu – UK, Mid-Khumbu – MK, Lower Khumbu – LK. The approximate area of comparison mapped in (Figs. 9, 11 and 14) is highlighted by the gray box. The approximate area presented in the Hyperion Imja and Lhotse Shar glacier analysis is highlighted with a yellow box in the lower right hand corner.

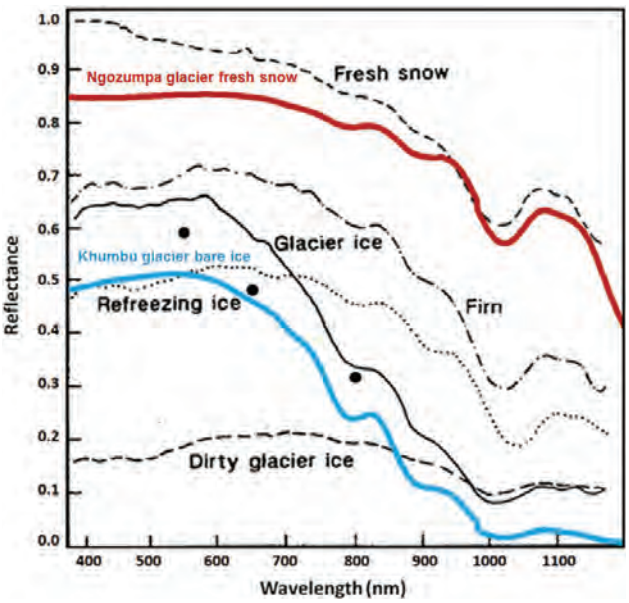

Fig. 4. Field spectra of Ngozumpa glacier fresh snow (red) and Khumbu glacier bare ice (cyan) measurements as compared to reference snow and ice spectral signatures by Qunzhu et al. (1985), ASTER derived surface reflectance values for the Khumbu glacier bare ice are over plotted in black circles. (Qunzhu et al. (1985) graph reprinted with permission from IAHS.)

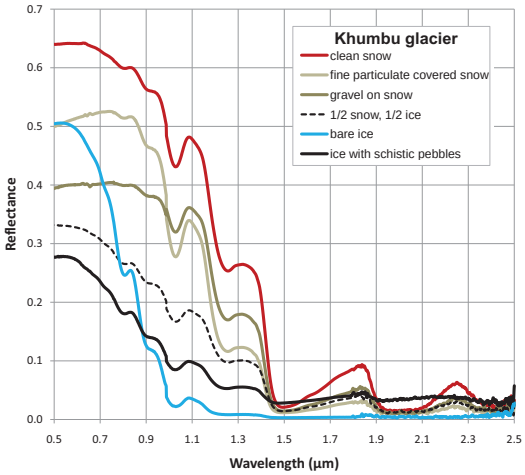

Fig. 5. Khumbu glacier clean snow, fine particulate covered snow, gravel on snow, mixed pixel half snow, half ice and bare ice spectra are plotted that were acquired in the ice pinnacles region near the Khumbu icefall. Spectral signatures represent an average of 20 individual spectral measurements. Particulate and gravel covered snow reduces reflectivity in the visible portion of the spectrum, with debris composition beginning to be expressed in the gravel on snow signature (see reference spectral signature for sillimanite gneiss in Appendix A). The mixed pixel (half snow, half ice) spectral measurements result in a change in the slope of the reflectance from visible to near infrared. Clean snow and bare ice spectral acquisitions are displayed for comparison.

553

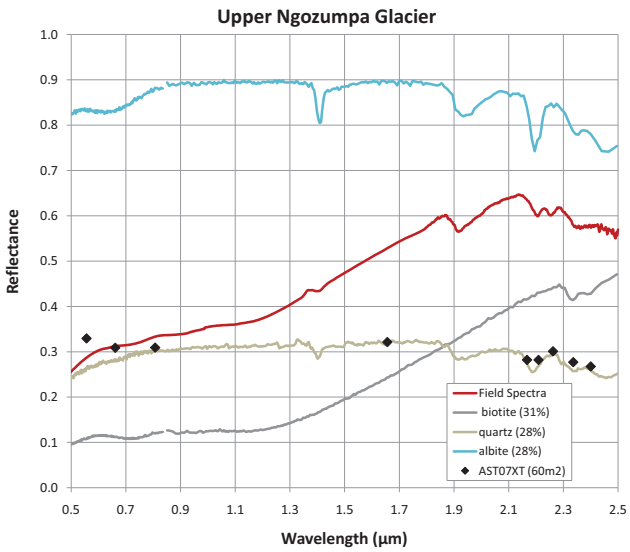

Fig. 6. Upper Ngozumpa glacier collected spectral signature of debris from 27 November 2009, corresponding with sample 3N of sand. Field measured reflectance is plotted in red along with spectral library reference reflectances of the 3 major minerals determined by XRD analysis: biotite (31%), quartz (28%), and albite (28%) (ASTER spectral library reference numbers: USGS231-HS28, AP-958-111, and USGS231-HS324, respectively). Corresponding ASTER (AST_07XT) surface reflectance (60 m^2 comparison – 4 × 4 pixels in visible bands 1–3, 2 × 2 pixels in SWIR bands 4–9) from 29 November 2005 is over plotted in black diamonds.

554

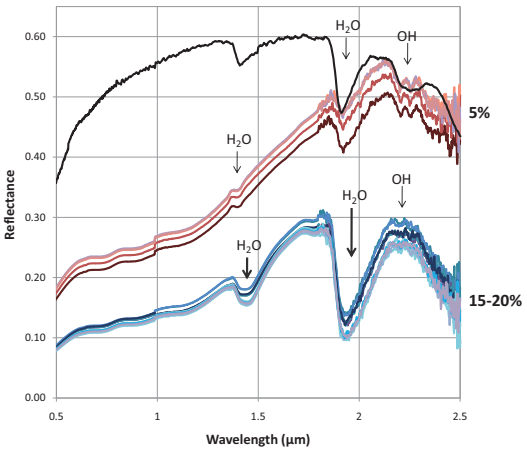

Fig. 7. Graph of two sets of reflectance field spectra acquired on 27 November 2009 at the upper Ngozumpa glacier site over mud of varying degrees of moisture (corresponding with debris sample ID's 1N, 2N). The set of spectra plotted by the red hues was visibly drier than the set of spectra plotted by blue hues. A spectral library reference reflectance profile of the dominant mineral determined by XRD analysis, quartz, is over plotted in black (ASTER spectral library No.382). Water content in the upper set of spectra is estimated at 5%, and 15–20% in the lower set of spectra. Water absorption bands are shown at 1.4 and 1.9 µm, and hydroxyl absorption at 2.2 µm. Water absorption features increase with greater moisture content and conversely, hydroxyl absorption decreases with increasing moisture. While sediment grain size is a factor in the intensity of the reflectance, moisture content dominates the intensity of the signal.

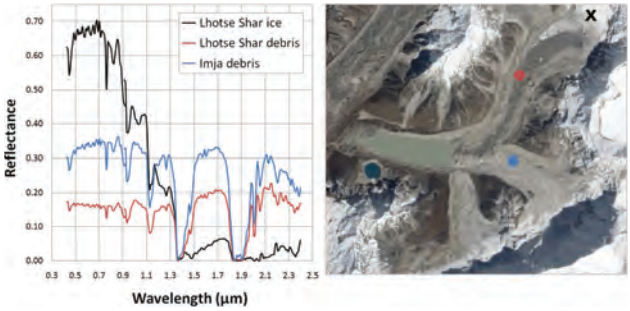

Fig. 8. Hyperion (13 May 2002) derived at-sensor reflectance plot (left) of Imja glacier debris (blue) vs. Lhotse Shar glacier debris (red) spectral signatures with a Lhotse Shar ice spectral signature shown for reference (black). An ALI (4 October 2010) 10 m pan-enhanced true color composite is shown on the right (courtesy NASA Earth Observatory) with the locations of the Hyperion derived spectra for debris shown in blue and red dots and ice in the black X.

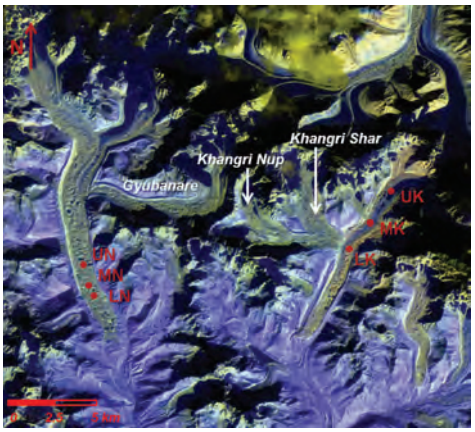

Fig. 9. SWIR, TIR Landsat bands (5, 7, 6) (1.65, 2.2, 11 µm) false color composite from 24 January 2003 displaying geologic differences of Ngozumpa, Khumbu and Imja glacier debris. Silicon dioxide rich granites are indicated by yellow coloring, while the blue color highlights strong amounts of gneiss. The Khumbu glacier longitudinal schistic supraglacial debris band reported by Fushimi et al. (1980) can be visualized in blue in this false color composite, as well as similar longitudinal supraglacial debris bands on upper Ngozumpa glacier. Indication of limited mass flux can be seen by the distinct change in supraglacial composition that can be visualized at the confluence of the Khangri Shar, Khangri Nup and Khumbu glacier – negligible mass is input to the Khumbu glacier. A difference in supraglacial debris on Ngozumpa vs. Khumbu glacier can be visualized, XRD-derived mineralogy found Ngozumpa in situ samples to be quartz, feldspar and mica dominant vs. Khumbu in situ samples that were mica, feldspar and quartz dominant.

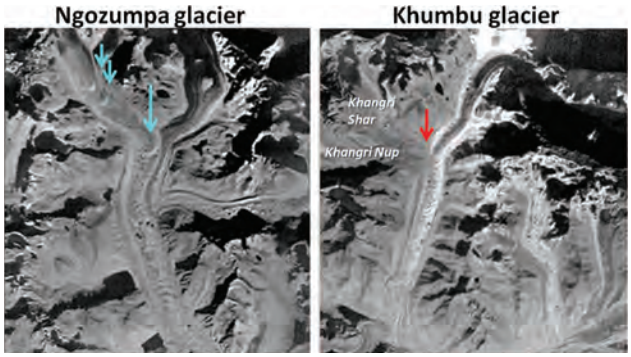

Fig. 10. ASTER (L1B radiance data 29 November 2005) SWIR based silicate index (Eq. 2) after Ninomiya et al. (2005) images of Ngozumpa glacier (left) and Khumbu glacier (right): darker shades indicate lower amounts of silicates, brighter shades indicate higher amounts of silicates. Cyan arrows on the Ngozumpa glacier point to areas of pulse like flow that are made more evident by the silicate index. The red arrow on the Khumbu glacier highlights the distinct transition in debris type at the convergence of the Khangri Shar, Khangri Nup and Khumbu glaciers. The Khumbu glacier longitudinal non-silicate rich schist band vs. the lateral longitudinal glacier silicate-rich granite bands are evident.

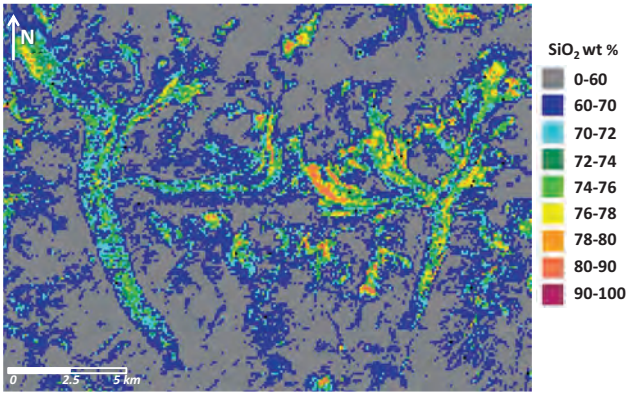

Fig. 11. SiO_2 weight percent distribution thematic map based on ASTER thermal emissivity bands after Miyatake (2000). Debris covered glacier areas are evident by elevated SiO_2 content in this region, perhaps due to the high supraglacial activity in terms of sediment transport, deposition and glacial erosion.

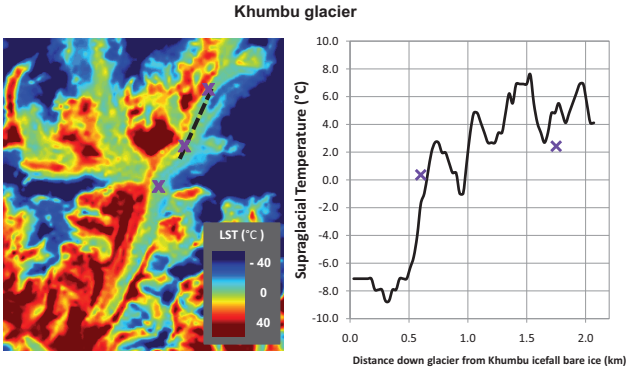

Fig. 12. Khumbu glacier regional Landsat TM (31 October 2009) derived surface temperature map is displayed on the left. A graph showing a surface temperature transect down glacier is shown on the right. In situ ground temperature measurements are indicated on the map and graph by the purple "X" annotations. Glacier surface temperature increases approximately 15 °C two kilometers down glacier from the Khumbu icefall. In situ average temperatures of 0.4 °C for upper Khumbu, 2.4 °C for mid-Khumbu, and 6.7 °C for lower Khumbu sample sites relate to Landsat TM LST's of −3.2, 4.8, 3.4 °C, respectively.

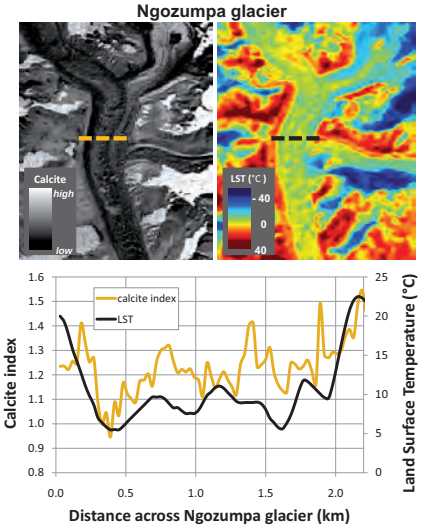

Fig. 13. The top portion of the image shows a ASTER L1B (29 November 2005) derived calcite index Eq. (3, left), and a Landsat TM (31 October 2009) derived LST map of Ngozumpa glacier study area. The graph below shows transect values of calcite index (light brown) and LST (blue) across the upper Ngozumpa ablation area. It may be possible to analyze ablation rate influences of different mineral types, for example as shown in the transect graph in the lower portion of the image, calcite rich areas correspond with higher glacier surface temperatures.

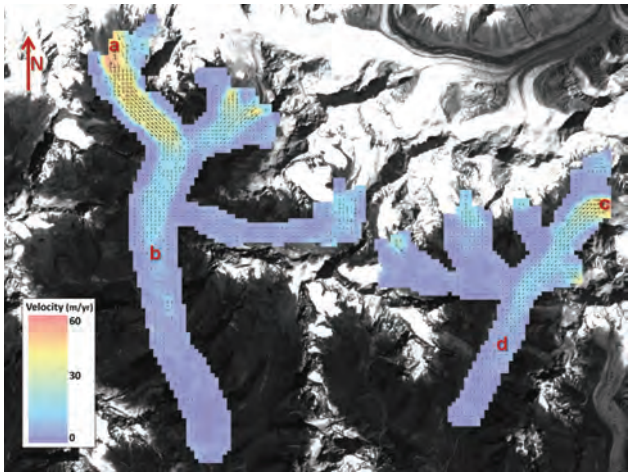

Fig. 14. Glacier surface velocity and flow directions are presented for Ngozumpa (left) and Khumbu (right) glaciers based on repeat feature tracking of Landsat ETM+ 15 m pan band images (30 October 2000, 4 October 2002). Velocity shown in meter per year displacement (by color) and flow direction (by black arrows). Theoretical supraglacial particulate streamline estimate the travel time from a to b on Ngozumpa glacier at 380 years, and travel time from c to d on Khumbu glacier at 450 years. The streamline interpolation stops where velocities are below the error margin of around 4 m/yr. So, the ages from streamlines are minimum ages. (Background image is Landsat ETM+ 15 m pan band from 4 October 2002.)

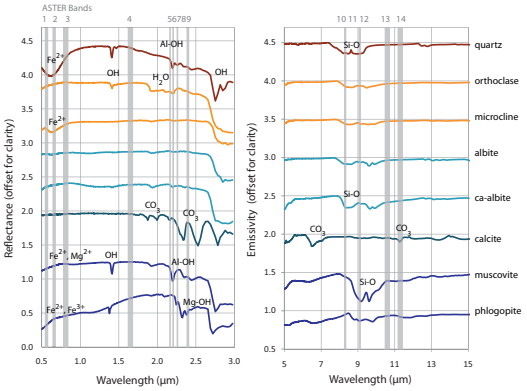

Figure A1. Reflective (VNIR-SWIR, left plot) and emissive (TIR, right plot) reference spectral library mineral signatures are displayed with ASTER multispectral band wavelength positions over plotted in gray. A *y*-axis offset of 0.5 has been applied to the mineral spectra for visualization purposes (maximum reflectance of spectra is 1). Emissivity values were calculated using Kirchoff's Law ($E = 1 - R$) where E is emissivity and R is reflectance. Note that measurements are from the USGS spectral library of specimens collected in different regions, at different grain sizes, and measured with differing laboratory conditions. Hence, signatures should be visualized with respect to general shape and potential characteristic features – which can be modified with substitution of different cations, among other factors). (Specific ASTER and USGS VNIR-SWIR and TIR spectral library references: quartz HS117.3B-5842, 32B; orthoclase HS13.3B, NMNH113188; microcline NMNH135231; albite GDS30-144, NMNHC5390; Ca-albite HS143.3B-5025, HS143.3B-3176; calcite WS272-1520, 194B; muscovite GDS108-4689, PS-16A; phlogopite HS23, NMNH12458.)

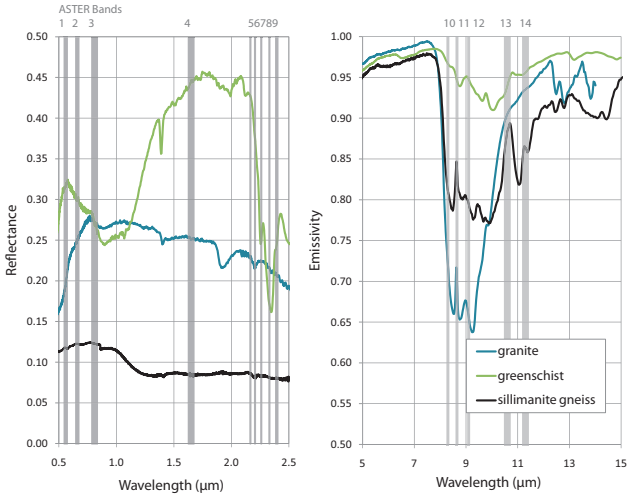

Figure A2. Reflective (VNIR-SWIR, left plot) and emissive (TIR, right plot) rock spectral signatures are displayed with ASTER multispectral band wavelength positions over plotted in gray. Emissivity values were calculated using Kirchoff's Law ($E = 1 - R$) where E is emissivity and R is reflectance. Note that measurements are from the USGS spectral library of specimens collected in different regions, and measured with differing laboratory conditions. Hence, signatures should be visualized with respect to general shape and potential characteristic features). (ASTER rock spectral library references: granite NMNH113640-17, greenschist 392, sillimanite gneiss Ward80.)

III

7.3 Publication II

K.A. Casey, R. Xie, O. Røyset, H. Keys. Supraglacial dust and debris geochemical variability: data from Svalbard, Norway, Nepal and New Zealand. *Revision submitted to Journal of Glaciology*.

IV

7.4 Publication III

K.A. Casey, A. Kääb. Supraglacial dust and debris reflectance and emissivity variability, relation to geochemical composition, surface temperature and glaciologic impacts. *Manuscript in preparation for submission.*

8

Appendix: K.A. Casey Publications

Peer-reviewed journal publications

K.A. Casey, A. Kääb. Supraglacial dust and debris reflectance and emissivity variability, relation to geochemical composition, surface temperature and glaciologic impacts. *Manuscript in preparation for submission.*

K.A. Casey, R. Xie, O. Røyset, H. Keys. Supraglacial dust and debris geochemical variability: data from Svalbard, Norway, Nepal and New Zealand. *Revision submitted to Journal of Glaciology.*

K.A. Casey, A. Kääb, D.I. Benn. Characterization of glacier debris cover via in situ and optical remote sensing methods: a case study in the Khumbu Himalaya, Nepal. The Cryosphere Discussions, 5, 499-564, 2011. *Revision submitted to The Cryosphere.*

Foster, J.L., D.K. Hall, J.B. Eylander, G.A. Riggs, S.V. Ngheim, M. Tedesco, E. Kim, P. Montesano, R.E.J. Kelly, **K. Casey**, B. Choudhury. A blended global snow product using visible, passive microwave and scatterometer satellite data. International Journal of Remote Sensing, 32, 5, 1371-1395, 2011.

8. APPENDIX: K.A. CASEY PUBLICATIONS

Hall, D.K., J.E. Box, **K.A. Casey**, S.J. Hook, C.A. Shuman and K. Steffen. Comparison of satellite-derived and in-situ observations of ice and snow surface temperatures over Greenland. Remote Sensing of Environment, 112, 3739-3749, 2008.

Hall, D.K., R.S. Williams, Jr., **K.A. Casey**, N.E. DiGirolamo and Z. Wan. Satellite-derived, melt-season surface temperature of the Greenland Ice Sheet (2000-2005) and its relationship to mass balance. Geophysical Research Letters, 33, L11501, 2006.

Hall, D.K., J.Key, **K.A. Casey**, G.A. Riggs and D. Cavalieri. Sea ice surface temperature product from the Moderate Resolution Imaging Spectroradiometer (MODIS). IEEE Transactions on Geoscience and Remote Sensing, 42, 5, 1076-1087, 2004.

Sholkovitz, E.R., H. Elderfield, R. Szymczak, **K. Casey**. Island weathering: river sources of rare earth elements to the Western Pacific Ocean. Marine Chemistry, 68, 39-57, 1999.

Proceedings publications

Paul, F., G. Bippus, **K. Casey**, H. Frey, A. Kääb, R. LeBris, T. Nagler, E. Rinne, H. Rott, A. Sheperd, T. Strozzi. Results from the ESA project GlobGlacier: Products, documents, challenges and future work. EARSeL 6th Workshop on Remote Sensing of Land Ice and Snow, 7-9 February 2011, Bern, Switzerland.

Zemp, M., Paul, F., Andreassen, L.M., Arino, O., Bippus, G., Bolch, T., Braithwaite, R., Braun, L., Càceres, B.E., Casassa, G., **Casey, K.A.**, Ceballos, C.L., Citterio, M., Delgado, H., Demuth, M., Espizua, L.E., Farokhnia, A., Fischer, A., Foppa, N., Frey, H., Fujita, K., Gärtner-Roer, I., Glowacki, P., Haeberli, W., Hagen, J.O., Hoelzle, M., Holmlund, P., Giesen, R.H., Kääb, A., Khromova, T., Kotlarski, S., Le Bris, R., Li, Z., Meier, M., Meneghel, M., Mool, P., Nussbaumer, S.U., Peduzzi, P., Plummer, S., Popovnin, V.V., Prinz, R., Rack, W., Rastner, P., Raup, B., Rinne, E., Seifert, F.M., Seiz, G., Severskiy, I., Shepherd, A., Sigurdsson, O., Strozzi, T., Vincent, C., Wheate, R., Yakovlev, A. Summit of International Glacier Monitoring in Zermatt, Switzerland. GlobGlacier Final User Group Meeting, 31 Aug - 1 Sep 2010, and WGMS General Assembly of the National Correspondents, 14 Sep 2010. Ice and Climate News.

K.A. Casey. Proposed methodology for detection of geochemical species on glaciers. Proceedings of 10th Biennial Meeting of the SGA, 16-22 August 2009, Townsville, Australia.

K.A. Casey, E.J. Kim, M.T. Hallikainen, J.L. Foster, D.K. Hall, G.A. Riggs. Validation of the AFWA-NASA blended snow-cover product in Finland, 2006-2007. Proceedings of the 65th Eastern Snow Conference, 28-30 May 2008, Fairlee, Vermont.

Hall, D.K., R. Solberg, **K.A. Casey**, J-G. Winther. Comparison of MODIS and SnowStar Snow Maps in Scandinavia. Proceedings of the 61st Eastern Snow Conference, 9-11 June 2004, Portland, ME.